UNITED STATES DEPARTMENT OF COMMERCE
DANIEL C. ROPER, Secretary
NATIONAL BUREAU OF STANDARDS
Lyman J. Briggs, Director

✦

Journal of Research

of the

National Bureau of Standards

✦

Volume 19, Number 4

October 1937

[Published with approval of the Director of the Budget]

UNITED STATES
GOVERNMENT PRINTING OFFICE
WASHINGTON : 1937

For sale by the Superintendent of Documents, Washington, D. C. - - - - - Price 25 cents
$2.50 per year on subscription

The prices of the separate Research Papers appearing in this JOURNAL are given on the front cover page. If 100 or more copies of any separate are ordered, a discount of 25 percent is allowed. Those who desire copies of separate Research Papers should send their orders and remittances without delay to the Superintendent of Documents, U. S. Government Printing Office, Washington, D. C. This will aid him to determine the number of copies to be printed for sale. Research Papers are not printed from electrotypes, and usually no more reprints can be had when the first and only printing is exhausted.

U. S. DEPARTMENT OF COMMERCE NATIONAL BUREAU OF STANDARDS

RESEARCH PAPER RP1031

Part of Journal of Research of the National Bureau of Standards, Volume 19, October 1937

STUDY OF TRANSPARENT PLASTICS FOR USE ON AIRCRAFT

By Benjamin M. Axilrod and Gordon M. Kline

ABSTRACT

Various transparent organic plastics, including both commercially available and experimental materials, were examined to determine their suitability for use as flexible windshields on aircraft. The properties studied include light transmission, haziness, distortion of vision, resistance to weathering, scratch resistance, indentation hardness, impact strength, dimensional stability, resistance to water and various cleaning fluids, bursting strength at normal and low temperatures, and flammability.

The two types of transparent plastics which are now in use on aircraft—namely, cellulose acetate and acrylate resin—were found to have certain defects which, it is believed, can be overcome in part by suitable modification of the composition and processing of the plastic.

Cellulose acetate plastic was found to have excellent impact strength, bursting strength, and flexibility, but the commercial products tested varied considerably in resistance to weathering and were all subject to marked shrinkage in 1 year's time. The shrinkage produces warping and sets up strains in the plastic sheets, which cause them to craze and crack. These strains are believed to be the cause of the spontaneous cracking of cellulose acetate windshields after they have been in service for 6 months or longer. This is particularly true of windshields exposed to low temperatures, as by ascent to high altitudes, thereby introducing additional strains in the windshield because of thermal contraction. A great deal of variation was observed in the weathering resistance between cellulose acetate sheets received from different manufacturers, and also between different lots of the material from the same manufacturer.

The acrylate resin plastic was found to be remarkably transparent, more stable to light and weathering and more resistant to scratching than cellulose acetate, but its impact strength and flexibility are much poorer. Surface crazing of the acrylate resins was noted after 1 year's exposure on the roof and also after storage for a similar period. It is claimed, however, that a method of processing has been developed which eliminates this tendency to craze. Further tests on modified samples of both cellulose acetate and acrylate resins are in progress to determine whether more uniformly durable products than have been on the market to date can be made available to the aircraft industry.

Other transparent plastics, such as cellulose nitrate, ethylcellulose, vinyl chloride-acetate resin, and vinyl acetal resins, failed in resistance to weathering after approximately 3 months. Glyceryl-phthalate, styrene, and phenol-formaldehyde resin plastics discolored markedly on exposure to sunlight or ultraviolet light from a carbon-arc lamp, and were also lacking in the flexibility which is desirable for aircraft windshields. A sample of cellulose acetobutyrate was practically unchanged after 12 months' exposure. With the exception of the cellulose nitrate, cellulose acetate, and acrylate resin plastics, the materials tested were of an experimental nature and were not recommended for use on aircraft. Many of the undesirable properties observed for these experimental materials will undoubtedly be eliminated in the course of the development of these plastics and it is not improbable that some of them will later become available in a form suitable for windshield use.

CONTENTS

		Page
I.	Introduction	368
II.	Clarity	369
	1. Description of hazeometer	370
	2. Test procedure and definitions	370
	3. Results of measurements of clarity	371
	(a) Light transmission	372
	(b) Haziness	372
III.	Index of refraction	373
IV.	Visibility distortion tests on plastics	373
V.	Resistance to weathering	374
VI.	Accelerated aging	379
VII.	Scratch resistance	382
	1. Description of apparatus	383
	2. Results of scratch-width measurements	383
VIII.	Indentation hardness	384
IX.	Impact strength	387
	1. Charpy test	387
	2. Falling-ball test	388
X.	Shrinkage	389
XI.	Resistance to water, alcohol, and kerosene	392
XII.	Bursting strength	394
XIII.	Flammability	397
XIV.	Conclusion	400

I. INTRODUCTION

Although no organic plastic has yet been developed that has the scratch resistance and low price of glass, nevertheless, plastic materials are now widely used as windows on airplanes. Two important properties of the plastics—namely, light weight and flexibility—have brought about this invasion of a field previously limited to glass. The organic plastics are approximately one-half as heavy as glass, a distinct advantage for aeronautical purposes. Flexibility is desirable in order to permit the use of curved transparent inclosures which offer minimum wind resistance.

The plastic sheets used in this country for aircraft windows (fig. 1) are made from cellulose acetate, known commercially under such trade names as Fibestos, Lumarith, and Plastacele, or from polymerized esters of acrylic and methacrylic acids, designated in the trade as Lucite and Plexiglas. Cellulose nitrate transparent sheeting is also employed to a limited extent; this type of product is variously designated as Celluloid, Fiberloid, Pryalin, and the like, by its manufacturers. A transparent synthetic resin made from glycerol and phthalic anhydride has been used in England as a window material on aircraft, but this product is not as flexible as the cellulose derivatives. None of the organic plastics possesses the surface hardness typical of glass, and the abrasive action of sand, dust, dirty rags, and flying insects soon impairs their transparency. For this reason a laminated product, made by sandwiching a plastic material between two layers of glass and commonly called safety glass, is used in locations where clear and undistorted vision is demanded, as through the windshield directly in front of the pilot. These parts must be designed for flat pieces, however, since the commercial production of laminated glass in curved shapes is very difficult to achieve and costly, although it has been accomplished experimentally.

Although the cellulose acetate sheets are more satisfactory with respect to weathering than the nitrate product, they are very suscep-

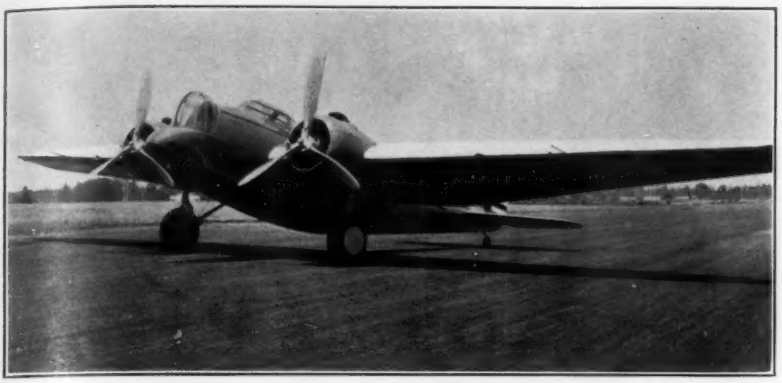

FIGURE 1.—*Transparent plastic covering on turret and cockpit of a bomber.*

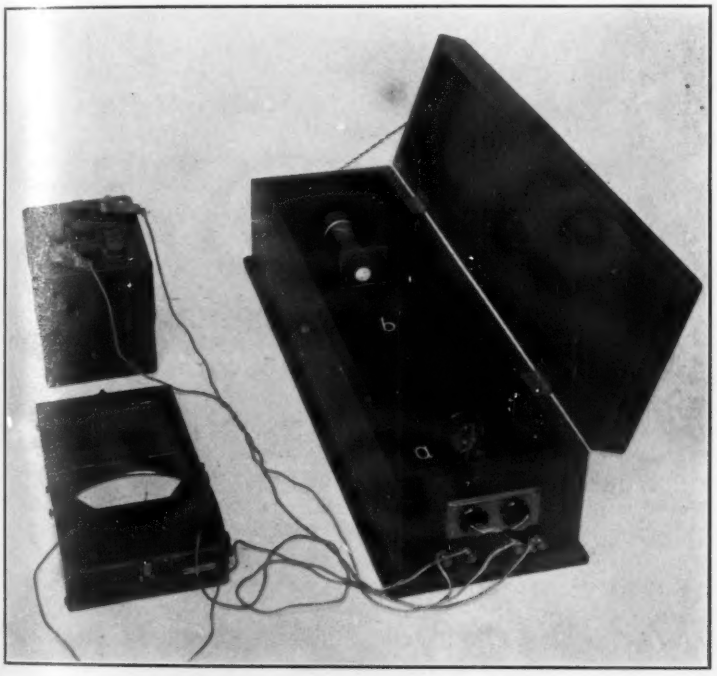

FIGURE 2.—*Hazeometer.*

UNIV. OF MICH.

tible to scratching and have been observed to develop a surface cracking after a few months in service. These factors lead to an impairment of vision through such material. Recognizing the need for an improved flexible material for use in curved windows on aircraft, the National Advisory Committee for Aeronautics established a project at the National Bureau of Standards to study the available transparent plastics with regard to their suitability for this purpose.

The following types of transparent plastics were found to be available commercially or experimentally for examination in connection with our investigation: Cellulose nitrate, cellulose acetate, cellulose acetobutyrate, ethylcellulose, acrylate (which term is used to include the polymerized esters of both acrylic and methacrylic acids), vinyl chloride-acetate, vinyl acetal, glyceryl-phthalate, styrene, and phenol-formaldehyde. Laminated glass for use on aircraft is made at the present time with four different plastic materials, as binders—namely, cellulose nitrate, cellulose acetate, acrylate resin, and vinyl acetal resin. Samples of these various products were obtained for investigation through the courtesy of the respective manufacturers.

The properties of transparent plastics of primary importance in their use for aircraft are as follows: Light transmission, freedom from haze, surface imperfections and constituents which reduce or distort vision, resistance to weathering, resistance to surface abrasion, impact strength, dimensional stability, resistance to the action of water and cleaning fluids, bursting strength at normal and low temperatures, and flammability.

II. CLARITY

The clarity of plastics is generally considered to be dependent upon two factors, light transmission and scattering of light by particles or by surface imperfections. Distortion caused by wavy surfaces and nonhomogeneous material is also an important factor in visibility through windshield materials and will be considered in section IV of this paper. The military services until recently specified that the plastic sheet should transmit at least 68 percent of white light when tested within 30 days of the date of manufacture and should be free from wrinkles, bubbles, scratches, pits, or depressions. The light transmission is usually measured with a visual or photoelectric photometer, employing in the latter a photoelectric cell which is sensitive mainly to the visible portion of the spectrum. The transparent plastics now in use generally transmit more than 85 percent of the incident light. The haziness has been measured by several methods, including visual inspection with or without a background of light from Cooper-Hewitt lamps, comparison of the plastic specimen with graded samples of varying degrees of haziness, counting the "star dust" visible in a small area under the microscope, and the determination of a small portion of the light scattered when the sample is placed at a suitable angle with relation to the light source and photometer. Although the latter method has the desirable feature of utilizing one instrument for measuring both light transmission and haziness, there is the possibility of introducing considerable error since only a small portion of the scattered light is measured.

A photometer of simple construction, called the "hazeometer", which can be used effectively to measure the haziness of a plastic as well as the light transmission, was developed in the course of this investigation.

1. DESCRIPTION OF HAZEOMETER

The apparatus is shown in figure 2. A 6-volt automobile-type bulb is mounted in front of a reflector. A cylindrical shield, blackened inside and with a circular aperture *b* in the center of the base, causes an approximately parallel beam of light to be radiated toward the photoelectric cell. A blackened disk with a circular aperture, *a*, is mounted in front of the photoelectric cell. In the instrument as built for experimental purposes the two openings, *a* and *b*, are each 1 inch in diameter and are spaced 18 inches apart. The photoelectric cell is of the Weston photronic type. The spectral response of this cell deviates considerably from the luminosity curve of the eye, and hence the light transmission obtained is not the same as would be measured with a visual photometer but is a close approximation to such value for samples containing little or no dye. A filter can be obtained from the manufacturer which will approximately correct the response of the cell to that of the eye. The meter has an internal resistance of 50 ohms and a range of 100 microamperes. Spring clamps are fastened to the frame at each aperture to hold the plastic in place. A 6-volt storage battery is used to operate the lamp. All the parts are housed within a wooden box finished in a dull black which reduces reflections to a minimum. The lid of the box is closed during measurements to keep rays of light from outside sources from reaching the photoelectric cell. This instrument is only applicable for measuring the haze in sheets which have approximately parallel surfaces and are free from imperfections which act as lenses or prisms.

2. TEST PROCEDURE AND DEFINITIONS

To obtain a measure of the light transmission of the plastic, the light is adjusted in intensity so that a current of 100 microamperes is obtained from the photoelectric cell. A flat sample is then placed in front of the cell at aperture *a*. Of the light incident on the sample, a fraction is transmitted undeviated, and a fraction is scattered by the surfaces and the interior of the sample. The photoelectric cell receives the undeviated fraction of the light and that part of the scattered light which is not deflected at angles greater than about 90°. The light transmission of the plastic is defined as that fraction of the light received by the photoelectric cell through the unobstructed aperture, which continues to reach the sensitive element when the plastic is placed over the aperture *a* directly in front of the photoelectric cell.

To obtain a measure of the haziness the specimen is placed at aperture *b*, 18 inches distant from aperture *a*. The photoelectric cell still receives the undeviated fraction of the light, but collects only that small portion of the scattered light which is confined to the small solid angles subtended by aperture *a* at points in opening *b*. The difference between the photoelectric currents with the sample at *a* and *b* is a measure of the light scattered, assuming that a linear relation exists between the photoelectric current and the total light incident upon the sensitive element of the cell. The current is practically proportional to the total incident light for no external resistance; the deviation is only slight for the 50-ohm resistance in the microammeter used. Haziness is defined as the percentage of the total light transmitted at position *a*, which is scattered when the sample is placed at position *b*.

3. RESULTS OF MEASUREMENTS OF CLARITY

The initial white-light transmission and haziness of the materials submitted by cooperating manufacturers were measured with the hazeometer. The results are presented in table 1. Each value in the table is the average for three specimens, each 1¼ by 2½ inches. The results of measurements of light transmission and haziness on several varieties of plain and laminated glass are given in table 2 for comparison.

TABLE 1.—*Optical properties of transparent plastics*

Material	Sample	Thickness	White-light transmission	Haze value	Index of refraction
		Mils	*Percent*	*Percent*	n_D^{21}
Cellulose acetate	*A1*	64	88.8	3.9	1.500
Do	*A2*	95	85.9	6.1	1.500
Do	*A3*	133	83.0	7.6	1.501
Do	*B1*	63	91.4	7.1	1.501
Do	*B2*	93	90.6	5.1	1.502
Do	*B3*	64	91.7	4.0	1.500
Do	*B4*	98	89.1	4.0	1.495
Do	*B5*	101	88.7	3.9	1.498
Do	*C1*	56	88.2	6.1	1.500
Do	*C3*	125	81.8	10.4	1.501
Do	*D1*	162	77.1	6.7	1.475
Cellulose acetobutyrate	*S1*	41	92.3	6.0	1.494
Cellulose nitrate	*E1*	67	91.6	3.7	1.501
Do	*F1*	64	85.0	4.1	1.501
Ethylcellulose	*G1*	57	82.1	27.2	1.479
Do	*H1*	29	86.1	9.8	1.472
Do	I1	38	91.1	7.0	1.483
Acrylate resin	*J1*	66	93.6	4.6	1.496
Do	*J2*	76	93.7	4.2	1.492
Do	*K1*	117	94.1	1.9	1.496
Do	*K2*	88	94.2	1.8	1.483
Vinyl chloride-acetate resin	*L1*	56	82.5	5.3	1.525
Do	*L2*	100	79.2	7.2	1.529
Vinyl acetal resin	*M1*	62	88.8	5.4	1.509
Do	*N1*	126	84.4	11.5	1.490
Glyceryl-phthalate resin	*P1*	159	86.2	4.8	1.578

TABLE 2.—*Optical properties of glass windshield products*

Type of glass	Type of plastic lamination	Sample	Thickness	White-light transmission	Haze value
			Mils	*Percent*	*Percent*
Thin plate	None	*X1*	85	[a]86.9	0.9
Thin plate safety	Acetate	*X5*	186	[a]82.8	1.3
10-oz sheet	None	*X2*	53	93.2	1.2
10-oz sheet safety	Acetate	*X6*	130	91.3	1.2
¼-inch plate	None	*X4*	225	91.0	0.9
Thin sheet safety	Acrylate	*Y1*	107	92.8	1.2
Do	do	*Y2*	130	92.4	1.2
Plate safety	do	*Y3*	248	89.4	1.2
Plate safety	Nitrate	*Z1*	234	[a]73.7	1.8
Do	Vinyl	*Z2*	261	[a]71.6	1.4
Sheet safety	do	*Z3*	144	92.0	1.6

[a] These glasses distinctly colored, probably by iron oxide.

(a) LIGHT TRANSMISSION

It will be noted that the white-light transmission of all of the plastics tested exceeds the 68-percent requirement formerly specified by the military services. The highest values were obtained with samples of acrylate resins, the percentage transmission varying between 93.6 and 94.2 for these materials. The samples of cellulose acetate which gave white-light transmissions exceeding 90 percent did not contain blue dye, whereas those tinted blue gave values varying between 77 and 83 percent. The effect of the addition of blue coloring on the transmissivity is shown in table 2 for the glass products and in table 3 for a special series of cellulose acetate transparent plastics. Because of the pronounced lowering of the percentage of light transmitted, the practice of adding blue dye to cellulose acetate transparent sheet has been discontinued by some manufacturers. For undyed materials approaching the transparency of polished glass, most of the loss of light is due to reflection at the two surfaces and can be approximately calculated from the refractive index.

TABLE 3.—*Light-transmission and haziness values of transparent cellulose acetate plastics with and without the addition of blue dye*

Thickness	Dye	Light-transmission		Haziness value $\left(\frac{A-B}{A}100\right)$
		Sample at photoelectric cell (A)	Sample 18 in. from photoelectric cell (B)	
Mils		*Percent*	*Percent*	*Percent*
53	Blue	86.3	83.9	2.8
53	do	86.2	83.7	2.9
67	None	90.7	87.6	3.4
68	do	91.2	87.5	4.1
65	do	91.0	85.8	5.7
67	do	90.7	85.3	6.0
67	do	90.7	85.2	6.1
85	do	89.7	84.0	6.4
31	Blue	4.2	3.8	9.0
35	do	86.7	78.4	9.6
35	do	86.7	77.6	10.5
105	do	75.0	64.3	14.3
105	do	75.1	63.8	15.0

(b) HAZINESS

The haze values for two of the acrylate samples, namely, 1.8 and 1.9 percent, compare favorably with measurements made on laminated safety glass and are the lowest of any of the plastics studied. The values for the cellulose acetate products show considerable variation. Apparently a minimum of about 4 percent of haze for sheets up to 100 mils thick is the best that can be done and for thicker sheets this would be somewhat higher. The fog or cloudiness in sheets, with haze values of this order is quite easily detected by the naked eye and is a much more serious defect than the lowering of white-light transmission by blue dye. The values recorded in table 1 for the materials other than cellulose nitrate, cellulose acetate, and acrylate resin, were obtained on experimental samples only, such products not being available in sheet form for aircraft windshields at the present time.

III. INDEX OF REFRACTION

The index of refraction is of interest in considering the light-transmission characteristics of plastics. This property was measured by means of an Abbe refractometer on the same specimens used in the light-transmission and haze tests. Two contact liquids, alpha-bromonaphthalene and mercuric iodide, were employed in order to guard against incorrect values resulting from reaction between the sample and the contact liquid. The data obtained are presented in table 1. The refractive indices for the materials studied range from 1.47 to 1.58.

IV. VISIBILITY DISTORTION TESTS ON PLASTICS

Visibility distortion tests were made in accordance with the procedure suggested by the American Standards Association for laminated safety glass using sheets 12 inches square. In this test, a line is projected with a lantern so as to fall midway between two parallel lines 1 inch apart marked on a screen. The test specimen is 25 feet from the screen and the lantern is adjusted so that the center 10- by 10-inch square fills the beam. The sample in a suitable frame is moved across the beam and the movement of the projected line observed; the safety-glass specification requires that the projected line shall not deviate more than ½ inch as the sheet is moved across the beam. Several materials were tested but none failed to meet the specification. Measurements were then made on each sample of the deviation of the projected line as the square was moved an inch at a time across the beam. This measurement was made at the top, center, and bottom of the screen for the sample normal to the incident light; this was repeated just at the center of the screen for angles of 75, 60, 45, and 30°. The data did not prove suitable for giving an estimate of the visibility because a specimen with many relatively small ripples simply causes the projected line to move back and forth rapidly as well as causing it to get out of focus; a sample which is slightly wedge-shaped or one with a large wave in its surface might cause the line to deviate as much or more, yet it would be far superior as regards distortion.

The above considerations led to the following method for evaluating the distortion of the transparent plastic sheets. A projection lantern is focused on a screen 40 feet distant; the specimen is placed in front of and parallel to the screen. The sample is moved toward the light and its shadow observed. When light and dark patches begin to appear in the shadow, the distance of the specimen from the screen is noted and is taken as a measure of the relative distorting characteristics of the sheet. The less distortion, the greater is the distance at which the shadow becomes nonuniform. Observations were made by three individuals on 12- by 12-inch samples of the plastics. The averages of these observations are shown in table 4. The acrylate resin sheets are found to be considerably better than other plastic materials in this test.

TABLE 4.—*Measurements of distortion of light by transparent plastics*

Material	Sample	Distance where shadow becomes spotty
		Inches
Acrylate resin	*K4*	28
Vinyl chloride-acetate resin	*L1*	11
Cellulose nitrate	*F1*	7
Cellulose acetate	*A2*	5
Vinyl acetal resin	*N1*	4
Cellulose acetate	*C2*	4
Do	*B7*	2
Do	*D1*	0.5

V. RESISTANCE TO WEATHERING

Specimens of transparent plastics 7 by 7 inches were prepared for weather-exposure tests by fastening them in brass frames curved cylindrically to a radius of 5 inches. Most of the materials were flexible enough to bend to the curvature of the frame without special heat treatment and could be drilled in the flexed position without cracks forming at the holes. Two samples of the acrylate resin sheets, *J2* and *K1*, were softened in water warmed to about 60° C for 15 minutes and then bent and drilled. Another acrylate sample, *K3*, was softened by heating for 10 minutes at 70° C in an oven. One manufacturer of these resinous sheets has recently recommended bending them by warming at 90 to 125° C, depending on the thickness, using as the heating medium either water or preferably, hot air, pressing the sheet around a wood or metal form covered with rubber or glove cloth, and allowing it to cool in the bent position. Determinations of initial white light transmission and haze were made on the specimens in the frames before placing them on the roof. In addition, the light transmission was measured with red, green, and blue filters in order to follow any color changes in the various materials during exposure. The frames were fastened to exposure racks on the roof of the Industrial Building of the National Bureau of Standards, the racks facing south and being inclined at an angle of 45° to the horizontal. The tests were started on the roof during March 1936, and the changes in clarity after 1, 2, 3, 6, 9, and 12 months were determined quantitatively. The specimens were cleaned with lens paper soaked in tap water, and for some of the materials in kerosene, prior to each measurement of their clarity.

The data for light transmission and haze made on the transparent plastics are given in tables 5, 6, and 7.

TABLE 5.—*Effect of outside exposure on white-light transmission*

Material	Sample	Light transmission					Remarks on condition at last test period
		Initial	3 months	6 months	9 months	12 months	
		Percent	*Percent*	*Percent*	*Percent*	*Percent*	
Cellulose acetate	*A1*	88.2	90.6	83.4	85.5	77.1	Crazed; discolored.
Do	*A2*	85.2	88.2	81.7	81.2	71.1	Do.
Do	*A3*	82.2	86.4	84.9	83.5	72.9	Do.
Do	*B1*	90.8	91.6	91.2	91.3	91.3	Surface roughened; cracked.
Do	*B2*	89.9	90.7	90.5	90.7	90.7	Do.
Do	*B3*	90.7	90.7	90.5	90.4	88.8	Crazed.
Do	*C1*	87.1	87.6	88.7	89.2	89.3	Pebbled; crazed at edge.
Do	*C2*	81.1	83.1	83.5	84.7	84.6	Do.
Do	*D1*	76.6	87.9	86.7	80.9	57.4	Crazed and cracked.
Cellulose acetobutyrate	*S1*	92.0	92.2	92.2	92.1	92.2	Unchanged.
Cellulose nitrate	*E1*	91.0	84.8	43.2	37.0	35.1	Surface crazed; opaque.
Do	*F1*	83.7	79.1	39.0	34.2	32.2	Do.
Ethylcellulose	*G1*	79.7	51.8	----------	----------	----------	Opaque; cracked.
Do	*H1*	85.3	86.2	----------	----------	----------	Cracked loose from frame at 6 months.
Do	*I1*	90.3	89.8	60.2	24.0	----------	Opaque; friable.
Acrylate resin	*J1*	92.9	92.7	92.9	92.6	92.3	Roughened; crazed.
Do	*J2*	93.2	93.0	93.1	92.8	92.6	Crazed.
Do	*K1*	93.3	92.7	91.7	91.7	91.4	Slightly discolored.
Do	*K2*	93.2	93.7	93.6	93.5	93.1	Roughened; crazed.
Do	*K3*	93.5	93.5	93.3	92.6	----------	Slight crazing.
Vinyl chloride-acetate resin	*L1*	81.6	77.4	30.0	33.4	36.0	Discolored; crazed.
Do	*L2*	78.9	70.2	4.1	3.9	4.4	Discolored; opaque.
Vinyl acetal resin	*M1*	88.0	87.1	78.7	57.1	52.3	Crazed; opaque.
Do	*N1*	84.3	69.4	53.6	43.8	----------	Do.
Glyceryl-phthalate resin	*O1*	85.5	----------	82.8	82.4	----------	Slightly discolored.

TABLE 6.—*Effect of outdoor exposure of transparent plastics on light transmission using various color filters*

Material	Sample	Color transmission											
		Red filter [a]				Green filter [b]				Blue filter [c]			
		Initial	After 3 months	After 6 months	After 1 year	Initial	After 3 months	After 6 months	After 1 year	Initial	After 3 months	After 6 months	After 1 year
		Per-cent	*Per-cent*	*Per-cent*	*Per-cent*	*Per-cent*	*Per-cent*	*Per-cent*	*Per-cent*	*Per-cent*	*Per-cent*	*Per-cent*	*Per-cent*
Cellulose acetate	*A1*	91.2	91.6	84.5	75.1	87.1	89.1	80.6	72.3	88.3	88.0	78.6	71.1
Do	*A2*	89.1	89.6	83.6	68.9	83.8	85.7	78.4	65.1	85.4	84.8	75.3	64.1
Do	*A3*	87.5	87.9	87.1	71.7	80.0	83.6	82.0	66.8	83.0	83.1	79.0	65.7
Do	*B1*	91.3	91.7	91.5	91.7	89.5	90.0	90.2	90.3	89.2	90.3	89.4	90.1
Do	*B2*	90.8	90.8	90.8	91.1	88.4	89.0	89.4	89.6	87.9	89.3	88.5	89.3
Do	*B3*	91.6	91.8	91.7	88.8	89.8	89.1	89.0	87.2	89.4	88.2	86.7	86.0
Do	*C1*	89.3	89.0	89.6	90.2	85.4	85.2	87.2	87.5	86.4	86.4	86.9	88.0
Do	*C2*	85.4	85.8	86.2	87.7	78.0	78.9	81.3	82.6	80.2	81.5	81.3	83.6
Do	*D1*	84.4	87.7	86.2	52.6	75.1	85.0	84.1	49.4	80.9	86.1	83.7	50.2
Cellulose acetobutyrate	*S1*	92.2	92.2	92.4	92.4	91.2	91.0	91.6	91.1	90.9	91.2	91.3	90.9
Cellulose nitrate	*E1*	91.6	87.0	40.3	29.8	90.0	80.3	31.8	23.3	89.1	76.7	31.5	24.0
Do	*F1*	83.3	79.9	35.0	25.4	84.7	76.8	29.4	20.9	85.0	73.3	27.2	20.7
Ethylcellulose	*G1*	82.7	44.2	------	------	74.7	41.7	------	------	72.6	42.4	------	------
Do	*H1*	86.5	86.2	------	------	83.3	83.9	------	------	81.8	83.2	------	------
Do	*I1*	91.2	90.0	57.9	------	89.2	87.7	53.3	------	88.5	87.7	51.6	------
Acrylate resin	*J1*	92.9	92.5	92.7	92.9	92.2	91.7	92.5	92.3	92.1	91.6	91.6	91.8
Do	*J2*	93.2	92.8	93.1	93.6	92.5	92.0	92.4	92.7	92.4	92.0	91.8	92.6
Do	*K1*	93.1	93.0	92.6	93.1	92.7	91.1	90.3	90.5	92.6	90.1	87.9	88.7
Do	*K2*	94.1	93.4	93.5	93.5	93.0	92.7	92.9	93.0	93.2	92.8	92.8	93.1
Do	*K3*	93.7	93.3	[d]92.5	------	93.1	93.0	[d]91.5	------	93.2	92.2	[d]91.5	------
Vinyl chloride-acetate resin	*L1*	86.5	82.7	52.2	54.3	83.3	72.7	19.8	22.4	84.9	74.7	33.2	37.4
Do	*L2*	85.1	77.4	12.0	13.3	76.9	62.8	6.2	4.4	76.6	65.4	15.2	15.1
Vinyl acetal resin	*M1*	89.0	87.3	79.2	48.0	86.6	84.7	74.9	40.3	85.8	84.2	73.1	41.2
Do	*N1*	85.6	71.8	[d]42.4	------	81.2	65.3	[d]35.0	------	79.6	64.1	[d]36.5	------
Glyceryl-phthalate resin	*O1*	87.7	------	[d]87.0	------	80.2	------	[d]78.5	------	79.3	------	[d]77.7	------

[a] Pyrometer red filter (Corning Glass Works).
[b] No. 61 Wratten filter (Eastman Kodak Co.).
[c] No. 47 Wratten filter (Eastman Kodak Co.).
[d] After 9 months.

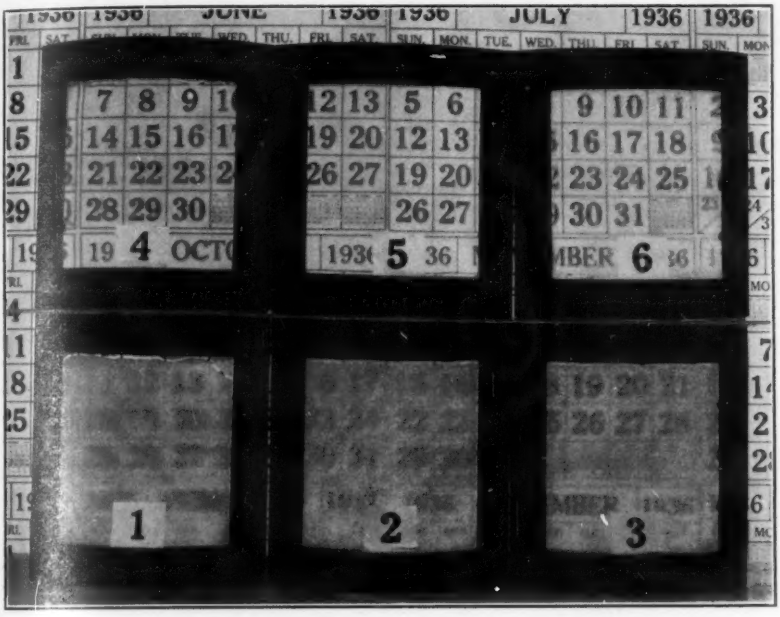

FIGURE 3.—*Exposure panels after 1 year out-of-doors.*

Identification number	Material	Sample
1	Cellulose acetate	*A1*
2	do	*A2*
3	do	*A3*
4	do	*B1*
5	do	*B2*
6	do	*B3*

FIGURE 4.—*Exposure panels after 1 year out-of-doors.*

(Sample 24 exposed for 9 months only.)

Identification number	Material	Sample
7	Cellulose acetate	*C1*
8	do	*C3*
9	do	*D1*
10	Cellulose nitrate	*E1*
11	do	*F1*
24	Vinyl acetal resin	*N1*

FIGURE 5.—*Exposure panels after 1 year out-of-doors.*

(Sample 25 exposed for 9 months only.)

Identification number	Material	Sample
16	Acrylate resin	*J2*
17	do	*K1*
18	do	*K2*
25	do	*K3*
14	Ethylcellulose	*I1*
15	Acrylate resin	*J1*

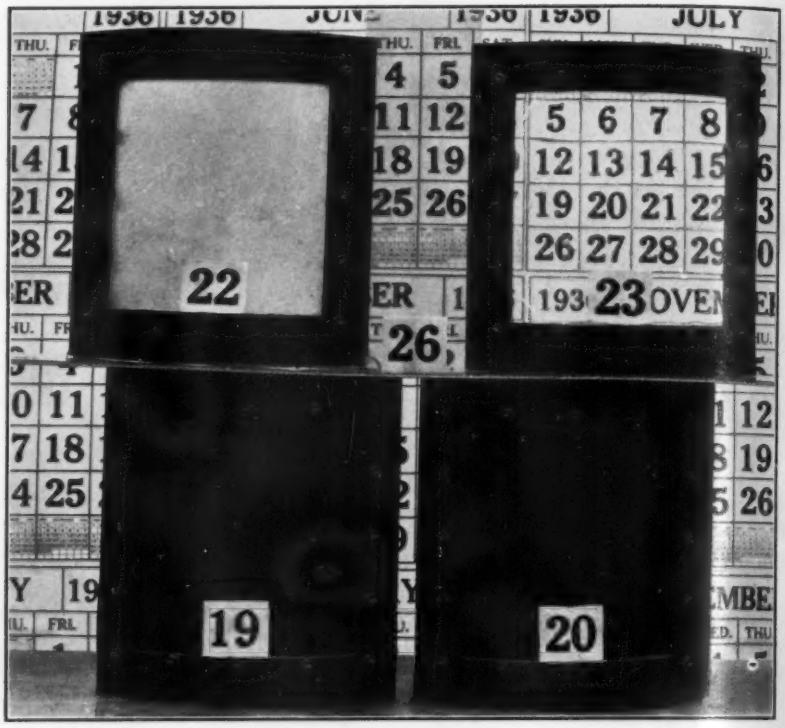

FIGURE 6.—*Exposure panels after 1 year out-of-doors.*

(Sample 26 exposed for 9 months only.)

Identification number	Material	Sample
19	Vinyl chloride-acetate resin	*L1*
20	do	*L2*
22	Vinyl acetal resin	*M1*
23	Cellulose acetobutyrate	*S1*
26	Glyceryl-phthalate resin	*O1*

TABLE 7.—*Effect of outside exposure on haziness of transparent plastics*

Material	Sample	Haze value				
		Initial	3 months	6 months	9 months	12 months
		Percent	*Percent*	*Percent*	*Percent*	*Percent*
Cellulose acetate	*A1*	4.1	4.7	14.4	24.1	38.5
Do	*A2*	6.0	6.9	14.5	21.4	30.8
Do	*A3*	7.7	7.5	11.5	20.6	24.3
Do	*B1*	6.7	7.5	8.3	8.3	9.3
Do	*B2*	4.7	5.0	7.2	7.9	7.9
Do	*B3*	3.6	3.8	5.1	6.4	10.0
Do	*C1*	6.4	7.5	11.5	10.4	11.3
Do	*C2*	9.4	9.7	12.2	11.9	12.5
Do	*D1*	7.2	11.8	16.5	33.0	56.4
Cellulose acetobutyrate	*S1*	5.4	4.7	4.6	4.6	6.0
Cellulose nitrate	*E1*	3.2	7.8	83.8	96	97
Do	*F1*	4.2	7.5	84.8	97	98
Ethylcellulose	*G1*	26.0	78.8	----	----	----
Do	*H1*	9.0	17.0	----	----	----
Do	*I1*	5.8	7.2	86.3	99	----
Acrylate resin	*J1*	4.4	4.7	5.3	5.3	5.2
Do	*J2*	3.5	4.5	4.8	4.7	4.4
Do	*K1*	2.7	2.8	2.5	3.2	3.7
Do	*K2*	2.6	3.2	3.4	3.1	3.8
Do	*K3*	1.3	1.7	2.8	4.0	----
Vinyl chloride-acetate resin	*L1*	6.3	7.2	11.1	18.2	25.9
Do	*L2*	10.6	15.0	38	55	64
Vinyl acetal resin	*M1*	3.2	10.3	74	95	96
Do	*N1*	8.4	27.8	90	94	----
Glyceryl-phthalate resin	*O1*	7.7	----	9.4	10.0	----

The condition of the samples after 12 months of exposure on the roof is shown in figures 3 to 6. Examination of the photographs indicates clearly that the samples of acrylate resins, nos. 15, 16, 17, and 18, are in the best condition after the year's exposure. This same conclusion is reached from a consideration of the values for light transmission in tables 5 and 6 and for haze in table 7. The surfaces of three of these samples, however, had begun to craze and crack. These cracks are not readily visible when viewed by directly transmitted light, but become very pronounced when illuminated so that the light scattered by them can be observed. Figure 7 shows panels 16, 17, and 18 taken at a suitable angle to show this crazing. It should be kept in mind that these frames are curved and that cracks like those which show at the center portion of panels 16 and 18 are present throughout the whole sheet. Sample 17 (*K1*) did not show any evidences of crazing; however, it contained a plasticizer which caused a slight yellowing of the sheet upon exposure. This discoloration is indicated by the results of the light-transmission measurements using a blue filter, shown in table 6. Some samples of acrylate resin kept in storage for approximately 18 months developed similar crazing, as shown in figure 8. One of the manufacturers of this type of plastic has stated that his product has been modified so as to avoid this failure. Tests on these new materials are in progress.

The cellulose acetate transparent sheets tested are shown in figures 3 and 4, panels 1 to 9, after 12 months' exposure. The products of different manufacturers and of different samples from the same

manufacturer varied considerably in their behavior upon weathering. Panels 1 to 3 had crazed badly, discolored, and become practically opaque. Panels 4 and 5 were in the best condition of any of the cellulose acetate samples after 1 year on the roof. Even these had become considerably hazy and one had cracked at the top of the frame because of shrinkage. These two samples tended to become coated with a frosty layer when left untouched for several weeks. This surface coating was readily removed with lens paper soaked in kerosene, and would be constantly eliminated by normal cleaning in service. Panel 6 was a sample submitted as a supposedly improved product, but it is quite apparently inferior to panels 4 and 5, made by the same manufacturer. Panels 7 and 8 were beginning to show large surface cracks after 1 year and their surfaces had become roughened or "pebbled", thereby causing distortion of vision through them. Panel 9 had become practically opaque in 1 year; the cracking which caused this had taken place fairly regularly over the period of exposure as indicated by the haze values in table 7.

It is well known that deterioration of cellulose nitrate is accelerated by ultraviolet light. Samples 10 and 11 show how completely opaque this plastic becomes during 1 year of exposure to sunlight. Table 7 indicates that the major portion of the breakdown occurred between the 3- and 6-months period, namely, during June, July, and August. The condition of these samples after 3 months of exposure is shown in figure 9. The crazing which occurs is confined to the outer surface of the material, the back remaining smooth and transparent.

The ethylcellulose sheets tested were among the first samples of this plastic which became available in this country. As indicated in table 7, figure 9 (panel 12 after 3 months) and figure 5 (panel 14 after 12 months) these materials were not resistant to exposure on the roof. A marked increase in the haziness of two of the samples took place within 3 months, and the third sample deteriorated rapidly during the following 3 months. It is understood that manufacturers of these materials have improved the stability of ethylcellulose sheets during the interval which has elapsed since these materials were received. New materials are being tested to determine whether a grade which would be suitable for airplane use has been developed.

The vinyl resin sheets, all of which were experimental samples, did not have satisfactory resistance to weathering. The polyvinyl chloride-acetate sheets (panels 19 and 20 in fig. 6) discolored rapidly, becoming dark purple. This purple discoloration was entirely a surface-layer effect and extended only one-fifth of the way through the sample, the remainder being apparently unaffected. The vinyl acetal samples (panel 22 in fig. 6 after 12 months, and panel 24 in fig. 4 after 9 months) did not discolor but became opaque and showed evidences of surface cracking.

The sheet of cellulose acetobutyrate (panel 23 in fig. 6) was cast from a solution in organic solvents. The bubbles which are seen were present in the sheet as it was received. As indicated in tables 5, 6, and 7, no marked changes in the light-transmission and haze characteristics of this material took place during the exposure period. The streak which is present on one side of the picture of panel 23 is an optical effect only, no cracks having appeared in the exposed sample.

The glyceryl-phthalate resin was too brittle to be bent to the 5-inch radius of curvature of the test frames. A flat piece was exposed

FIGURE 7.—*Acrylate resin samples after 1 year of exposure, showing crazing.*

Identification number	Material	Sample
16	Acrylate resin	*J2*
17	do	*K1*
18	do	*K2*

FIGURE 8.—*Acrylate resin samples after approximately 1 year in storage, showing crazing.*

Identification number	Material	Sample
16	Acrylate resin	*J2*

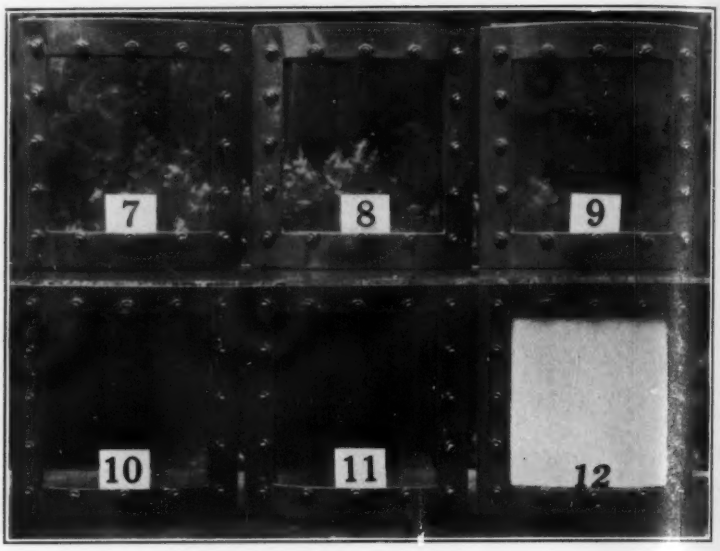

FIGURE 9.—*Exposure panels after 3 months out-of-doors*

Identification number	Material	Sample
7	Cellulose acetate	*C1*
8	do	*C3*
9	do	*D1*
10	Cellulose nitrate	*E1*
11	do	*F1*
12	Ethylcellulose	*G1*

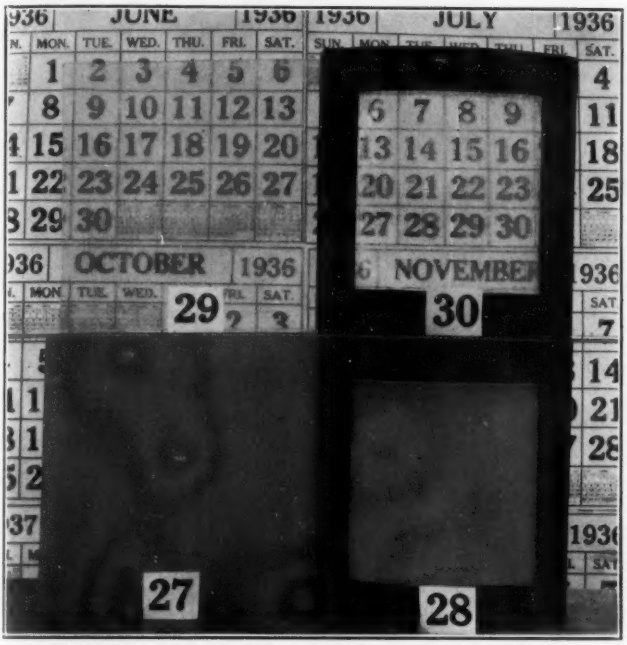

FIGURE 10.—*Exposure samples of cellulose acetate and cellulose nitrate after 9 months out-of-doors.*

Identification number	Material	Sample
27	Cellulose nitrate	*E1*
28	do	*E1*
29	Cellulose acetate	*B8*
30	do	*B6*

UNIV. OF MICH.

for 9 months on the roof and is shown in figure 6 (no. 26). No cracking or crazing is evident but the material had discolored considerably.

The possible effects on crazing of the bolting of the materials in a stressed state in the test frames was studied by exposing flat sheets of cellulose acetate and cellulose nitrate simultaneously with the same materials fastened in the curved panels. Figure 10, which shows the condition of the specimens after 9 months of exposure on the roof, indicates that the crazing took place equally rapidly under the two conditions. The crack down the middle of panel 30 was the result of strain caused by shrinkage due to loss of volatile material.

The effect of 1 year of exposure out-of-doors on the white light transmission and haziness of laminated and ordinary glass is shown in table 8. No marked breakdown of these products took place during this period. The laminated glass made with an acrylate plastic gave somewhat erratic results in the measurement of haze because the plastic tended to squeeze out at the edges, thereby leaving the product slightly wedge-shaped. However, there was no apparent change at the end of 1 year on the roof in the clarity or appearance of this type of laminated glass.

TABLE 8.—*Effect of outdoor exposure on white light transmission and haziness of glass windshield products*

Type of glass	Type of plastic lamination	Sample	Thickness	Light transmission		Haze value	
				Initial	After 12 months	Initial	After 12 months
			Mils	*Percent*	*Percent*	*Percent*	*Percent*
Thin plate	None	*X1*	85	86.7	86.8	1.3	1.2
Thin plate safety	Acetate	*X5*	186	81.6	82.5	1.5	1.7
10-oz sheet safety	do	*X6*	130	91.2	92.0	1.1	1.3
12- to 14-oz sheet	None	*X3*	67	93.1	93.1	1.0	1.2
12- to 14-oz sheet safety	Acetate	*X7*	152	91.2	91.9	1.4	1.3
¼-in. plate	None	*X4*	225	91.2	91.1	0.9	0.8
¼-in. tempered plate	do	*X8*	248	92.5	91.7	1.4	1.1
Thin sheet safety	Acrylate	*Y1*	107	92.8	92.0	0.9	1.3
Do	do	*Y2*	130	92.6	92.2	1.4	1.1
Plate safety	do	*Y3*	248	89.5	89.2	1.1	0.6
Plate and thin sheet safety	do	*Y4*	228	91.3	90.7	1.2	1.0
Plate and sheet safety	do	*Y5*	238	89.9	89.3	0.9	1.0
Plate safety	Nitrate	*Z1*	234	73.3	*73.0	1.5	*1.4
Do	Vinyl	*Z2*	261	71.4	*71.2	1.5	*1.7
Sheet safety	do	*Z3*	144	91.8	*91.5	1.6	*1.4

* After 9 months of exposure.

VI. ACCELERATED AGING

Accelerated aging tests were made in an apparatus having a carbon-arc light. Specimens 6 by 1½ inches were used, a portion of each being covered with aluminum to obtain a ready comparison of exposed and unexposed material. The samples were rotated around the carbon arc at a distance of 2 feet, at the rate of one revolution every 20 minutes. Tap water was sprayed on the plastics at one location in the apparatus; the duration of its application to each sample was about 15 seconds. The samples were tested after 500 and 1,000 hours. The results of these tests are shown in table 9. Figure 11

shows the condition of the specimens after 1,000 hours of exposure. The unexposed portion is at the top of each specimen in the photograph.

TABLE 9.—*Accelerated aging of transparent plastics by carbon-arc light with intermittent water spray*

Material	Sample	White-light transmission			Remarks on condition after 1,000 hours
		Initial	500 hr	1,000 hr	
		Percent	*Percent*	*Percent*	
Cellulose acetate	*A1*	88.2	90.2	89.2	Warped, cracked, and slightly clouded.
Do	*B1*	91.3	92.3	91.7	Surface roughened.
Do	*B3*	91.4	92.6	91.8	Warped and slightly clouded.
Do	*C1*	87.9	89.0	89.6	Warped.
Do	*C3*	81.7	84.6	84.8	Slightly warped.
Do	*D1*	76.8	82.5	86.0	Cracked and bleached.
Cellulose acetobutyrate	*S1*	92.2	92.2	92.2	Slightly warped.
Cellulose nitrate	*E1*	91.2	91.5	87.6	Warped, discolored, and slight crazing.
Do	*F1*	84.7	86.0	86.7	Discolored.
Ethylcellulose	*G1*	82.3	81.3	----------	Opaque at 800 hr; friable.
Do	*H1*	85.0	85.0	85.0	Warped and cloudy.
Do	*I1*	91.3	89.6	78.3	Warped; surface frosty.
Acrylate resin	*J1*	93.3	93.4	93.3	Surface pitted.
Do	*J2*	93.4	93.3	92.7	No marked change.
Do	*K1*	93.6	93.1	92.5	Do.
Do	*K2*	94.0	93.9	93.3	Do.
Vinyl chloride-acetate resin	*L1*	82.4	82.7	17.1	Discolored purple.
Do	*L2*	79.2	59.2	0.7	Discolored purple; opaque.
Vinyl acetal resin	*M1*	89.0	[a] 88.3	(b)	Warped and cloudy.
Styrene	*R1*	74.7	72.8	59.8	Darkened and cracked.

[a] 163 hr.
[b] Too warped to measure.

The cellulose acetate materials in general were improved in regard to light transmission, because of bleaching of the blue dye added to the original plastic. The specimens were held only by light spring clamps and many of the cellulose acetate specimens warped during the test. The cellulose nitrate samples were less affected by 1,000 hours in the accelerated aging apparatus than by 3 months (March, April, and May) of exposure out-of-doors. One sample of ethylcellulose was in a very friable state after 1,000 hours of exposure to the carbon-arc light. The acrylate resins were practically unchanged after this treatment. The effect of the carbon-arc light on the polyvinyl chloride-acetate samples was very pronounced, and they were converted from the transparent condition to purplish-colored opaque masses. This change was confined to a thin layer at the surface of the sample, which indicated practically complete absorption of the harmful light radiation. The styrene and vinyl acetal samples were rapidly deteriorated in this test. The cellulose acetobutyrate was practically unaffected. Salt deposited during the alternate wetting and drying cycles prevented accurate determination of haze changes.

A second group of specimens was subjected to the light from the carbon-arc lamp without a water spray so that haze measurements could be made. The samples were subjected to a somewhat higher temperature in this test, approximately 55° C instead of 40° C when

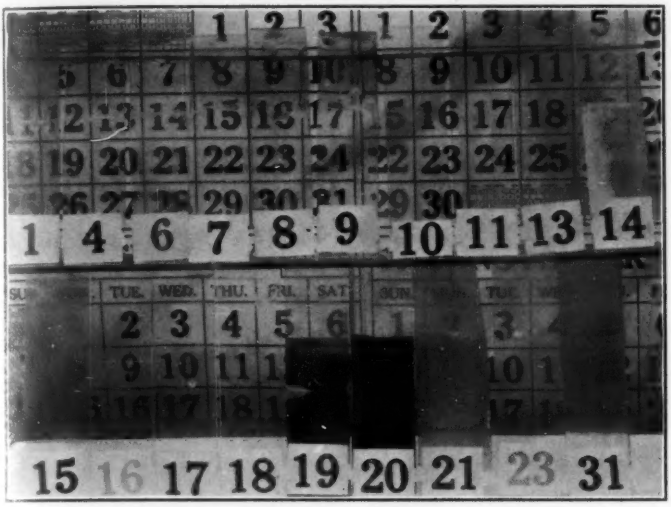

FIGURE 11.—*Condition of samples after exposure to carbon-arc light for 1,000 hours with intermittent water spray*

Identification number	Material	Sample	Identification number	Material	Sample
1	Cellulose acetate	*A1*	15	Acrylate resin	*J1*
4	do	*B1*	16	do	*J2*
6	do	*B3*	17	do	*K1*
7	do	*C1*	18	do	*K2*
8	do	*C3*	19	Vinyl chloride-acetate resin	*L1*
9	do	*D1*	20	do	*L2*
10	Cellulose nitrate	*E1*	21	Styrene	*R1*
11	do	*F1*	23	Cellulose acetobutyrate	*S1*
13	Ethylcellulose	*H1*	31	Phenol-formaldehyde resin.	*U1*
14	do	*I1*			

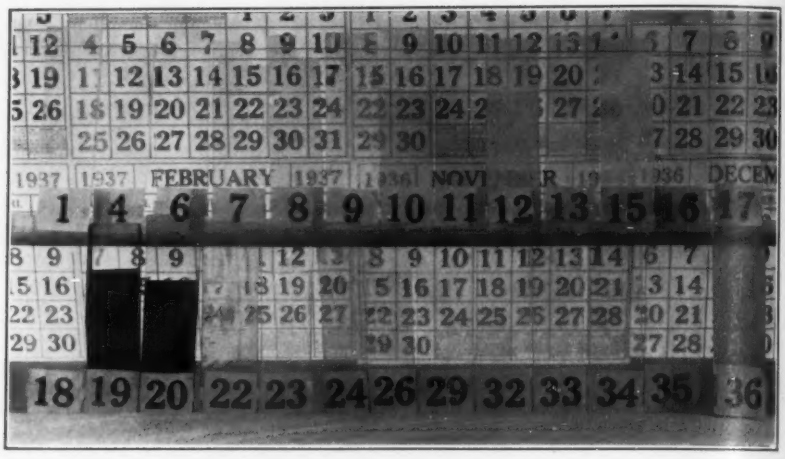

FIGURE 12.—*Condition of samples after exposure to carbon-arc light for 500 hours without water spray*

Identification number	Material	Sample	Identification number	Material	Sample
1	Cellulose acetate	*A1*	19	Vinyl chloride-acetate resin.	*L1*
4	do	*B1*	20	do	*L2*
6	do	*B3*	22	Vinyl acetal resin	*M1*
7	do	*C1*	23	Cellulose acetobutyrate	*S1*
8	do	*C3*	24	Vinyl acetal resin	*N1*
9	do	*D1*	26	Glyceryl-phthalate resin	*O1*
10	Cellulose nitrate	*E1*	29	Cellulose acetate	*B6*
11	do	*F1*	32	do	*B9*
12	Ethylcellulose	*G1*	33	do	*B4*
13	do	*H1*	34	do	*B5*
15	Acrylate resin	*J1*	35	Acrylate resin	*K3*
16	do	*J2*	36	Glyceryl-phthalate resin	*T1*
17	do	*K1*			
18	do	*K2*			

the water spray was employed. The data for light transmission after 500 hours of exposure, shown in tables 9 and 10, indicate that the cellulose nitrate and vinyl chloride-acetate resin samples are deteriorated more rapidly in the drier and warmer condition. Figure 12 shows the condition of the specimens after 500 hours of exposure. The unexposed portion is at the top of each specimen in the photograph. Sample *J1*, an acrylate resin, was quite markedly affected by the higher temperature, and became translucent because of surface roughening.

TABLE 10.—*Accelerated aging of transparent plastics by carbon-arc light without water spray*

Material	Sample	White-light transmission		Haze value		Remarks on condition at 500 hr
		Initial	500 hr	Initial	500 hr	
		Percent	*Percent*	*Percent*	*Percent*	
Cellulose acetate	*A1*	89.2	90.8	3.8	4.4	Surface slightly roughened.
Do	*B1*	91.5	91.8	7.4	8.4	No marked change.
Do	*B3*	91.7	91.9	3.6	4.0	Surface slightly roughened.
Do	*B4*	89.1	87.6	4.5	5.5	Do.
Do	*B5*	88.3	87.0	4.4	5.0	Surface slightly roughened; discolored yellow.
Do	*B6*	91.3	91.8	3.2	4.0	Surface slightly roughened.
Do	*B8*	90.6	90.8	3.8	4.1	Do.
Do	*C1*	88.5	90.2	6.0	6.0	Do.
Do	*C3*	82.3	84.3	10.0	10.0	Do.
Do	*D1*	77.4	86.6	7.0	9.3	Blue dye faded; cracked.
Cellulose acetobutyrate	*S1*	92.8	91.8	5.5	4.1	Warped; no marked change.
Cellulose nitrate	*E1*	91.7	81.4	3.8	6.9	Discolored brown; cracked.
Do	*F1*	85.2	73.2	3.6	4.1	Discolored brown.
Ethylcellulose	*G1*	82.7	83.1	26.6	29.6	Cracked badly and discolored.
Do	*H1*	85.6	84.4	9.9	10.2	No marked change.
Do	*I1*	91.4	90.6	6.1	(a)	Cracked badly and became friable.
Acrylate resin	*J1*	93.7	93.7	6.1	10.6	Surface badly pebbled.
Do	*J2*	93.7	93.3	b 6.1	b 4.7	No marked change.
Do	*K1*	94.0	93.1	3.6	3.5	Slightly yellowed.
Do	*K2*	94.4	94.3	1.4	1.9	No marked change.
Do	*K5*	94.2	93.8	1.6	1.4	Do.
Vinyl chloride-acetate resin	*L1*	82.6	ca. 0	5.0	--------	Opaque; discolored purple.
Do	*L2*	80.3	ca. 0	8.7	--------	Do.
Vinyl acetal resin	*M1*	88.7	85.5	3.9	7.8	Discolored yellow.
Do	*N1*	85.6	83.0	9.5	10.8	Surface roughened; discolored yellow.
Glyceryl-phthalate resin	*O1*	85.8	81.0	5.2	5.8	Discolored brown.
Do	*T1*	66.2	65.0	(a)	(a)	Discolored yellow.

[a] Specimen broke before these values could be determined.
[b] Specimen slightly prismatic, making haze measurement doubtful.
[c] Surfaces of specimen unpolished.

The haze values in tables 7 and 10 show that the results of the accelerated test do not indicate the same relative order of stability as is found upon exposure out-of-doors. The two cellulose nitrate samples became clouded at about the same rate on the roof, whereas *E1* broke down more rapidly than *F1* in the accelerated test. Similar discrepancies are noted for the ethylcellulose and vinyl acetal resins. The amount of discoloration of the samples by the carbon-arc light can be judged from the data in table 11 for light transmission using various color filters. There was a considerable drop in the light transmitted,

using the green and blue filters, for the cellulose nitrate samples and the glyceryl-phthalate resin *O1*. A slight drop was also noted for acrylate resin *K1*. On the other hand, the light transmission, using the green filter, showed a marked increase after 500 hours of exposure to ultraviolet light for those samples which contained blue dye, notably for cellulose acetate *D1*.

TABLE 11.—*Effect of accelerated aging of transparent plastics by carbon-arc light without water spray on light transmission using various color filters*

Material	Sample	Color transmission					
		Red filter [a]		Green filter [b]		Blue filter [c]	
		Initial	500 hr	Initial	500 hr	Initial	500 hr
		Percent	*Percent*	*Percent*	*Percent*	*Percent*	*Percent*
Cellulose acetate	*A1*	91.3	91.6	87.3	89.5	89.4	90.6
Do	*B1*	91.7	92.1	89.3	90.5	89.8	91.2
Do	*B3*	92.3	92.2	90.2	90.8	90.0	91.4
Do	*B4*	89.1	88.8	86.2	85.7	86.2	86.6
Do	*B5*	89.6	88.7	87.0	84.7	87.4	85.6
Do	*B6*	92.1	92.1	89.8	90.6	89.6	91.4
Do	*B8*	91.1	91.3	91.4	89.2	89.0	90.2
Do	*C1*	90.6	91.2	86.3	88.5	87.8	89.6
Do	*C3*	86.7	87.5	78.7	81.3	81.8	84.4
Do	*D1*	84.9	88.2	75.7	84.0	82.6	84.6
Cellulose acetobutyrate	*S1*	92.8	91.8	91.2	90.7	91.4	90.6
Cellulose nitrate	*E1*	92.0	90.7	89.8	74.2	89.4	72.0
Do	*F1*	83.8	82.8	84.9	66.7	85.8	65.6
Ethylcellulose	*G1*	86.1	86.2	78.2	80.3	76.6	80.8
Do	*H1*	86.7	86.0	82.7	82.6	81.6	82.4
Do	*I1*	92.2	[d]	89.7	[d]	89.6	[d]
Acrylate resin	*J1*	93.3	92.9	92.3	92.7	92.8	92.8
Do	*J2*	93.5	93.2	92.4	92.3	92.4	92.4
Do	*K1*	93.2	93.3	92.6	91.7	92.6	91.4
Do	*K2*	93.9	93.7	93.0	93.4	93.4	93.4
Do	*K5*	93.7	93.3	93.0	92.7	93.2	92.6
Vinyl chloride-acetate resin	*L1*	87.5	ca. 0	83.8	ca. 0	87.2	ca. 0
Do	*L2*	86.3	ca. 0	77.3	ca. 0	79.2	ca. 0
Vinyl acetal resin	*M1*	89.3	88.3	86.2	82.3	85.6	80.4
Do	*N1*	86.8	85.7	82.4	80.3	81.4	78.6
Glyceryl-phthalate resin	*O1*	88.5	86.6	81.2	74.8	80.6	76.4
Do	*T1*	69.3	70.3	57.2	58.8	62.4	63.0

[a] Pyrometer red filter.
[b] No. 61 Wratten filter.
[c] No. 47 Wratten filter.
[d] Specimen broke before these values could be determined.

VII. SCRATCH RESISTANCE

The comparative ease with which transparent organic plastics are scratched is a major obstacle to their substitution for glass in many applications where their toughness and nonsplintering characteristics would be advantageous. However, the plastics vary considerably in scratch resistance, and it is desirable to have a method of measuring this property. The effect of tumbling with sand of a standard grade was tried, but after a short period a polishing action produced by fine fragments tended to undo the action of the coarse grains of sand. Furthermore, it was very difficult to remove the fine dust from the samples preparatory to determining the amount of abrasion by measuring the light transmission.

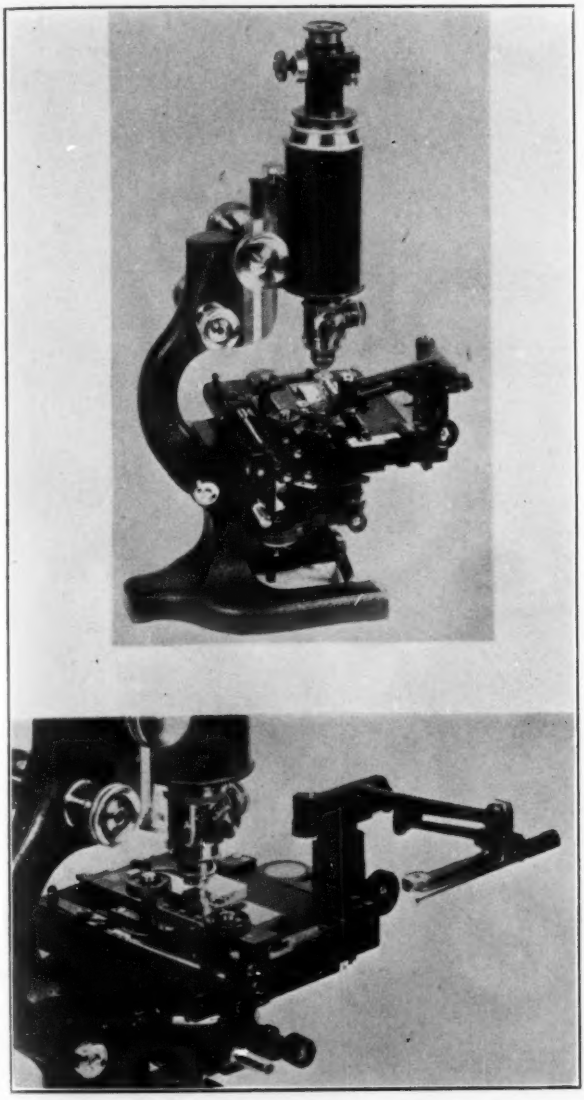

FIGURE 13.—*Bierbaum scratch-resistance apparatus.*

Above: Diamond tool in scratching position.
Below: Diamond tool swung aside and microscope in position to measure scratch width.

UNIV. OF MICH.

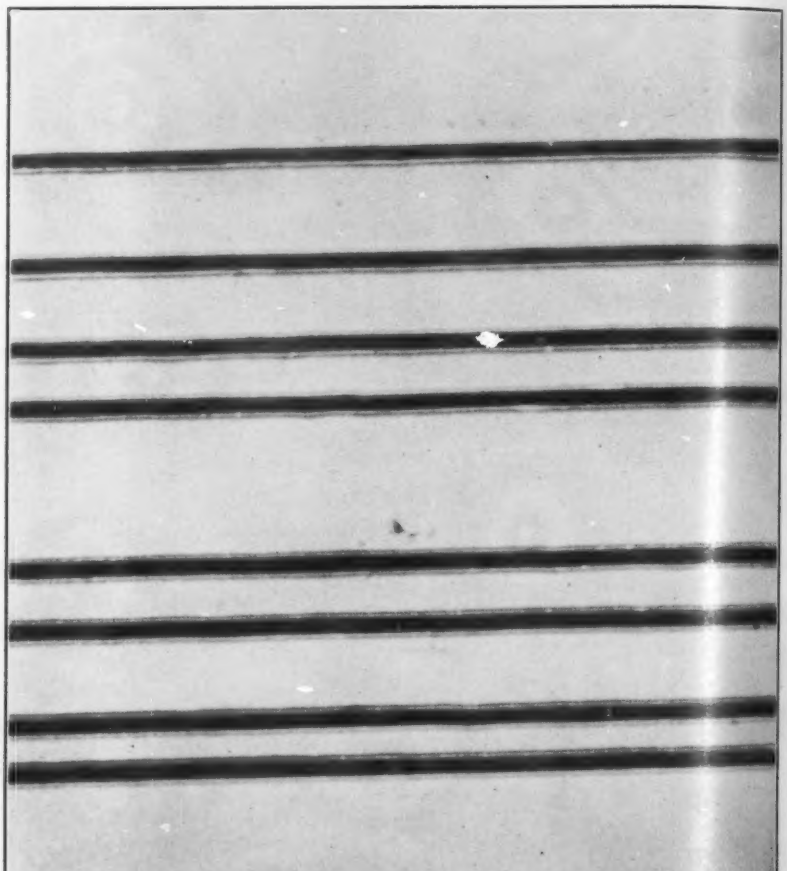

FIGURE 14.—*Scratches on cellulose acetate plastic* ($\times 150$).

These difficulties are avoided when a sclerometer is used to produce a band of scratches from which the relative resistance of the material can be judged by determining the average width of the scratches. Various types of sclerometers have been developed for use in making scratch tests on metals. These are discussed in detail by O'Neill.[1]

1. DESCRIPTION OF APPARATUS

The instrument used in this work on plastics was developed by Bierbaum and is called the Microcharacter (fig. 13). The cutting diamond is in the form of a corner of a cube, mounted so that the diagonal of the cube is normal to the test surface and one edge is in line with the direction of the scratch. The diamond is suspended from a balanced arm pivoted on sapphire bearings. One end of the arm is provided with a spirit level and the other with a 3-gram weight which constitutes the standard load for the diamond point. The diamond is mounted at the small end of a tapered steel spring; the other end of the spring is fastened to the lower side of the suspension area. A vertical rack is provided for raising and lowering the bracket that carries the cutting tool. This bracket is attached to a microscope mechanical stage provided with suitable clamps and screw mechanism to permit the specimen to be moved slowly under the diamond point. The width of the scratch (fig. 14) is measured with a microscope having a calibrated filar micrometer eyepiece. The plastics were conditioned at 21° C and 65-percent relative humidity for at least 24 hours, and the test was conducted under these conditions. The scratch resistance is defined as the quotient of the load in kilograms divided by the square of the scratch width in millimeters.

2. RESULTS OF SCRATCH-WIDTH MEASUREMENTS

The data obtained with the Bierbaum Microcharacter on various plastics are shown in table 12. Each value is the average of 15 measurements on 5 scratches, each scratch being measured at 3 points. The speed of the diamond point was approximately 0.2 mm/sec. To determine whether or not a material was anisotropic, two bands of scratches at right angles to each other were ruled on the specimen. A few cellulose acetates, notably samples *A3*, *B5*, and *C3* give some indication of anisotropism. The results show that most of the materials are isotropic as far as scratch resistance is concerned.

The scratch resistance of cellulose acetate varied with the products of different manufacturers, presumably because of differences in types and amounts of plasticizer present. The acrylate resins were the most resistant to scratching of the materials studied.

[1] H. O'Neill, Hardness of Metals and Its Measurement (Sherwood Press, Cleveland, 1934).

TABLE 12.—*Scratch resistance of transparent plastics measured with the Bierbaum Microcharacter*

Material	Sample	Thickness	Scratch resistance [a]		
			Scratches ruled parallel to length of sample	Scratches ruled perpendicular to length of sample	Average
		Mils	kg/mm²	kg/mm²	kg/mm²
Cellulose acetate	*A1*	62	9.9	9.9	9.9
Do	*A2*	90	11.9	11.8	11.9
Do	*A3*	125	11.1	9.2	10.2
Do	*B1*	60	8.3	8.1	8.2
Do	*B3*	60	8.2	8.1	8.2
Do	*B4*	100	9.3	9.2	9.3
Do	*B5*	100	5.6	6.9	6.3
Do	*B6*	60	7.3	7.9	7.6
Do	*C1*	60	7.6	7.1	7.4
Do	*C2*	90	8.1	7.0	7.6
Do	*C3*	125	7.7	7.3	7.5
Do	*D1*	150	5.7	5.0	5.4
Cellulose acetobutyrate	*S1*	40	4.5	4.5	4.5
Cellulose nitrate	*E1*	60	10.0	9.9	10.0
Do	*F1*	62	10.3	9.9	10.1
Ethylcellulose	*G1*	60	5.6	5.5	5.6
Do	*H1*	30	6.3	6.2	6.3
Do	*I1*	40	4.0	4.5	4.3
Acrylate resin	*J1*	70	15.0	15.0	15.0
Do	*J2*	65	18.4	18.1	18.3
Do	*K1*	120	15.1	14.9	15.0
Do	*K5*	120	16.8	16.4	16.6
Vinyl chloride-acetate resin	*L1*	50	10.3	10.1	10.2
Do	*L2*	100	9.8	9.6	9.7
Do	*L3*	100	10.7	10.6	10.7
Vinyl acetal resin	*N1*	100	7.0	7.0	7.0
Glyceryl-phthalate resin	*O1*	125	14.0	----------	14.0
Styrene	*R1*	80	10.6	10.4	10.5

[a] Scratch resistance is defined as the quotient of the load in kilograms divided by the square of the scratch width in millimeters.

A value of 14.8 for the scratch resistance of acrylate resin sample *K1* was obtained when a 6-gram load on the diamond point was used. Comparison of this value measured with a 6-gram load with the one in table 12 obtained with a 3-gram load, namely, 15.0, shows that the calculated scratch resistance value is substantially independent of the load used. This would be expected to be true, since the diamond tool is of such shape that the scratches made with different loads are geometrically similar. The widths of the microcuts obtained with the 3- and 6-gram loads for this acrylate resin were, respectively, 14.2 and 20.3 microns.

VIII. INDENTATION HARDNESS

A number of instruments for measuring indentation hardness previously developed for use with metals have been applied to the determination of the so-called hardness of plastics, including the Brinell, Martens, Rockwell, Vickers, and Shore machines. Table 13 presents the results of measurements made on unconditioned samples of plastics with some of these instruments. There is relatively good agree-

FIGURE 15.—*Vickers hardness testing machine.*

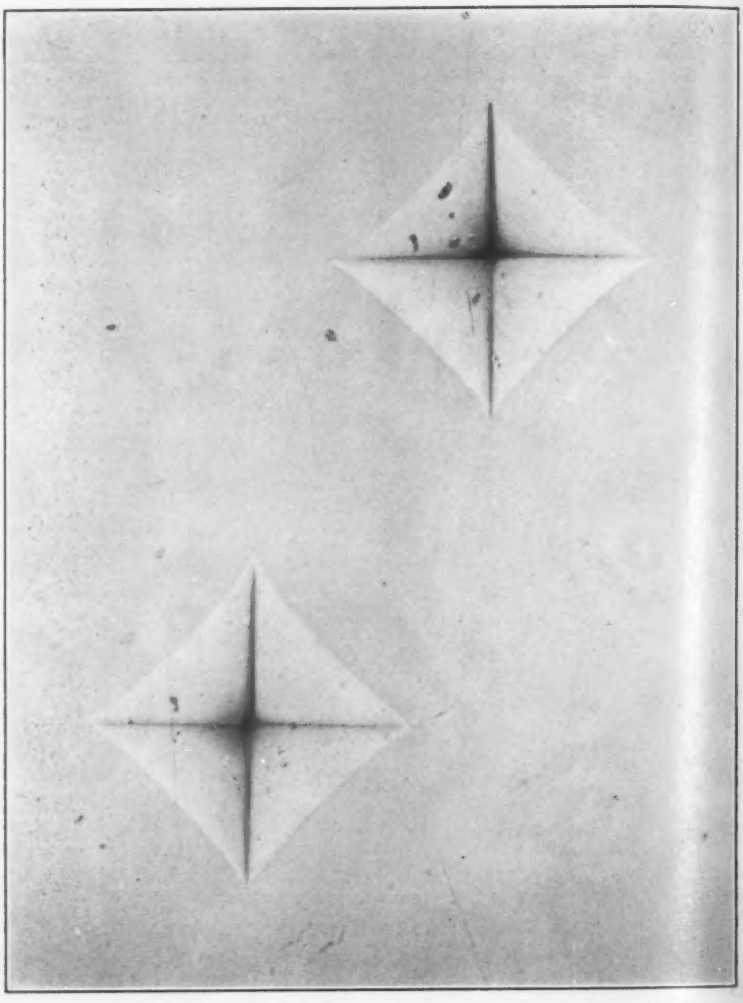

FIGURE 16.—*Pyramidal indentations on vinyl resin plastic* (×70).

ment between the degrees of hardness indicated by the Vickers, Rockwell, and Brinell machines. The Shore scleroscope is not considered very satisfactory because the hardness values indicated for the plastics were all much higher than those for a mild-steel specimen, the Brinell hardness of which was about 10 times that of the plastics. The data in the last two columns in table 13 show the effect of time of application of the load on the hardness values obtained. The relatively soft plastics undergo very little increase in indentation after 30 seconds loading time, but for the materials above Brinell number 15 a considerable effect on the area of the indentation is noted.

TABLE 13.—*Hardness of transparent plastics as measured by various instruments*

Material	Sample	Thickness	Shore scleroscope number [a]	Vickers number [b]	Rockwell number [c] (15-T scale)	Brinell number [d] (30 sec)	Brinell number [e] (3 min)
		Mils					
Cellulose acetate	*A1*	62	57	8.7	15.1	13.0	12.4
Do	*B1*	60	58	11.0	16.2	13.1	12.6
Do	*B2*	90	61	8.4	16.0	13.9	12.3
Do	*C1*	60	53	7.0	9.9	11.5	11.4
Do	*C3*	125	54	6.2	11.2	10.9	11.0
Cellulose nitrate	*E1*	60	63	12.7	29.7	16.6	15.8
Do	*F1*	62	60	11.7	23.2	15.8	15.0
Ethylcellulose	*G1*	60	50	6.3	7.7	10.6	10.6
Acrylate resin	*J1*	70	73	18.4	30.5	17.5	14.7
Do	*J2*	65	84	24.0	81.6	27.4	20.9
Do	*K1*	120	75	15.0	31.5	16.0	14.5
Vinyl chloride-acetate resin	*L1*	50	62	16.2	32.7	16.4	14.0
Vinyl acetal resin	*M1*	63	45	3.0	[f]	[f]	[f]
Styrene resin	*R1*	80	65	20.0	65.0	20.0	16.4
Phenol-formaldehyde resin	*U1*	125	80	12.6	15.5	15.8	15.3
Plate glass	*X1*	85	121				
Mild steel		1,000	25	[g] 159		[h] 159	

[a] Rebound, measured on an arbitrary scale of 140, of a hammer with a diamond striking point falling freely from a height of approximately ¾ inch; model D instrument.
[b] 5-kg load applied on a diamond pyramid for 7 seconds.
[c] 15-kg load applied on a ball of ⅛ inch diameter for 30 seconds; Rockwell superficial hardness tester.
[d] 15-kg load applied on a ball of ⅛ inch diameter for 30 seconds (usual Brinell time).
[e] 15-kg load applied on a ball of ⅛ inch diameter for 3 minutes.
[f] Too soft to measure.
[g] 50-kg load.
[h] 3,000-kg load on a ball of 10 mm diameter.

The Vickers hardness-testing machine (fig. 15) was used for making a more detailed study of indentation hardness of plastics. The indenting tool in this instrument is a diamond in the form of a square pyramid, having an angle between opposite faces of 136°, the value obtained therewith being substantially independent of the testing load. The lengths of the diagonals of the indentation (fig. 16) made with this tool are more readily measured than the diameter of the indentation made by a spherical tool. A load of 5 kilograms was used. The machine is so constructed that the load is applied slowly and progressively to the test specimen, remains for a given time, and is then automatically removed. The lengths of the diagonals of the indentation are measured by means of a micrometer ocular in the microscope attached to the apparatus. The Vickers hardness number is the quotient of the applied load, in kilograms, divided by the pyramidal area of the impression in square millimeters. The plastics

were conditioned at 21° C and 65-percent relative humidity for not less than 24 hours prior to testing.

The effects of variations in the time of application of full load on the values obtained for Vickers hardness numbers are shown in table 14. The time was found to be an important factor in this test as in the Brinell test. A more detailed study of the Vickers hardness of the transparent plastics was made on the same samples used for the scratch resistance test. A full load time of 10 seconds was selected. The values obtained are shown in table 15. Each value given in tables 14 and 15 is the average of four determinations. Lack of uniformity in the sheet is believed to be responsible in large part for the differences noted for the indentation hardness of a given plastic sample in the two tables.

TABLE 14.—*Variation of Vickers hardness number with time of loading*

Material	Sample	Vickers number		
		5-kg load applied for 10 seconds	5-kg load applied for 30 seconds	5-kg load applied for 90 seconds
Cellulose acetate	*A1*	6.3	5.8	5.9
Do	*B1*	7.2	6.7	6.7
Do	*B2*	6.8	6.3	6.3
Do	*C1*	5.6	5.2	4.8
Do	*C3*	5.2	4.6	4.2
Cellulose nitrate	*E1*	11.7	11.2	10.5
Do	*F1*	10.5	10.4	9.3
Ethylcellulose	*G1*	5.2	4.9	4.8
Acrylate resin	*J1*	14.0	12.1	11.2
Do	*J2*	18.9	17.2	15.4
Do	*K1*	14.1	12.7	11.3
Vinyl chloride-acetate resin	*L1*	14.9	14.7	13.4
Styrene	*R1*	20.1	18.7	16.6
Phenol-formaldehyde	*U1*	13.0	11.3	9.3

TABLE 15.—*Vickers indentation hardness numbers of various transparent plastics*

(Samples conditioned at 21° C and 65-percent relative humidity; 5-kg load applied for 10 seconds.)

Material	Sample	Thickness	Vickers number
		Mils	
Cellulose acetate	*A1*	62	6.9
Do	*A2*	90	7.7
Do	*A3*	125	7.1
Do	*B1*	60	7.9
Do	*B2*	90	6.6
Do	*B3*	60	6.8
Do	*B4*	60	7.0
Do	*B5*	60	4.3
Do	*B6*	60	6.2
Do	*B9*	60	6.6
Do	*C1*	60	5.6
Do	*C2*	90	5.5
Do	*C3*	125	5.2
Do	*D1*	150	7.0
Cellulose acetobutyrate	*S1*	40	4.8
Cellulose nitrate	*E1*	60	11.6
Do	*F1*	62	10.5
Ethylcellulose	*G1*	60	5.6
Do	*H1*	30	8.0
Do	*I1*	40	4.6
Acrylate resin	*J1*	70	15.4
Do	*J2*	65	19.2
Do	*K1*	120	13.6
Do	*K6*	120	16.7
Vinyl chloride-acetate resin	*L1*	50	15.3
Do	*L2*	100	15.0
Do	*L3*	100	15.0
Vinyl acetal resin	*M1*	63	ca. 0.5
Do	*N1*	100	11.0
Glyceryl-phthalate resin	*O1*	125	27.1
Styrene resin	*R1*	80	19.8
Phenol-formaldehyde resin	*U1*	125	13.0

The glyceryl-phthalate resin was the most resistant to indentation of the materials tested; the cellulose derivatives were indented more readily than the resins with the exception of the vinyl acetal sheets, one of which was very soft. Some evidence was also obtained in measurements of the indentation diagonals that a few of the cellulose acetate sheets were anisotropic, but the variations in the two directions were not large enough to warrant reporting in detail.

It is interesting to compare the Vickers hardness numbers in table 15 with the scratch-resistance data in table 12. Good correlation is evident for the cellulose nitrate, ethylcellulose, and acrylate resin plastics. However, the scratch resistance values for the vinyl and styrene resins are much lower than the indentation values, and for the cellulose acetate samples, the two coefficients are not similar. It is, therefore, believed to be impractical to substitute the better-known and more-rapid indentation-hardness measurement for scratch-resistance data obtained with a sclerometer.

IX. IMPACT STRENGTH

1. CHARPY TEST

The resistance of the transparent plastics to impact was determined with a Charpy impact machine and by a falling-ball method. For the Charpy tests, two sets of notched specimens 0.5 by 2.5 inches were

prepared. The notch, located at the center of the specimen, was 0.1 inch deep and was produced with an ordinary 60° triangular file. One set was tested for impact strength at 70° F and the other at about 25° F. The samples were broken individually and not as a composite specimen. The capacity of the Charpy machine (fig. 17) was 2.9 ft lb, while its striking velocity was about 8 ft/sec. The results of these tests are shown in table 16. The cellulose nitrate, cellulose acetate, ethylcellulose and vinyl acetal samples have relatively high impact strength at 70° F, whereas the vinyl chloride-acetate and acrylate resins were relatively weak. At 70° F the cellulose acetate samples gave impact values of 1.9 to 3.6 ft lb/in. of notch, whereas at 25° F the strength varied from 0.25 to 1.5 ft lb/in. of notch; the comparable figures for cellulose nitrate were 3.8 to 4.4 at 70° F and 2.1 to 2.6 at 25° F, and for vinyl acetal resin were 2.9 at 70° F and 0.65 at 25° F. For the acrylate resins and ethylcellulose, the strength at 25° F was about 80 percent of the values observed at 70° F.

2. FALLING-BALL TEST

In tests made by the falling ball method to determine the impact resistance of the plastics, it was found to be impractical to use the 12- by 12-inch frame employed for testing laminated safety glass, in which the specimen is not clamped at the edge. In such a frame a cellulose acetate sample, 94 mils thick, failed only on the 24th impact of a ½ pound steel ball falling 65 feet. A nitrate specimen 65 mils thick pulled through the frame on the first impact. The following test procedure was, therefore, adopted. A steel ball weighing ½ pound was dropped from various heights on a disk 6½ inches in diameter held firmly between rubber gaskets in a metal frame (fig. 18) which had a circular opening 5½ inches in diameter. The test was continued until the sample was penetrated by the ball. The results are given in table 16. The cellulose plastics failed when the ball dropped 50 to 65 feet, some requiring several impacts from the latter height. All of the acrylate resin samples failed when the ball was dropped 10 feet. The vinyl chloride-acetate resin samples failed at 8 feet, whereas a vinyl acetal resin now being developed particularly for safety-glass construction broke only after an average of 11½ impacts with the steel ball from 65 feet.

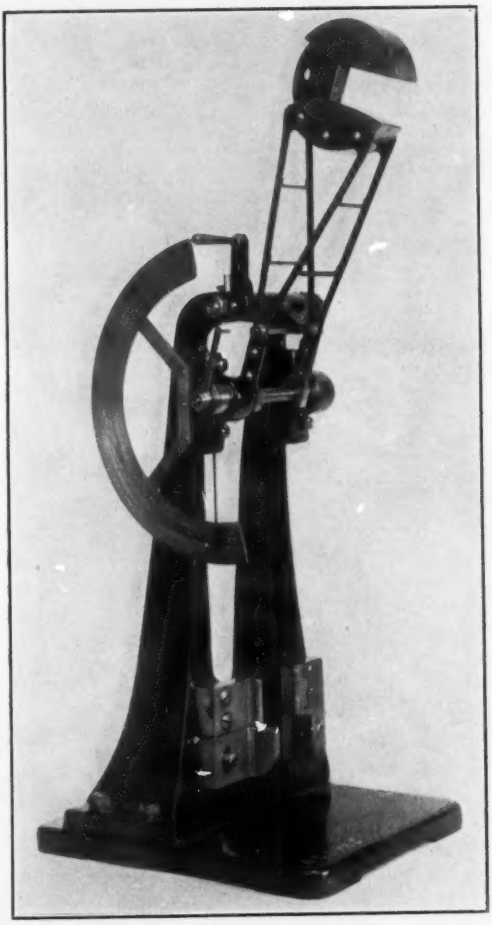

FIGURE 17.—*Apparatus for determining Charpy impact strength.*

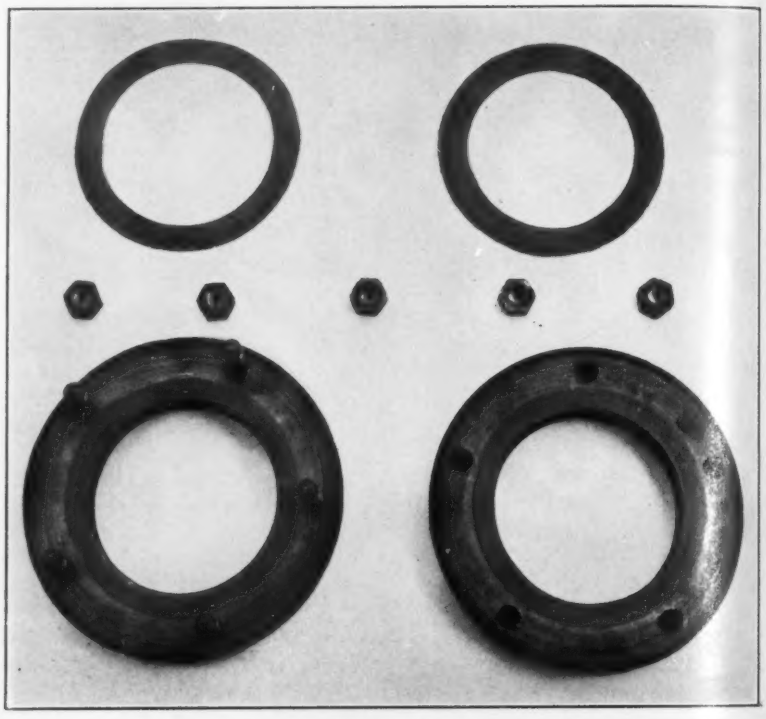

FIGURE 18.—*Frame used to hold plastics in the falling-ball impact test.*

TABLE 16.—*Charpy and dropped-ball impact tests on transparent plastics*

Material	Sample	Thickness	Charpy impact strength (notched)		Ball impact strength	
			70° F	25° F	Ball height	Average number of balls required for failure
		Mils	ft lb/in. of notch	ft lb/in. of notch	ft	
Cellulose acetate	*A1*	65	2.8	0.51	65	2.5
Do	*A2*	96	3.2	.37	50	7
Do	*A3*	135	2.1	.25	50	9
Do	*B2*	94	1.9	.33	65	6
Do	*B4*	98	3.0	1.51	65	2.5
Do	*B5*	100	3.6	1.33	65	10
Do	*B6*	67	2.7	0.89	65	1
Do	*B7*	95	2.4	1.16	65	6
Do	*B9*	92	2.3	0.29	65	5
Do	*C1*	57	2.8	1.02	65	3
Do	*C3*	125	2.4	0.84	65	9
Do	*D1*	165	2.3	.30	50	6
Cellulose nitrate	*E1*	66	3.8	2.13	65	4
Do	*F1*	63	4.4	2.60	65	4.5
Ethylcellulose	*G1*	59	3.1	2.49	----	----
Acrylate resin	*K1*	117	0.46	0.33	3	2
Do	*K4*	88	.45	.26	----	----
Do	*K7*	222	.44	.37	10	2
Do	*K8*	218	.40	.36	10	3
Vinyl chloride-acetate resin	*L3*	102	.4	.15	8	2
Vinyl acetal resin	*N1*	122	2.9	.65	65	11.5

In order to determine the effect of impacts of a comparatively inelastic body on the plastic, a tennis ball partially filled with 1 pound of shot was used in a series of tests. Results of tests on a few cellulose acetate samples indicate that a given sample will withstand three times as many impacts from this type of falling body as from a ½-pound steel ball.

X. SHRINKAGE

The shrinkage which transparent plastics undergo in service is an important factor in their durability. Excessive shrinkage causes buckling and in some cases cracking of the plastic sheet.

The shrinkage of transparent plastics occurring during exposure on the roof and also as a result of accelerated aging was studied. Specimens approximately 11 by 1 inch were conditioned at 21° C and 65-percent relative humidity and gage lengths of 10 inches were marked off. One set of samples was placed on an exposure rack on the roof, while a second set was subjected to accelerated aging at 70° C in an oven in which the air was circulated. After various periods the samples were removed to the conditioning room for 24 hours and the change in length was measured. The results are presented in tables 17 and 18.

TABLE 17.—*Accelerated shrinkage tests at 70° C of transparent plastics*

Material	Sample	Thickness	Decrease in length			
			4 days	2 weeks	1 month	2 months
		Mils	*Percent*	*Percent*	*Percent*	*Percent*
Cellulose acetate	*A3*	133	0.9	1.0	1.3	2.2
Do	*A1*	64	1.2	1.5	1.6	3.4
Do	*A2*	95	1.0	1.1	1.5	[b]
Do	*B2*	93	1.0	1.1	1.3	2.0
Do	*B3*	64	[a] 1.3	2.1		
Do	*B4*	96	1.1	1.5	1.8	1.7
Do	*B5*	100	2.0	3.5	4.2	4.8
Do	*B6*	66	1.7	2.0	2.5	3.1
Do	*B9*	89	1.4	1.8	2.2	2.3
Do	*B10*	63	1.1	1.6	2.2	2.4
Do	*B11*	64	1.0	1.6	2.2	2.5
Do	*B12*	61	0.8	1.1	1.2	1.2
Do	*C3*	125	.9	1.0	1.3	1.9
Do	*D1*	169	1.1	1.4	1.5	2.3
Cellulose acetobutyrate	*S1*	41	2.5	3.1	3.5	4.0
Cellulose nitrate	*E1*	67	0.4	0.4	0.6	1.1
Do	*F1*	64	.5	.5	.7	[c] 0.9
Ethylcellulose	*G1*	53	1.2	1.5	1.9	2.4
Do	*H1*	29	0.4	0.5		
Do	*I1*	38	.5	.6	0.8	2.5
Acrylate resin	*J1*	66	2.2	[b]	[b]	[b]
Do	*J2*	76	0.2	0.2	0.2	0.7
Do	*K1*	124	2.0	2.0	2.0	
Do	*K2*	88	1.8	1.8	1.8	2.0
Do	*K3*	71	1.5	1.6	1.7	1.7
Do	*K5*	118	0.2	0.3	0.3	
Do	*K9*	60	[a] 1.9	1.9		
Vinyl chloride-acetate resin	*L1*	64	4.2	4.3	4.6	3.2
Vinyl acetal resin	*M1*	63	0.2	0.8	1.0	1.5
Do	*N1*	127	[c] .4	[c] .6	[c] 0.6	[c] 0.9
Glyceryl-phthalate resin	*O1*	162	.1	.1	.1	.1
Do	*T1*	290	.7	.7	.7	.7
Phenol-formaldehyde resin	*U1*	170	1.0	1.4	1.6	1.9

[a] 3 days. [b] Warped. [c] Increase in length.

TABLE 18.—*Outdoor shrinkage tests of transparent plastics*

Material	Sample	Decrease in length					
		1 month	2 months	3 months	6 months	9 months	1 year
		Percent	*Percent*	*Percent*	*Percent*	*Percent*	*Percent*
Cellulose acetate	*A1*	1.3	1.8	2.5	2.7	3.1	3.4
Do	*A2*	0.5	0.6	1.1	1.1	1.4	1.3
Do	*A3*	.4	.6	0.9	1.0	1.1	1.1
Do	*B2*	.4	.4	.6	0.6	0.7	0.8
Do	*B6*	.8	1.2	1.6	1.8	2.1	2.3
Do	*C3*	.5	0.7	1.1	1.2	1.3	1.3
Do	*D1*	.6	.9	1.4	1.4	1.6	1.5
Cellulose acetobutyrate	*S1*	.5	.7	0.9	1.0	1.0	1.1
Cellulose nitrate	*E1*	.2	.3	.4	0.4	0.4	0.5
Do	*F1*	.2	.3	.4	.4	.5	.6
Ethylcellulose	*G1*	0.6	1.1	1.5	[a]	[a]	[a]
Do	*H1*	1.0	1.5	2.0	[a]	[a]	[a]
Do	*I1*	0.8	1.1	1.4	1.8	[a]	[a]
Acrylate resin	*J1*	.05	0.1	0.1	0.1	.1	.1
Do	*J2*	.0	.0	.0	.0	.0	.0
Do	*K1*	.0	.2	.2	.2	.2	.2
Do	*K2*	.06			.1	.1	.1
Do	*K6*	.0		.0	.05	.06	
Do	*K9*	.04	.1	.2	.2	.2	.2
Vinyl chloride-acetate resin	*L1*	.0	.0	.0	.0	.03	.03
Vinyl acetal resin	*N1*	.4	[a]	[a]	[a]	[a]	[a]
Glyceryl-phthalate resin	*O1*	.0			[b] .1	[b] .1	[b] .1
Do	*T1*	.0	.0	.0	.1	.1	.1
Phenol-formaldehyde resin	*U1*	.8	1.0	1.2	1.4	1.5	1.5

[a] Gage lines obliterated by deterioration of sample. [b] Increase in length.

When the shrinkage is accelerated by heating at 70° C, the decrease in length after 4 days is very nearly the same for many of the materials as that observed after 2 weeks in the oven. For cellulose acetate plastics, the shrinkage after 2 weeks was about 1 percent for 120-mil stock and 2 percent for the 60-mil material; after 2 months these values had increased to approximately 2 and 3 percent, respectively. The lowest shrinkage of all the cellulose acetate samples was undergone by sample *B12*, a 60-mil sheet, the change in length being 1.2 percent in 2 months. The two cellulose nitrate samples had decreased 0.5 percent in length in 2 weeks and 1 percent in 2 months. The acrylate resin plastics, which were first submitted, shrunk almost 2 percent in 2 weeks at 70° C and did not change appreciably thereafter. A later sample of this type of resin, identified as *K5*, which was given a final heat treatment by the manufacturer, shrunk approximately 0.3 percent in 2 weeks, after which no further change in the length was observed. A sample of unplasticized acrylate resin, *J2*, decreased in length only 0.2 percent in 2 weeks, but showed 0.7 percent shrinkage after 2 months. The greatest shrinkage during the 2 months of heating at 70° C occurred with a vinyl chloride-acetate resin; the decrease in length being 8.2 percent. A glyceryl-phthalate resin, *O1*, underwent the least shrinkage, namely, 0.1 percent; another sample of this resin, made by a different company, decreased 0.7 percent in length.

The degree of shrinkage of materials during outdoor exposure was somewhat different than under accelerated aging. In general, the outdoor shrinkage of the synthetic resins was small compared to that of the cellulose plastics. Reasonably good correlation was observed between the shrinkages for the various cellulose derivatives exposed on the roof and heated at 70° C in the oven. The cellulose acetate samples decreased in length from 0.8 to 3.4 percent in 1 year on the roof, whereas the same samples decreased 2.0 to 3.4 percent when heated for 2 months at 70° C. The cellulose nitrate samples averaged 0.55-percent shrinkage for 1 year on the roof and 1 percent for 2 months' heating at 70° C. The ethylcellulose plastics deteriorated rapidly on the roof, making measurements impossible after approximately 6 months. They had shrunk 2.0 percent at the end of 3 months on the roof compared with an average value of about 3 percent for the accelerated test. The acrylate resins had decreased in length only about 0.2 percent in 1 year on the roof; the heat-treated resin shrunk approximately 0.05 percent in 6 months. The greatest disparity between the natural and accelerated aging was noted in the case of the vinyl chloride-acetate resin, which, although it shrunk 8.2 percent in 2 months at 70° C, had decreased in length less than 0.05 percent after 1 year on the roof.

Presumably it would be possible to reduce the shrinkage of the cellulose plastics by heat treatment during the process of manufacture as was done for the acrylate resin sample *K5*. The impact strength of sample *K5* as measured on the Charpy apparatus was the same as that of the ordinary acrylate stock. As indicated in tables 12 and 15, the values of scratch resistance and indentation hardness are higher for the preshrunk than for the ordinary acrylate. Samples of ordinary cellulose acetate and cellulose nitrate were preshrunk by heating at 100° C for 4- and 24-hour periods. Impact measurements were made

at 21° C with the Charpy apparatus on both the untreated and heated materials. The decrease in length was also determined; the specimens used to measure shrinkage were placed on the roof to detect further shrinkage. The results are given in table 19. The impact strength of the cellulose acetate sample was decreased only 5 percent by heating for 4 hours; the same treatment halved the impact strength of the nitrate and caused it to discolor. It would seem, therefore that a method of heat treatment which would remove residual volatile solvent, the gradual loss of which may be in large part responsible for the shrinkage of the cellulose acetate plastics, would yield a much improved material for windshields.

TABLE 19.—*Effect of heating cellulosic plastics at 100° C on impact strength and shrinkage*

Material	Sample	Thickness	Charpy impact strength on notched specimen			Shrinkage	
			Original	After 4 hours at 100° C	After 24 hours at 100° C	After 4 hours at 100° C	After 24 hours at 100° C
		Mils	ft lb/in. of notch	ft lb/in. of notch	ft lb/in. of notch	*Percent*	*Percent*
Cellulose acetate	*C5*	92	1.9	1.8	1.4	2.0	3.2
Cellulose nitrate	*W1*	93	3.6	1.8	1.8	1.6	2.6

XI. RESISTANCE TO WATER, ALCOHOL, AND KEROSENE

Resistance to water and to various organic solvents with which it is likely to come in contact is an important property of a transparent plastic which is to be used as an airplane windshield. Data were, therefore, obtained as to the amount of water, alcohol, and kerosene absorbed by the various plastics when immersed in these liquids and also as to their effect on the condition of the surface and appearance of the samples. The results of these tests are presented in tables 20 to 22. It will be noted in table 20 that the absorption of water is particularly pronounced in the case of the cellulosic plastics, with the exception of cellulose acetobutyrate. Two of the three ethylcellulose samples became cloudy when exposed to water for 48 hours. This behavior would be very objectionable in a material for windshields. The resinous materials absorb very little moisture, with the exception of the vinyl acetal sample, *M1*, a vinyl acetate polymer which has been hydrolyzed and condensed with formaldehyde. This resin also becomes cloudy when wet and warps badly. The acrylate and vinyl resins are not affected by water.

As shown by the data in table 21, alcohol has a decidedly detrimental effect on all the transparent plastics studied, with the exception of the vinyl chloride-acetate resin and, therefore, should not be used for cleaning windshields.

TABLE 20.—*Water absorption by transparent plastics at 70° F*

Material	Sample	Thickness	Gain in weight			Remarks
			After 2 hr	After 24 hr	After 7 days	
		Mils	*Percent*	*Percent*	*Percent*	
Cellulose acetate	*A1*	66	0.63	2.39	3.25	
Do	*B1*	64	.59	2.02	2.40	
Do	*B3*	62	.52	1.82	2.19	
Do	*C1*	58	.68	2.10	2.08	
Do	*C3*	126	.38	1.32	----------	
Do	*D1*	165	----------	----------	3.34	
Cellulose nitrate	*E1*	66	.19	0.73	1.23	
Do	*F1*	63	.25	.88	1.33	
Cellulose acetobutyrate	*S1*	36	.43	.85	0.76	
Ethylcellulose	*G1*	58	.56	1.91	2.91	Cloudy at 48 hr.
Do	*H1*	29	3.25	8.71	9.32	
Do	*I1*	35	2.50	3.21	3.61	Slightly cloudy at 48 hr.
Acrylate resin	*J1*	79	0.05	0.21	0.51	
Do	*J2*	70	.06	.29	.79	
Do	*K1*	116	.04	.14	.43	
Do	*K2*	88	.07	.27	.40	
Vinyl chloride-acetate resin	*L1*	57	.02	.05	.07	
Do	*L2*	100	.01	.03	.04	
Vinyl acetal resin	*M1*	61	.59	2.45	5.70	Cloudy after 2 hr.

TABLE 21.—*Absorption of ethyl alcohol (95%) by transparent plastics at 70° F*

Material	Sample	Gain in weight			Remarks
		After 2 hr	After 24 hr	After 7 days	
		Percent	*Percent*	*Percent*	
Cellulose acetate	*A1*	4.08	15.72	10.68	Surface rippled; slightly cloudy.
Do	*B1*	2.41	10.72	6.64	Do.
Do	*B3*	2.95	12.57	7.34	Do.
Do	*C1*	3.13	11.14	4.85	Do.
Do	*C3*	1.49	6.58	7.91	Do.
Do	*D1*	1.52	6.84	14.99	Quite cloudy.
Cellulose nitrate	*E1*	3.21	36.5	----------	Surface roughened in 2 hr; swollen after 1 week.
Do	*F1*	4.98	----------	----------	Surface roughened in 2 hr; swollen after 24 hr.
Cellulose acetobutyrate	*S1*	6.43	6.02	3.79	No effect on appearance.
Ethylcellulose	*G1*	----------	----------	----------	Dissolves.
Do	*H1*	----------	----------	----------	Do.
Do	*I1*	----------	----------	----------	Do.
Acrylate resin	*J1*	0.22	8.51	16.49	Surface pitted.
Do	*J2*	−.02	9.67	9.65	Surface roughened.
Do	*K1*	.00	3.23	20.92	Surface roughened after 2 hr; smooth at 1 week.
Do	*K2*	10.15	86.90	----------	Softened in 2 hr; swollen after 1 week.
Vinyl chloride-acetate resin	*L1*	−0.01	−0.03	0.00	No attack.
Do	*L2*	−.01	−.01	.04	Do.
Vinyl acetal resin	*M1*	5.70	18.16	11.79	Milk-white and opaque at 1 week.

TABLE 22.—*Kerosene absorption by transparent plastics at 70° F*

Material	Sample	Gain in weight		
		After 2 hr	After 24 hr	After 7 days
		Percent	*Percent*	*Percent*
Cellulose acetate	*A1*	−0.12	−0.22	−0.38
Do	*B1*	.01	−.03	−.14
Do	*B3*	−.06	−.10	−.22
Do	*C1*	−.14	−.31	−.59
Do	*C3*	−.08	−.17	−.36
Do	*D1*	−.04	−.11	−.22
Cellulose acetobutyrate	*S1*	−.14	−.22	−.44
Cellulose nitrate	*E1*	.00	−.03	−.06
Do	*F1*	−.01	.00	−.04
Acrylate resin	*J1*	.00	−.01	−.05
Do	*J2*	.01	.01	−.09
Do	*K1*	−.02	−.04	−.09
Do	*K2*	.01	.01	.01
Vinyl chloride-acetate resin	*L1*	.00	.02	−.02
Do	*L2*	−.03	−.04	−.06
Ethylcellulose	*G1*	.09	.67	2.00
Do	*H1*	.42	1.82	5.04
Do	*I1*	3.82	15.24	20.12
Vinyl acetal resin	*M1*	0.00	−0.03	−0.08

The absorption of kerosene by all the plastics except ethylcellulose was negligible according to the results shown in table 22. The three samples of ethylcellulose differed markedly in their affinity for kerosene. However, no impairment of transparency or roughening of the surface on any of these samples was noted. Kerosene is, therefore, a very suitable reagent for cleaning the surfaces of plastic windshields. It was found to be very effective in removing, before proceeding with measurements of light transmission and haziness, a frosty-appearing layer which accumulated on the surface of some of the cellulose acetate samples used in exposure tests and which was not fully removed by washing with water.

XII. BURSTING STRENGTH

Tests of bursting strength were made on a few specimens of cellulose acetate, cellulose nitrate, and acrylate resin. Circular disks 7 inches in diameter of the various materials were cut out and conditioned at 21° C and 65-percent relative humidity. In the testing apparatus the specimen was held between steel clamping rings having an opening 5 inches in diameter. Hydraulic pressure from a hand pump was applied to one side of the disk and was increased until the disk was ruptured. The pressure to produce rupture was taken as a measure of the bursting strength. These tests were repeated with the specimen protected from the steel rings by rubber gaskets 1/16 inch thick.

All specimens except the acrylate resins were greatly deformed by the test, and assumed a dome-like appearance. The results are presented in table 23.

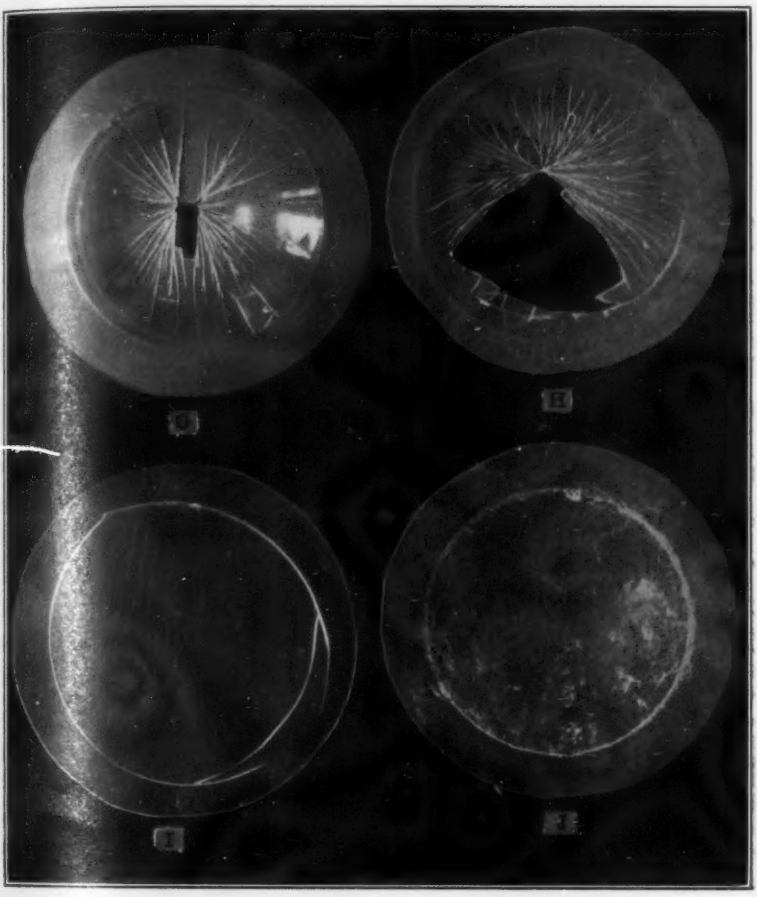

FIGURE 19.—*Samples of transparent plastics after bursting strength tests.*

G. Cellulose acetate burst at about 25° C.
H. Cellulose acetate burst when one surface was cooled with ethylene dichloride at −35° C.
I. Acrylate resin burst at about 25° C.
J. Acrylate resin burst when one surface was cooled with ethylene dichloride at −35° C.

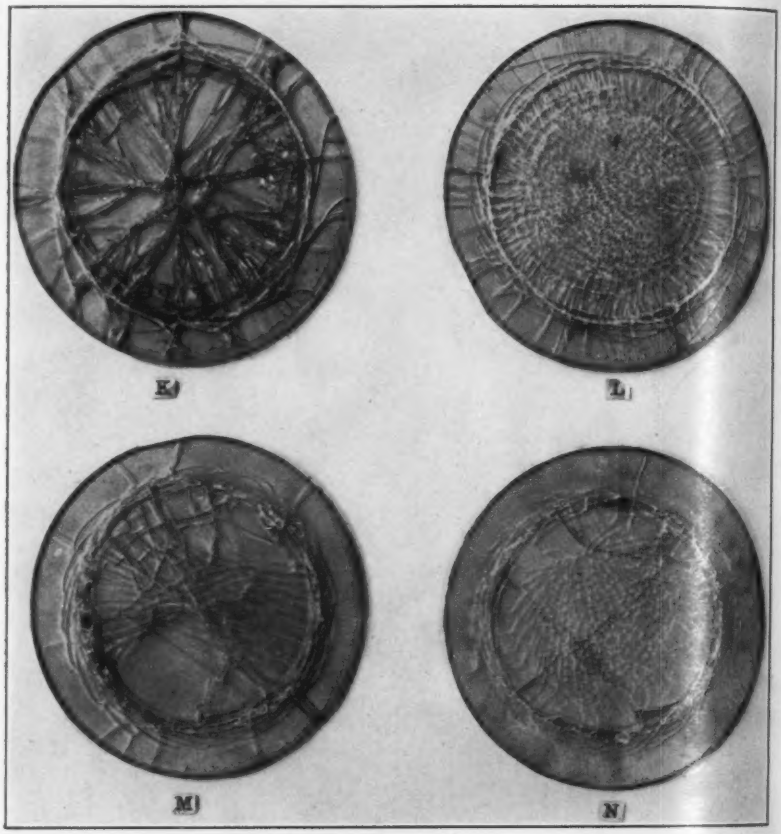

FIGURE 20.—*Samples of laminated glass after bursting strength tests.*

K. Glass bonded with cellulose nitrate plastic.
L. Glass bonded with cellulose acetate plastic.
M. Glass bonded with vinyl resin plastic.
N. Glass bonded with acrylate resin plastic.

TABLE 23.—*Bursting tests on 5-inch disks of transparent plastics at approximately 25° C*

A. WITHOUT RUBBER GASKETS

Material	Sample	Thickness	Bursting strength	Location of failure
		Mils	lb/in.²	
Cellulose acetate	*B2*	93	295	At clamping rings.
Do	*B3*	65	200	In center.
Do	*C1*	57	165	At clamping rings.
Do	*C3*	125	400	In center.
Cellulose nitrate	*W1*	93	375	At clamping rings.
Acrylate resin	*K5*	70	26	Do.
Do	*K10*	98	46	Do.
Vinyl acetal resin	*N1*	49	100	Pinhole developed between center and edge.
Do	*N1*	49	115	At clamping rings.

B. WITH RUBBER GASKETS

Cellulose acetate	*B2*	93	340	At clamping rings (slipped in grips).
Do	*C1*	56	190	In center.
Do	*C3*	125	430	Do.
Cellulose nitrate	*W1*	93	380	Do.
Acrylate resin	*K10*	97	44	Between clamping rings.
Do	*K11*	65	33	At clamping rings.
Do	*K11*	73	32	Do.
Do	*K12*	97	45	Do.
Do	*K12*	98	45	Do.
Do	*K13*	202	117	Do.
Do	*K13*	185	100	Do.

Figure 19 shows samples of cellulose acetate, *G*, and acrylate resin, *I*, after the bursting-strength determination. Without rubber gaskets most of the samples failed at the clamping rings. However, when protected by the rubber gaskets, only the acrylate resin and one cellulose acetate sample failed in this location. The other specimens failed in the center along radial lines. The gaskets had very little effect on the numercial value obtained for bursting strength.

The effect on the bursting strength of cooling one surface of the plastic to approximately −35° C was also determined. The cooling was accomplished by application of a mixture of solid carbon dioxide and an organic liquid to the outer surface and allowing the mixture to remain in contact with the plastic for 5 minutes before forcing water at room temperature against the opposite surface. The results of these tests are presented in table 24.

When kerosene or ethylene glycol was used as the cooling medium, the bursting strengths of the cellulose acetate and acrylate plastics were about the same as the values obtained at room temperature. Ethylene dichloride at −35° C had a deleterious effect on both cellulose acetate and acrylate resin and caused the bursting strengths to be much lower than were observed with kerosene and ethylene glycol.

Thus, one sample of an acrylate type of resin 0.2 inch thick failed at 100 to 117 lb/in.^{2} at room temperature, at 108 to 126 lb/in.^{2} at −35° C when cooled with the kerosene-carbon dioxide mixture, and at 64 lb/in.^{2} when ethylene dichloride was used as the cooling medium. Examination of the latter specimen revealed minute crazing of the cooled surface. Likewise, cellulose acetate approximately 0.1 inch thick, which failed at 350 lb/in.^{2} with the kerosene-carbon dioxide mixture, burst at 167 lb/in.^{2} when tested under similar conditions, except that ethylene dichloride was used in cooling the specimen. It is concluded that the spontaneous cracking of cellulose acetate windshields reported to occur on planes which have ascended to high altitudes, is due to loss in strength of the particular product because of poor aging characteristics rather than because of inherent weakness of the original cellulose acetate sheet.

TABLE 24.—*Bursting tests on 5-inch disks of transparent plastics cooled to approximately −35° C on outer surface*

A. WITHOUT RUBBER GASKETS

Material	Sample	Thickness	Cooling liquid applied on top surface	Bursting strength	Location of failure
		Mils		lb/in.^{2}	
Cellulose acetate	*B14*	107	Ethylene dichloride	167	In center.
Do	*B14*	107	Kerosene	350	In center and at rings.
Do	*C6*	127	do	370	In center.
Do	*C6*	127	Ethylene glycol	420	In center and at rings.
Acrylate resin	*K5*	73	Ethylene dichloride	(a)	At clamping rings; surface crazed.
Do	*K11*	65	Kerosene	33	At clamping rings.

B. WITH RUBBER GASKETS

Cellulose acetate	*B14*	107	Ethylene dichloride	180	At clamping rings.
Acrylate resin	*K7*	231	Kerosene	168	Do.
Do	*K7*	232	Ethylene glycol	142	Do.
Do	*K12*	97	Kerosene	51	Do.
Do	*K12*	97	do	58	Do.
Do	*K13*	199	do	126	Do.
Do	*K13*	201	do	108	Do.
Do	*K13*	192	Ethylene dichloride	64	In center and at clamping rings; surface crazed.

[a] Failed before appreciable load could be applied.

A few samples of laminated glass and plate glass were tested at 25° C in the same bursting-strength apparatus used for the plastic sheets. The results of these tests are presented in table 25, and the condition of the laminated-glass products after test is shown in figure 20. It will be noted that the bursting strengths of these materials are considerably less than those observed for the cellulose acetate plastic sheets.

TABLE 25.—*Bursting tests on 5-inch disks of laminated and plate glass*

Type of glass	Type of plastic lamination	Sample	Thickness	Bursting strength
			Mils	lb/in.²
Thin sheet safety	Acrylate	*Y1*	106	12
Sheet safety	Vinyl	*Z3*	117	19
Plate safety	Cellulose nitrate	*Z1*	196	33
Sheet safety	Cellulose acetate	*X6*	129	32
Thin plate	None	*X1*	83	12
¼-inch plate	do	*X4*	225	60

XIII. FLAMMABILITY

Two types of flammability tests for transparent plastic sheet were made on specimens 6 inches long and 0.5 inch wide. In one test, the specimen is suspended from a hook by a hole drilled ⅛ inch from one end and an alcohol flame is kept in contact with the bottom edge for 10 seconds. The time required for the sample to fall from the hook or for the flame to be extinguished is noted. A proposed specification required that the sample shall not fall from the hook or become completely enveloped in flames in less than 40 seconds from the time the flame is applied. In the second test, the sample is clamped at one end in a horizontal position longitudinally and at an angle of 45° to the horizontal laterally, ignited at the free end with an alcohol flame in contact with it for 10 seconds, and the time required to burn 3 inches or for the flame to be extinguished is determined. Army specification 94–12014–A for transparent sheet requires that the time for the flame front to travel 3 inches shall be not less than 1½ minutes.

The results of these tests are shown in table 26. It will be noted that for most of the materials two values are given. The first set of data was obtained after the specimens had been conditioned 24 to 48 hours at 21° C and 65-percent relative humidity, whereas the second set of specimens had been in the conditioning room for approximately 30 days when tested.

The second set of samples in general tended to be extinguished more quickly or burn at a slightly slower rate than those conditioned for the shorter time. The cellulose acetate, cellulose acetobutyrate, vinyl chloride-acetate resin, glyceryl-phthalate resin, and phenol-formaldehyde resin samples passed the above requirements for both the horizontal and vertical tests. Some of the acrylate resin strips were enveloped in flames in less than the 40 seconds specified for the vertical test, but this is a very difficult value to estimate. Only one acrylate specimen burned faster than the rate of 2 inches per minute allowed for the horizontal test. One vinyl acetal resin and the ethylcellulose samples, all of which were relatively thin materials, burned in the horizontal test at a somewhat greater rate than the 2 inches per minute. However, none of these plastics was found to approach the degree of flammability of cellulose nitrate, which burned at a rate of about 17 inches per minute when held in a horizontal position.

TABLE 26.—*Flammability tests on transparent plastics* [a]

Material	Sample	Thickness	Vertical test					Horizontal test		
			Self-extinguishing materials		Nonextinguishing materials			Self-extinguishing materials		Nonextinguishing materials
			Burning time of sample	Burning time of sample and drippings	Time at which sample was enveloped in flames	Time at which sample fell off hook	Total burning time of sample	Burning time of sample	Length of sample burned	Time for burning 3 inches of sample
		Mils	sec	sec	sec	sec	sec	sec	in.	sec
Cellulose acetate	*A1*	64	13					18	0.6	
			11					11		
Do	*A2*	94	12					12	.4	
			12					11		
Do	*A3*	131	12					23	.4	
			11					14		
Do	*B1*	63	16					24	.5	
			16					13	.5	
Do	*B2*	94	23					38		
			24					11		
Do	*B3*	65	19	49				24	.6	
			16					16		
Do	*B5*	100			45	65	120			237
					41	57	77			196
Do	*B13*	123	40					41	1.0	
			33					11		
Do	*C1*	54	18					23	0.7	
			26	41				75	1.8	
Do	*C2*	94	30					89	1.2	
			28	48						217
Do	*C3*	124	51	111				49	1.0	
			40	84				147	2.1	
Do	*D1*	150			80	79 82	229 169			171 199
Cellulose acetobutyrate	*S1*	40	11					17		
			14	41				18	0.8	
Cellulose nitrate	*E1*	66			5	7				9 10
Do	*F1*	63			4	7 8				10 12
Do	*W1*	94			4	10 11				13 11
Ethylcellulose	*G1*	58			36	39 45	49 50			60 73
Do	*H1*	31			45	40 51				49
Acrylate resin	*J2*	80			36	49 54	349 319			98 118
Do	*J3*	135			42	63 68	303 373			104 109
Do	*K1*	99			35	95 63	305 250			117 117
Do	*K2*	88			35	63 59	223 276			120 93
Do	*K3*	61			28	81 51	151 142			92 98
Do	*K6*	113			47	112 81	292 237			174 140
Vinyl chloride-acetate resin	*L2*	98	[b]	[b]				[b]	[b]	
Vinyl acetal resin	*N1*	119			78	64 90	136 157			118 108
Do	*N2*	52			55	44 68	51 78			88 77
Glyceryl-phthalate resin	*O1*	161			160	270 230	430 423			441 283
Phenol-formaldehyde resin	*V1*	260	[b]	[b]				[b]	[b]	

[a] The first value for each material was obtained on a specimen conditioned 24 to 48 hours at 21° C and 65-percent relative humidity; the second value is for a specimen left for 30 days in the conditioning atmosphere before testing.

[b] Would not ignite.

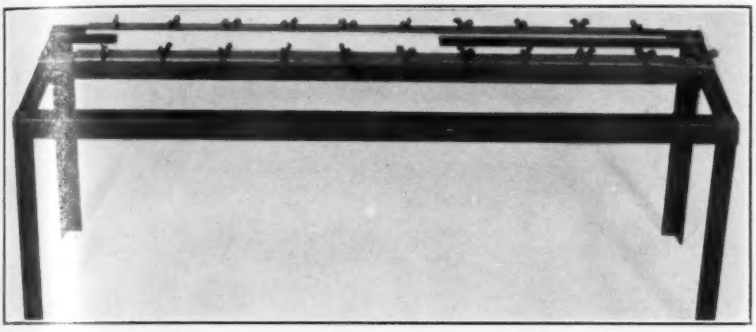

FIGURE 21.—*Apparatus for determining rate of burning.*

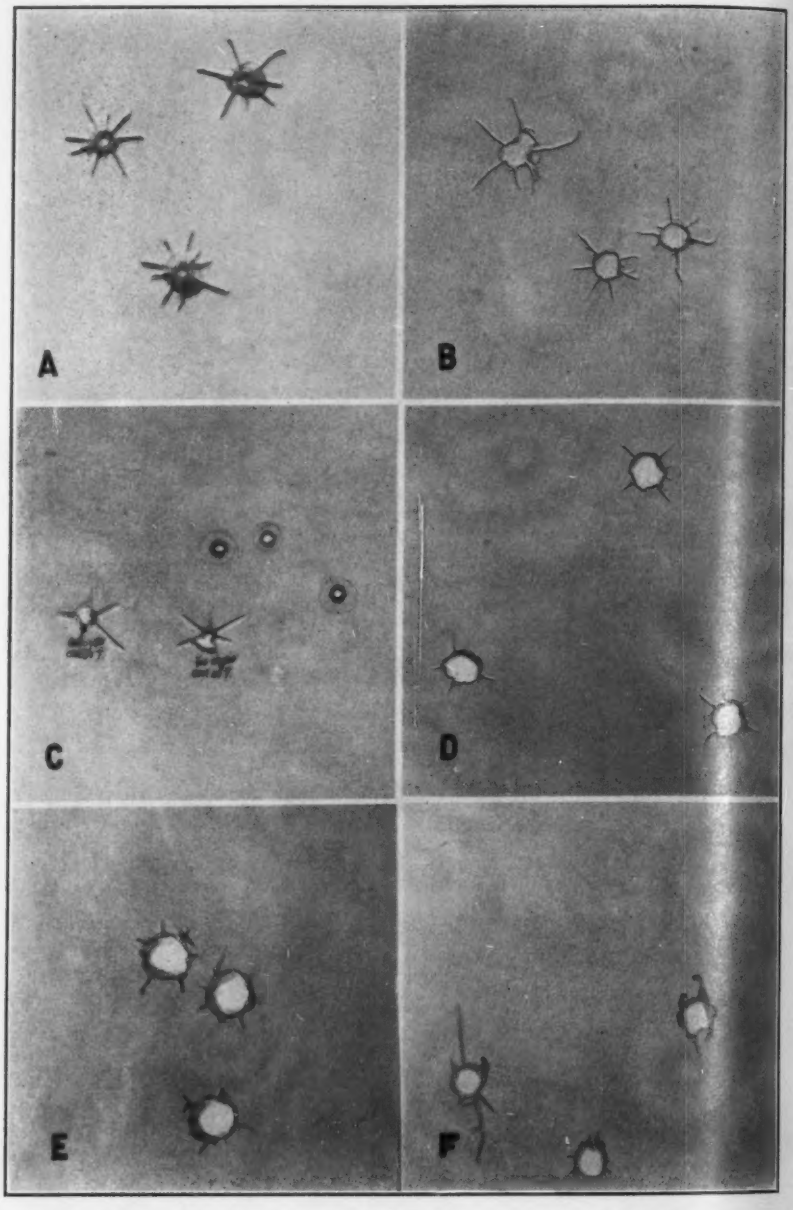

FIGURE 22.—*Effect of tracer bullets on transparent plastics.*

A. Acrylate resin, *K1*, 0.113 in. thick; three tracer bullets caliber .30, M1, at 100 yards.
B. Acrylate resin, *K9*, 0.067 in. thick; three tracer bullets caliber .50, M1, at 100 yards.
C. Cellulose nitrate, *F1*, 0.062 in. thick; three tracer bullets caliber .30, M1, at 100 yards; two tracer bullets caliber .30, M1, at 600 yards.
D. Cellulose nitrate, *E1*, 0.066 in. thick; three tracer bullets caliber .50, M1, at 100 yards.
E. Cellulose acetate, *C2*, 0.095 in. thick; three tracer bullets caliber .50, M1, at 100 yards.
F. Cellulose acetate, *B3*, 0.066 in. thick; three tracer bullets caliber .50, M1, at 100 yards.

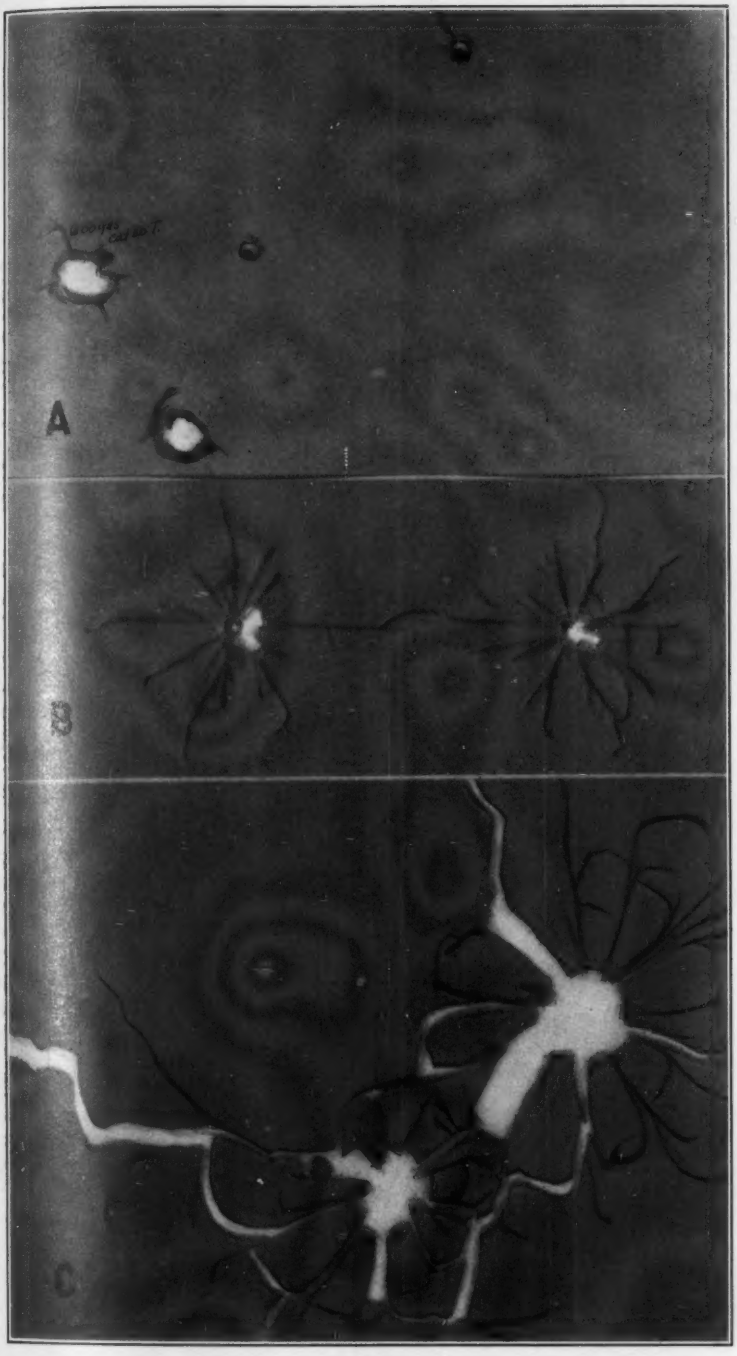

FIGURE 23.—*Effect of tracer bullets on transparent plastics.*

A. Cellulose acetate, *A2*, 0.095 in. thick; three tracer bullets caliber .30, M1, at 100 yards; one tracer bullet caliber .30, M1, at 600 yards.
B. Vinyl chloride-acetate resin, *L3*, 0.100 in. thick; two tracer bullets caliber .30, M1, at 100 yards.
C. Vinyl chloride-acetate resin, *L3*, 0.100 in. thick; two tracer bullets caliber .50, M1, at 100 yards.

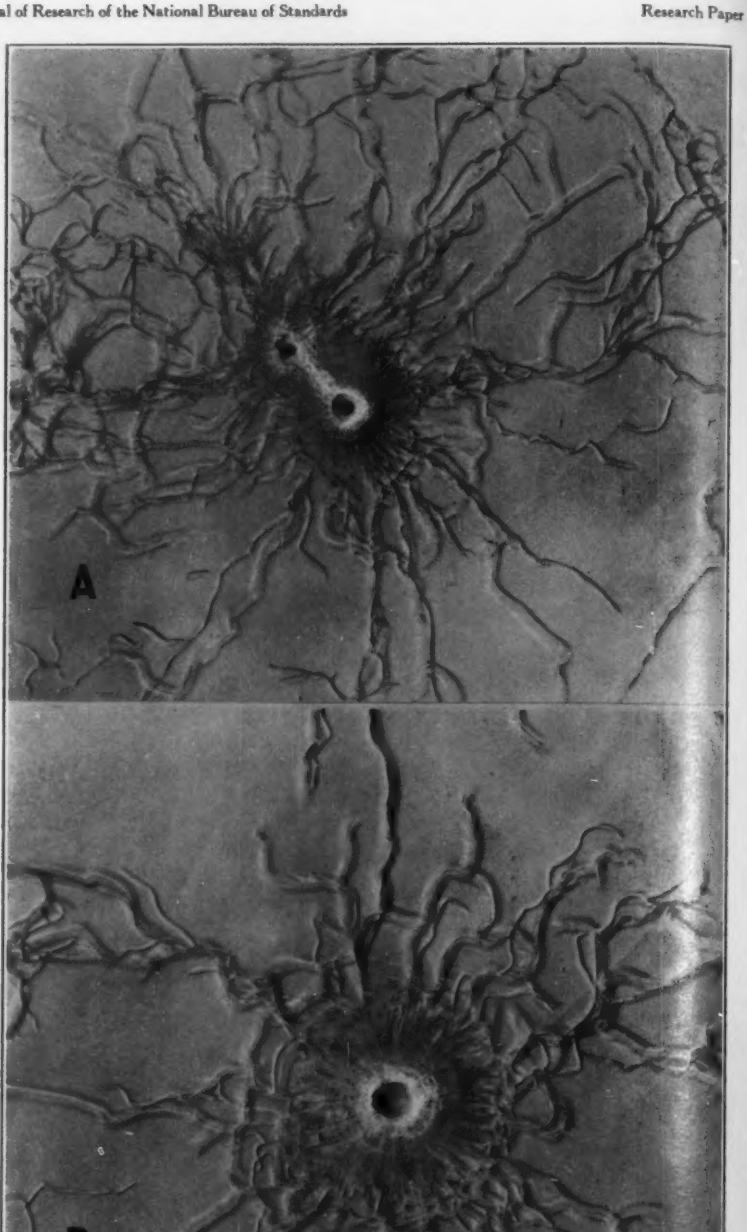

FIGURE 24.—*Effect of tracer bullets on laminated glass.*

A. Plate glass bonded with cellulose acetate plastic, X5, 0.188 inch thick; two tracer bullets caliber .30, M1, at 100 yards

B. Plate and sheet glass bonded with acrylate resin plastic, Y5, 0.238 inch thick; one tracer bullet caliber .50, M1, at 100 yards.

There is considerable question regarding the practical value of flammability tests of this type. The differences in ease of ignition or melting points greatly influence the results. Some samples tend to melt and separate the burning portion from the rest of the sample. The manner in which the strip is mounted for the test also is an important factor in the rate of burning. Data on the rates of burning in horizontal and vertical positions of plastics clamped in a metal frame (fig. 21) are presented in table 27. All the plastics including the cellulose nitrate burnt more slowly under these conditions. The cellulose acetate samples contained flame-retarding plasticizers which caused them to be extinguished in many of the tests shown in tables 26 and 27. Sample *B5*, and apparently *D1*, did not contain this type of plasticizer.

TABLE 27.—*Rate of burning of transparent plastics*

Material	Sample	Rate of burning of test strips ¾ by 3 inch			Rate of burning of test strips 1¼ by 3 inch		
		Horizontal strip ignited at one end	Vertical strip ignited at bottom	Vertical strip ignited at top	Horizontal strip ignited at one end	Vertical strip ignited at bottom	Vertical strip ignited at top
		in./min	in./min	in./min	in./min	in./min	in./min
Cellulose acetate	*C1*	0.93	(a)	(a)	(a)	1.86	(a)
Do	*C3*	0.35	(a)	(a)			
Cellulose nitrate	*E1*	3.75	9.75	2.22	4.28	9.90	2.12
Do	*F1*	3.96	8.55	2.12	5.00	10.30	2.08
Ethylcellulose	*G1*	1.24	2.81	0.75	2.10	3.00	1.25
Acrylate resin	*J1*	0.41	0.94	.31	0.52	0.84	0.31
Do	*J2*	.28	.61	.20	.51	.62	.23
Do	*K1*	.21	.30	.16	.31	.53	.18
Vinyl acetal resin	*M1*	.53	.88	.29	.83	1.41	.38
Styrene resin	*R1*	.54	.58	.41			

[a] Extinguished before burning 3 inches.

Tests made with incendiary bullets are of interest in connection with the establishment of specifications for the fire resistance of these materials. Tracer bullets of .30 and .50 caliber were fired through the samples at ranges of 100 and 600 yards.[2] None of the plastics, which included cellulose nitrate, cellulose acetate, vinyl chloride-acetate resin, and acrylate resin, was ignited. It is, therefore, apparent that, considered from the viewpoint of military requirements, the safe limits for the flammability of these materials should be based on storage and handling problems, which are serious only for the cellulose nitrate plastic, rather than on the danger of ignition from tracer bullets. The break caused by the impact of the bullet afforded useful information on the relative toughness of these materials. Some samples were merely penetrated by the bullets, which left small holes with no radial cracks, while others were completely shattered by the larger-caliber bullets. These effects of tracer bullets on transparent plastics are clearly shown in figures 22 and 23. Figure 24 shows the type of break which is obtained when laminated glass made with cellulose acetate and acrylate resin plastics, respectively, are penetrated by tracer bullets.

[2] The cooperation of Lt. Col. R. H. Hannum and other members of the staff of Frankford Arsenal in making these tests is gratefully acknowledged.

XIV. CONCLUSION

Pending the results of further tests on samples of cellulose acetate, acrylate resin, and other plastics, which have been prepared by the manufacturers using modified compositions and methods of processing to overcome the defective behavior noted during the course of this investigation, it is concluded that the problem of choosing between cellulose acetate and acrylate resin plastics for aircraft windows at present appears to be one of the required impact strength. If a relatively high impact strength is necessary, the cellulose acetate sheets are much superior to the acrylate resin in this respect. However, if high impact strength is not essential, then the superior clarity and weathering resistance of the acrylate resin makes it the more desirable material. Both the cellulose acetate and the acrylate resin have the advantages of being lighter in weight than glass and of being readily fitted to curved openings.

WASHINGTON, July 13, 1937.

U. S. Department of Commerce National Bureau of Standards

RESEARCH PAPER RP1032

Part of Journal of Research of the National Bureau of Standards, Volume 19, October 1937

ELECTRICAL CHARACTER OF THE SPARK DISCHARGE OF AUTOMOTIVE IGNITION SYSTEMS

By Melville F. Peters, George F. Blackburn, and Paul T. Hannen

ABSTRACT

To determine the character of a spark discharge it is necessary to determine current and voltage as functions of time. The measurement of these quantities is facilitated by the use of the cathode ray oscillograph, but due consideration must be given to the effect of the measuring circuit, including connections to the oscillograph, on the character of the discharge, especially in investigations of automotive ignition circuits.

Two methods suitable for measuring the current in the discharge with the cathode ray oscillograph are (1) measurement of the voltage across a known inductance, and (2) deflection of the cathode beam by the magnetic field set up by the current. The paper deals in detail with the application of these two methods, including, in the first method, the equations by which the current is derived, and the method of calibrating the measuring circuit in both methods.

An analysis is made of oscillograms obtained by both methods for the discharge in the calibrating circuits and in a typical ignition circuit. Crest currents of 50 to 80 amp were measured. The frequencies ranged from 6 to 10 Mc/s, the decrements from 0.08 to 0.40, and the energy expended from 0.0023 to 0.0135 j. The expended energy is found to agree with the energy known to be stored in the capacitance of the circuit at the beginning of the discharge.

CONTENTS

	Page
I. Introduction	402
II. Description of methods of current measurement	402
1. Measurement of voltage across a known resistance	402
2. Measurement of voltage across a known inductance	403
3. Measurement of magnetic deflection	404
III. Description of apparatus	405
IV. Experimental procedure	406
1. Determination of inductance of standard inductors	406
(a) Computation	406
(b) Measurement	407
2. Calibration of oscillograph	407
(a) Measurement of voltage across standard inductors	407
(b) Measurement of current by magnetic deflection	408
V. Determination of electrical characteristics from the oscillograms	409
1. Measurement of frequency	409
2. Measurement of decrement	410
3. Evaluation of resistance	410
4. Evaluation of energy	411
VI. Results	411
1. Spark characteristics by measurement of voltage across a known inductance	411
(a) Calibration	411
(b) Measurements on typical ignition circuit	413
2. Spark characteristics by measurement of magnetic deflection	414
(a) Measurements on typical ignition circuit	414
(b) Calibration	414
VII. Discussion of results	417
VIII. References	418
Appendix A. Derivation of expression for voltage across capacitance of oscillograph circuit	418
Appendix B. Displacement of line of zero voltage on an oscillogram	420

I. INTRODUCTION

The electrical character of a spark discharge may be determined if both current and voltage are known as functions of time. When these have been determined such quantities as crest voltage, crest current, frequency, decrement, and energy may be deduced. For the measurement of voltage and current the most suitable instrument is the cathode ray oscillograph. In making these measurements it is necessary to introduce apparatus into the discharge circuit which unavoidably changes the effective resistance, inductance, and capacitance of the circuit. If the electrical constants of the discharge circuit are large, as compared to those of the measuring apparatus, care must be taken in selecting the apparatus so that either the nature of the circuit is not seriously affected or correction may be made for the change in the character of the discharge.

In automotive ignition systems the capacitances of the individual leads from the spark coil or magneto to and including the spark plugs have been found to lie between 40 and 300 $\mu\mu$f. The inductances of the corresponding leads lie between 0.5 and 3 μh. The direct-current resistance of the leads is small.

A technique for measuring voltage across a spark-plug gap, using a low-capacitance voltage divider with the cathode-ray oscillograph, has been described by the authors [1][1]. Such additional considerations as are necessary will be taken up in appendix B.

The present paper considers three methods of measuring the discharge current using the cathode-ray oscillograph, viz: (1) By measuring the voltage drop across a resistance; (2) by measuring the voltage drop across an inductance, and (3) by deflecting the cathode beam magnetically by means of coils introduced into the circuit. The principles underlying these three methods are well known, but the magnitudes of the electrical constants of an automotive ignition circuit impose limitations upon their application to such circuits. One of the primary objects of this work is to develop technique which can be used to determine the character of spark discharges of automotive ignition systems without appreciably disturbing the ignition circuit.

This work was sponsored by the Bureau of Aeronautics of the U. S. Navy Department and was completed in April 1933.

II. DESCRIPTION OF METHODS OF CURRENT MEASUREMENT

1. MEASUREMENT OF VOLTAGE ACROSS A KNOWN RESISTANCE

The Dufour or cold cathode type of oscillograph is well suited to the observation and measurement of spark-discharge phenomena, because of the high-speed transients involved. Since the voltage sensitivity of this type of oscillograph is only about 0.004-cm deflection of the cathode beam per volt, a convenient deflection requires the application of several hundred volts. Assuming a crest discharge current of 50 amp, a resistance of 5 ohms would have to be inserted in the discharge circuit to produce a deflection of 1 cm. Since the effective resistance of the circuit during discharge, as determined from the decrement, is of the same order of magnitude as this, it is evident

[1] Figures in brackets here and throughout the text refer to the references given in sec. VIII, p. 418.

that the addition of the required resistance would produce a considerable change in the decrement of such a circuit.

A resistance of 0.1 ohm or less could be used if the voltage across the resistance were amplified. An objection to this procedure is that it is difficult to find a resistor which has negligible inductance. At high frequencies the presence of inductance in the resistor results in an inductive voltage component in the deflection, which may be greater than that due to the resistance. In the course of experiments with a specially built amplifier and so-called noninductive resistors this was found to be true and suggested the advisability of measuring peak current by measuring the voltage drop across a known inductance.

2. MEASUREMENT OF VOLTAGE ACROSS A KNOWN INDUCTANCE

When a capacitance C discharges through an inductance L and resistance R, the current at time t after the beginning of the discharge may be given by

$$i=\frac{V_0}{\omega L}\epsilon^{-\alpha t}\sin \omega t \tag{1}$$

if $\alpha^2<1/CL$. Here $\alpha=R/2L$, $\omega=\sqrt{1/CL-R^2/4L^2}$, and V_0 is the voltage of the capacitor at the beginning of the discharge.

The potential difference across a part L_1 of the inductance at a time t is given by

$$v_{L_1}=\frac{V_0 L_1}{\omega L}\sqrt{\alpha^2+\omega^2}\,\epsilon^{-\alpha t}\cos(\omega t+\theta), \tag{2}$$

where $\theta=\tan^{-1}\alpha/\omega$

From eq 1 and eq 2 the relation between a voltage crest and the current crest which follows the voltage crest by approximately one-quarter cycle is

$$I=\frac{V}{L_1\sqrt{\alpha^2+\omega^2}}\,e^{\left[\frac{\alpha}{\omega}\left(\frac{\pi}{2}+\theta\right)\right]} \tag{3}$$

If $\alpha=0$ this reduces to the relation between maximum voltage and current in an undamped sine wave,

$$I=\frac{V}{\omega L_1} \tag{4}$$

In a spark discharge in an ignition circuit α is usually very small compared with ω, so that in computing the crest current from eq 4 the error introduced by neglecting the damping factor is less than the error resulting from experimental errors in measuring V, ω, and L_1.

To apply this method of current measurement, a single-layer coil is constructed whose inductance can be measured or readily computed. The magnitude of the inductance must be such that the characteristics of the discharge are not affected to any considerable extent by its inclusion in the circuit, and that a convenient deflection on the oscillograph is produced by the discharge. The high-frequency resistance of the coil can be made negligibly small in comparison with its inductance, and the self-capacitance can also be made negligibly small. The quantities V and ω are obtained from oscillograms.

Figure 1 shows diagrammatically the arrangement used for measuring the potential difference across L_1. The capacitance C' represents that of the oscillograph plates and of the voltage divider, if one is used. The resistance and inductance of the connecting wires are represented by R' and L', respectively. In order to reduce the effect of the measuring circuit on the discharge circuit, C' should be small compared to C.

Assuming that the influence of the measuring circuit on the discharge circuit is negligible, it is next necessary to determine the effect of the electrical constants of the connecting leads on the pattern obtained in the oscillograph. In order to do this a damped high-frequency voltage whose maximum value is known is applied to the terminals of the inductance L_1 and the oscillograph deflection compared with the deflection due to the same voltage at low frequency. This serves to determine what correction, if any, must be applied to the current values obtained from the deflections measured on an oscillogram to obtain the true current in the discharge circuit. The maximum value, frequency, and damping of the current used for this calibration are made as nearly as practicable like those of the current in the ignition circuit to be studied, and it is then assumed that the same correction factor is valid for both circuits.

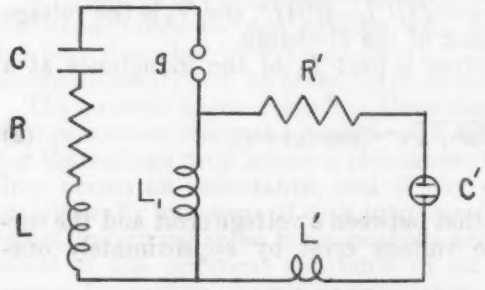

FIGURE 1.—*Schematic diagram of circuit used in measuring voltage across inductance.*

A detailed analysis of the relation between the voltage across the deflection plates and the voltage across the inductance L_1 will be found in appendix A, page 418. This analysis shows the correction to be applied in terms of the constants of both circuits. The manner of determining experimentally the correction factor will be described in section IV, page 407.

3. MEASUREMENT OF MAGNETIC DEFLECTION

In this method the cathode beam of the oscillograph is deflected by the magnetic field which is created when the discharge current flows through two coils placed adjacent to the beam, and with their common axis normal to its path. The deflection is proportional to the strength of field, and hence to the current, and takes place at right angles both to the direction of the field and that of the beam. For a given current the strength of field along the path traversed by the beam depends on the dimensions and location of the coils. The coils, which are symmetrically placed on opposite sides of the path of the beam, are connected in parallel in order to avoid setting up an electrostatic field.

To obtain a convenient deflection as the experimental conditions are changed requires a change either in the dimensions of the coils, or their positions, or both. With each change, a calibration is necessary to obtain the sensitivity in centimeters deflection per ampere.

This method is applicable to current of any wave form, or to non-oscillating current.

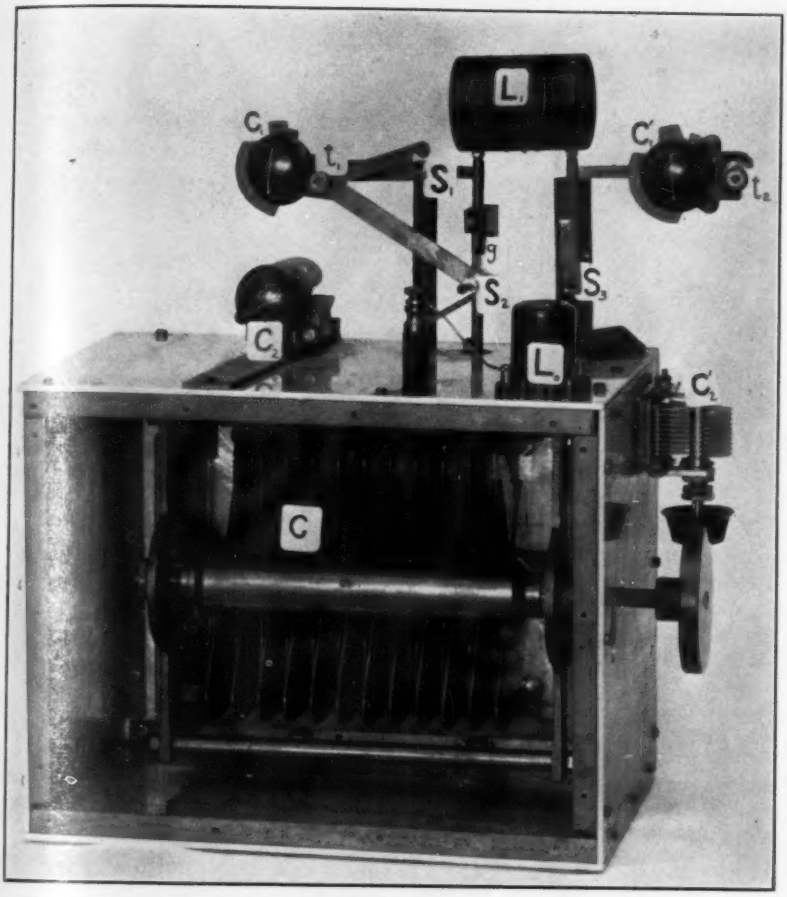

FIGURE 2.—*Arrangement used to supply heavy current discharges for calibrating the oscillograph.*

C, High-voltage variable air capacitor; L_0, choke coil; L_1, standard inductor; g, spark gap; C_1, C'_1, C_2, C'_2, variable air capacitors; s_1, s_2, s_3, switches; t_1, t_2, terminals.

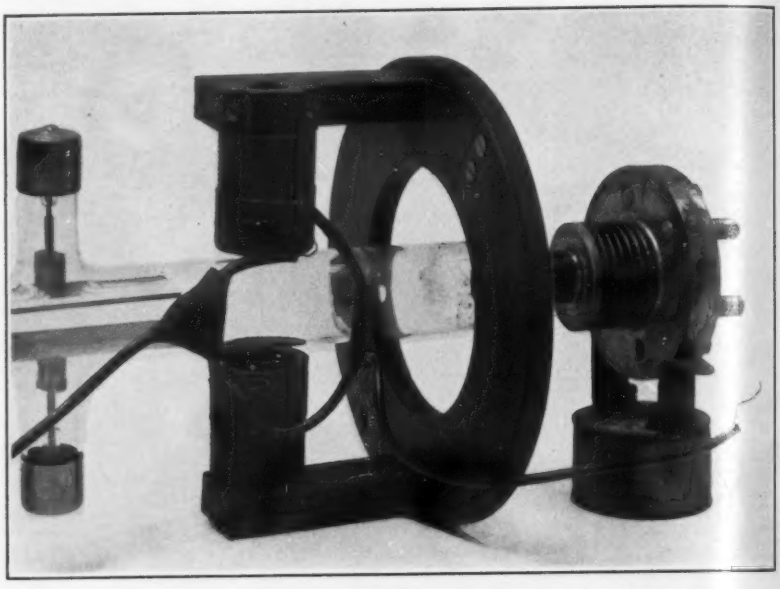

FIGURE 4.—*Deflecting coils as supported in their positions adjacent to the deflection tube.*

III. DESCRIPTION OF APPARATUS

The cathode ray oscillograph was of the high-voltage cold-cathode type. The cathode was operated at approximately 60,000 v, the supply being the secondary of a transformer. The primary was connected to a 60-c 110-v supply through rotary switches operated by a synchronous motor driven from the same source. The switches were constructed so that the negative voltage was applied to the cathode during one half cycle, once in every 100 cycles.

Figure 2 is a photograph and figure 3 a diagram of the standard circuit used to supply heavy-current spark discharges at high frequencies. The capacitor C is in the metal box and has a range of 50 to 300 $\mu\mu$f. The rotating plates of the capacitor are permanently connected to an aluminum shielding box, and the assembly was calibrated for capacitance. The spark gap is at g, and interchangeable inductors are inserted in the circuit at L_1. L_0 is a 60-mh choke coil to prevent oscillations from the magneto circuit affecting the standard

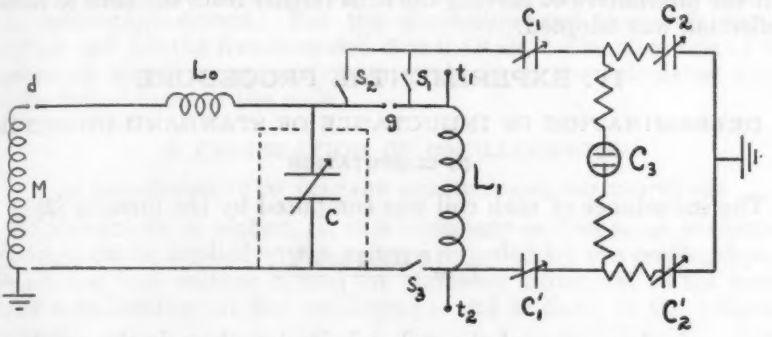

FIGURE 3.—*Diagram of circuit used to calibrate the oscillograph.*

circuit during the high-frequency discharge. The distributor gap of the magneto M is shown at d. The voltage divider consists of four capacitors: C_1, C_1', each having a maximum capacitance of 15 $\mu\mu$f, and C_2, C_2', each having a maximum capacitance of 100 $\mu\mu$f.

Provision is made at s_1 for connecting C_1 to the inductance coil L_1, and at s_2 to the high-voltage side of the spark gap. The latter connection is made for calibrating, since it is desired to compare in a single spark discharge the breakdown voltage of the gap with the crest voltage across the inductance coil. After being calibrated the measuring circuit with terminals t_1 and t_2 is connected in series with the circuit under investigation.

At s_3 is a switch used to open or close the circuit from the coil to the shielding box, which is grounded. When coil L_1 is connected in the circuit being studied, s_1 connects C_1 to the circuit, and s_2 and s_3 are opened.

Balancing of the capacitance voltage divider has been described by the authors [1]. Briefly, the divider is balanced by applying a high voltage, such as that generated by the magneto, to both sides of the divider. To accomplish this, s_1 and s_2 are closed and s_3 is opened slightly, so that it acts as a spark gap. If the divider is balanced the cathode beam is not deflected during the charging or the discharge

of the spark gap s_3. If the beam is deflected the divider may be balanced and the deflection reduced to zero by changing the capacitance of C_1 or C_2.

The calibration was made first with an inductance coil, L_1, 5.2 cm long and 5.1 cm in diameter wound with three turns of copper wire 0.07 cm in diameter, and then with a second coil 5.2 cm long, 5.1 cm in diameter wound with five turns of copper wire 0.07 cm in diameter.

Figure 4 shows how the magnetic deflection coils were placed in their supports adjacent to the deflection tube. A special tube was made to permit the use of these coils. The regular tube has two pairs of deflection plates, one pair horizontal and the other pair vertical. The special tube has the horizontal plates, but the vertical plates are omitted to prevent the shielding of the electron beam from the magnetic field by the eddy currents which would have been induced in the vertical plates by the magnetic field.

Sufficient deflection was produced under the prevailing conditions, with three turns of wire on each coil. Often less could have been used, but the alternative of moving the coils farther from the tube to reduce deflection was adopted.

IV. EXPERIMENTAL PROCEDURE

1. DETERMINATION OF INDUCTANCE OF STANDARD INDUCTORS

(a) COMPUTATION

The inductance of each coil was computed by the formula [2]

$$L_s=\frac{0.03948a^2n^2K,}{b} \tag{5}$$

where a is the radius of the coil, b is its length, n is the number of turns, and K is a factor which depends on the ratio of the diameter to the length. L_s is the inductance in microhenries of the current sheet of the given dimensions, and a correction must be made to take into account the size and shape of the cross section of the wire. The corrected value of the inductance is given by

$$L_o=L_s-0.01257an(A+B), \tag{6}$$

in which L_o is the inductance of the coil at low frequencies, A is a constant which takes into account the difference in self-inductance of a turn of wire from that of a current sheet, and B depends on the difference in mutual inductance of the turns of the coil from that of the turns of the current sheet. A is given as a function of the ratio of the diameter of the wire to the distance between centers of the wire measured along the axis, and B is a function of the number of turns.

The ratio of diameter to length of both coils was 1.02. For this ratio the factor K is 0.6884. For the three-turn coil the value of A is -2.640 and the value of B is $+0.166$. For the five-turn coil A is -2.144 and B is $+0.218$.

Substituting these values and the dimensions of the coils in equations 5 and 6, the resulting values of low-frequency inductance are 0.54 μh for the three-turn coil and 1.15 μh for the five-turn coil.

(b) MEASUREMENT

In order to check experimentally the computed inductance of the two coils, the total inductance of the standard discharge circuit, which includes the inductance of the coil and connecting circuit, was determined by the following method [2]. With the spark-gap electrodes in contact and the inductance loosely coupled to a variable-frequency oscillator, the calibrated variable capacitor C of the standard circuit was given various settings, and for each setting the natural frequency of the circuit was found, indicated by resonance with the oscillator. Since $1/\omega^2 = L(C+C_0)$, where $(C+C_0)$ is the total capacitance and L is the total inductance of the discharge circuit at high frequency, the plot $1/\omega^2$ versus C is linear. The slope of this line gives the inductance L, and the intercept on the C axis gives C_0.

With the three-turn coil the total inductance of the circuit was found to be 0.67 μh, and with the five-turn coil 1.27 μh. The difference between the experimentally determined inductance for the circuit and the computed value for the coil should equal the inductance of the connecting circuit. For the three-turn coil this difference is 0.12 μh and for the five-turn coil it is 0.11 μh. The closeness of this agreement serves as an experimental check on the calculated values of the inductances of the coils.

2. CALIBRATION OF OSCILLOGRAPH

(a) MEASUREMENT OF VOLTAGE ACROSS STANDARD INDUCTORS

As was shown in section II, it is necessary to find what correction, if any, must be applied to the voltage recorded by the oscillograph to obtain the true voltage across the standard inductors. This constitutes a calibration of the oscillograph and is done in the following manner.

The standard discharge circuit is used, with C set at the desired value and with one of the standard inductors L_1 in the circuit. Referring to figure 3, switch s_1 is open, s_2 and s_3 are closed. Thus the charging voltage applied to the capacitor C, to break down the gap g, is applied also to the oscillograph circuit, comprising the capacitors of the capacitance voltage divider, the inductance and resistance of the connecting wires, and any resistors that have been added to prevent the occurrence of parasitic oscillations in the oscillograph circuit. This charging voltage builds up at a relatively slow rate, and the voltage recorded by the oscillograph is then related to this charging voltage by a factor K which depends only on the settings of the capacitors of the voltage divider.

One method of determining the factor K consists in applying an alternating voltage of about 1,000 v at a frequency of several thousand cycles per second to one pair of deflecting plates and to the voltage divider, which is connected to the other pair. The slope of the resulting straight line on an oscillogram is a measure of the factor K.

Upon the breakdown of the gap g, the capacitor C discharges through the inductance and resistance of the circuit, usually in an oscillatory manner, and the oscillograph records the oscillations of voltage, and their decreasing amplitude. Any correction which is required because of the effect of the measuring circuit on the record obtained on an oscillogram is determined by comparing the deflection due to the gap breakdown voltage with the maximum deflection on the succeeding

cycle, after multiplying this maximum deflection by a factor to correct for the decay of voltage from one cycle to the next. In arriving thus at the correction factor, it is assumed, first, that no sensible error is introduced by regarding the inductance between the points of oscillograph connection to the discharge circuit as the total inductance of the discharge circuit; second, that the effect of the resistance of the circuit may be neglected in comparison with the inductance; and third, that the damping factor has approximately the same value for the first cycle as it does during the cycles immediately following the first. It has been found that the error arising by reason of these assumptions is less than the experimental error of measurement of the deflection on an oscillogram, which is usually 3 percent or more.

(b) MEASUREMENT OF CURRENT BY MAGNETIC DEFLECTION

Calibration of the oscillograph for this method of current measurement consists in determining the current sensitivity of the oscillograph, and is most conveniently carried out after a suitable oscillogram has been obtained of the current in the ignition circuit under test. With this procedure the deflection coils are placed adjacent to the deflection tube so as to give a convenient deflection by the current in the ignition circuit, and the coils are not disturbed during the calibration.

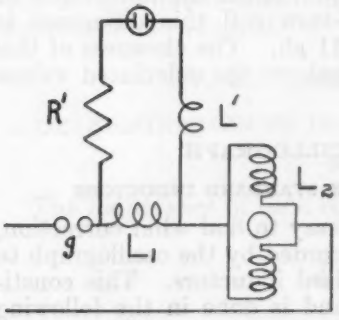

FIGURE 5.—*Schematic diagram of circuit used to calibrate the oscillograph for measurement of current by magnetic deflection.*

The calibration was carried out with high-frequency discharge current. The procedure for calibrating consists in modifying the circuit of figure 1 by putting the deflection coils L_2 in series with the inductor L_1 (fig. 5). Then one or more oscillograms are made of the deflection due to the discharge current in the standard circuit flowing in L_2, with the deflection plates disconnected from L_1. Besides the deflection, the frequency of the discharge also is obtained from this oscillogram. The deflection coils are then removed from the deflection tube to a distance such that their field cannot affect the cathode beam and the deflection plates connected to L_1. This arrangement gives oscillograms of the crest voltage across L_1 due to the discharge current, and from this deflection and the frequency the crest current is obtained, as in the method first described. Assuming that the crest currents in the discharges observed in these two ways are of equal value, the sensitivity of the oscillograph in centimeters deflection per ampere is deduced.

Since it is known that the breakdown voltage of the gap may be different for separate discharges, it is desirable to take the average of a number of oscillograms of each type. The ideal method would be to record the crest voltage across L_1 and the crest current through L_2 on the same discharge. However, the quadrature of phase between current and voltage causes the cathode beam to describe a spiral path, and it was found that at high frequencies the linear velocity of the beam across the photographic film at the outside of this spiral was too high to leave a well-defined trace, while toward the center considerable

fogging resulted from the action of the cathode beam at one spot prior to the discharge. At the time this work was done these difficulties had not been overcome, so that the method first described was considered preferable.

Subsequent experiments with a discharge circuit having a natural frequency of 5.0 Mc/s have shown that oscillograms of simultaneous current and voltage can be obtained by limiting the maximum deflection along both axes to a moderate amount and by sweeping the cathode beam across the film horizontally at a moderate rate, so as to avoid undue fogging of the film by the protracted presence of the cathode beam. The discharge is timed to occur while the beam is crossing the film. In this instance the sweep speed was about 10^4 cm/sec, and the film width was traversed in about 1.3×10^{-3} sec. Since the duration of the discharge was about 10^{-6} sec the displacement of the beam due to the sweep speed during the period of the discharge was only about 10^{-2} cm. The maximum deflection from the origin was 3 cm.

At this frequency it was found that the current sensitivity, about 0.03 cm deflection per ampere, was the same as for direct current.

V. DETERMINATION OF ELECTRICAL CHARACTERISTICS FROM THE OSCILLOGRAMS

If oscillograms have been obtained by either of the two methods of current measurement, it is possible to derive various quantities which are characteristic of or associated with the circuit producing the discharge. These will now be considered.

1. MEASUREMENT OF FREQUENCY

Since it is desired to know the voltage and current as functions of time, it is necessary to sweep the beam across the photographic film at a known rate of speed. This speed must be such that the deflections due to voltage or current, which are caused to take place at right angles to the direction of the time axis, are clearly delineated. This was accomplished by using a high-voltage oscillator to deflect the beam in a vertical direction across the film, at a frequency of 77.5 kc/s. This produced the time axis. Since the output voltage E at a time t is $E=E_{max}\sin 2\pi Ft$, where F is the sweep frequency in cycles per second, the motion of the beam across the film is given by $d=D\sin 2\pi Ft$, where D is the amplitude and d is the deflection at time t, t being referred to the epoch t_0 when $d=0$. Thus, since $t=(1/2\pi F)(\sin^{-1}d/D)$, the time interval between any two points is given by

$$t_2-t_1=\frac{1}{2\pi F}\left(\sin^{-1}\frac{d_2}{D}-\sin^{-1}\frac{d_1}{D}\right).$$

This expression is valid only if t_1 and t_2 refer to the time at the beginning of the quarter-cycle ($d=0$) in which d_1 and d_2 occur. If d_1 and d_2 lie on opposite sides of the point $d=0$, the terms within parentheses must be added.

The position of the time axis being vertical, the voltage or current to be measured is applied so as to produce a horizontal deflection and the oscillations whose frequency is to be measured are then spread out along the time axis. A convenient number n of these

oscillations is chosen, and the time interval (t_2-t_1) between these cycles measured. The frequency is then

$$f=\frac{n}{t_2-t_1}=\frac{2\pi Fn}{\sin^{-1}\frac{d_2}{D}-\sin^{-1}\frac{d_1}{D}} \tag{7}$$

2. MEASUREMENT OF DECREMENT

The decrement of a damped alternating current is usually defined as the natural logarithm of the ratio of a current maximum to the next current maximum in the same direction.

$$\delta_n=\log\frac{I_n}{I_{n+1}} \tag{8}$$

If v is the potential difference produced by this damped current, then

$$\delta_n=\log\frac{V_n}{V_{n+1}} \tag{9}$$

By evaluating V_n and V_{n+1} from eq 2, the decrement is found to be

$$\delta_n=\frac{2\pi\alpha_n}{\omega}=\frac{\pi R_n}{\omega L} \tag{10}$$

since $\alpha_n=R_n/2L$.

When R, which is the total resistance in the circuit, is constant, the damping is logarithmic. When R varies in such a way that the oscillations diminish in amplitude by a constant difference, the damping is linear. The actual damping in ignition circuits is usually found to lie between these two extremes. The decrement may also be measured by measuring the double amplitude, which is sometimes more easily done than measuring the amplitude. That is, if I_n' is the maximum current in the opposite direction following I_n, and I'_{n+1} is the maximum current following I_{n+1}, then

$$\delta_n=\log\frac{I_n+I_n'}{I_{n+1}+I_n'_{+1}} \tag{11}$$

Another relation that is sometimes useful is

$$\frac{I_n}{I_n'}=\left[\frac{I_n+I_n'}{I_{n+1}+I_n'_{+1}}\right]^{\frac{1}{2}} \tag{12}$$

although it is strictly true only if the damping is logarithmic.

3. EVALUATION OF RESISTANCE

Equation 10 can be written

$$R_n=\frac{\omega L\delta_n}{\pi}$$

If $\omega^2=1/LC$, which is nearly true if R^2_n is small in comparison with $4L/C$, then R_n is given by

$$R_n=\frac{\delta_n}{\pi\omega C} \tag{13}$$

in which the capacitance C measured at low frequency is taken as the capacitance at the discharge frequency.

The effective resistance R has three components, namely, gap resistance, circuit resistance, and radiation resistance. In the case of a shielded ignition harness, the radiation is very small and the radiation resistance probably negligible. In such a circuit, the distributed nature of the capacitance and inductance makes it difficult to calculate the high-frequency resistance. For these reasons no attempt has been made to separate the losses in the gap from those in the rest of the circuit.

The fact that in the discharge in an ignition circuit δ is not constant indicates that R is not constant. The variation in R is due to the variation in the gap resistance. The gap resistance probably varies in some manner with the instantaneous current in the gap, but the value of R given by eq 13 is the effective value of the total resistance of the circuit, and is assumed to be the effective resistance during any cycle in which the decrement is δ. With ignition circuits this effective resistance usually varies from a minimum value of 2 or 3 ohms at the beginning of a discharge to 10 or more ohms near the end.

4. EVALUATION OF ENERGY

Another way of defining the effective resistance of the discharge circuit during one cycle is to say that it is that value of resistance which, when multiplied by the square of the instantaneous current, integrated over the cycle, gives the total energy expended during that cycle. Thus,

$$W=R\int_0^{\frac{2\pi}{\omega}} i^2 dt \tag{14}$$

If the damping factor be neglected in carrying out this integration, the result is

$$W_n=R_n I_n^2/2f,$$

where R_n and I_n are the effective resistance and crest current in the nth cycle, f is the frequency, and W_n is the energy expended in that cycle. The total energy expended in a train of N oscillations is then

$$W=\frac{1}{2f}\sum_{n=1}^{N} I_n^2 R_n \tag{15}$$

This sum should be equal to the energy stored in the capacitor at the beginning of the discharge. The degree to which such equivalence is obtained is an indication of the accuracy with which R has been determined.

VI. RESULTS

1. SPARK CHARACTERISTICS BY MEASUREMENT OF VOLTAGE ACROSS A KNOWN INDUCTANCE

(a) CALIBRATION

Figure 6 is an oscillogram made with the standard discharge circuit, using the five-turn coil as inductance L_1. The capacitance C was 200

$\mu\mu$f. The oscillograph was connected across the spark gap and the inductance L_1. The discharge voltage was applied to that pair of deflection plates which produced a horizontal deflection. A time scale was made by applying alternating voltage of 77.5-kc/s frequency to the other pair of plates, which produced a vertical deflection. The relatively low rate of rise of voltage across the spark gap is shown by the deflection of the beam to the right of the zero voltage line during about two cycles of the timing wave, until the point a is reached. Here the gap breaks down, and the subsequent oscillations of voltage during the discharge, which can be more easily seen on the original oscillogram, are indicated in figure 6 by marking the deflection peaks.

In this oscillogram the true line of zero voltage is the line xy, rather than the heavy white line. This displacement of the zero line is due to a residual charge left on the capacitance voltage divider at the end of the preceding spark. (See appendix B.)

The position of the line xy was determined from the turning points, using eq 12. It was found that the assumption of logarithmic or linear damping made no appreciable difference in the position of this line.

Using eq 7 and measurements from figure 6, the frequency is found to be 10 Mc/s, which agrees with the frequency computed from the circuit constants.

Amplitude measurements were made on the left side of figure 6, because several of the oscillations of low amplitude on the right side were poorly defined. These amplitudes are given in table 1, column 2. These are plotted and a smooth curve drawn through them (plot 1(a), fig. 10). The adjusted amplitudes, in column 3, are taken from this curve; and ratios of successive amplitudes (column 4), decrements (column 5) and resistance (column 6) are all based on these adjusted values. This results in a set of resistance values which vary more uniformly than if they were computed directly from the measured amplitudes.

TABLE 1.—*Analysis of spark discharge from oscillogram of figure 6*

$$I_n=\frac{V_n}{\omega L_1}=\frac{13.3\times180\times\text{amplitude}}{2\pi\times10\times10^6\times1.27\times10^{-6}}=30.1\times\text{amplitude}.$$

$$R_n=\frac{\delta_n}{\pi\omega C}=25.4\,\delta_n.$$

$$W=\frac{45500}{2\times10\times10^3}=0.0023\text{ j}.$$

Oscillation number	Measured amplitude	Amplitude from plot 1 (a), fig. 10	Ratio $\frac{I_n}{I_{n+1}}$	Decrement	Decrement from plot 1 (b), fig. 10	Effective resistance	Crest current	I^2R
	cm						amp	w
1	1.95	1.95	1.08	0.08	0.08	2.0	58	6,700
2	1.80	1.80	1.09	.09	.09	2.3	54	6,700
3	1.65	1.65	1.12	.11	.10	2.5	50	6,200
4	1.50	1.47	1.13	.12	.11	2.8	44	5,400
5	1.30	1.30	1.13	.12	.12	3.0	39	4,600
6	1.15	1.15	1.13	.12	.13	3.3	34	3,800
7	1.05	1.02	1.16	.15	.14	3.6	30	3,200
8	0.85	0.88	1.16	.15	.15	3.8	26	2,600
9	.75	.76	1.17	.16	.16	4.1	23	2,200
10	.65	.65	1.18	.17	.18	4.6	19	1,700
11	.55	.55	1.22	.20	.21	5.3	16	1,400
12	.45	.45	1.29	.25	.25	6.4	13	1,100
13	.35	.35			.35	8.9	10	900
Total								45,500

FIGURE 6.—*Oscillogram of spark discharge, obtained for calibration of oscillograph for measurement of voltage across inductance.*

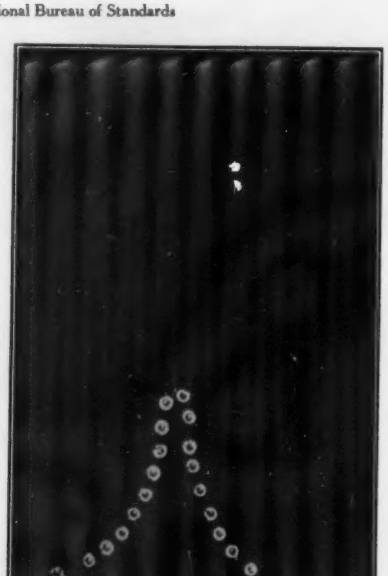

FIGURE 7.—*Oscillogram of spark discharge in a typical ignition circuit, using the voltage drop across inductance to produce deflection.*

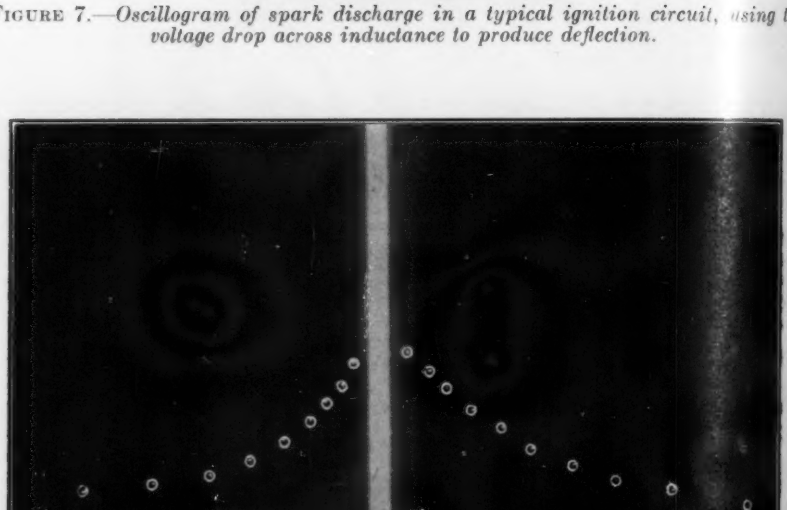

FIGURE 8.—*Oscillogram of spark discharge in a typical ignition circuit, using the magnetic field of the current to produce deflection.*

To calibrate the oscillograph circuit, or in other words to determine what correction must be applied to the measured voltage to obtain the true voltage, it is only necessary to compare the amplitude a with the amplitude a_1, after multiplying the latter by the ratio which has been found to exist between successive amplitudes. From table 1, this ratio for the amplitudes b and b_1 is 1.08. The deflection at a is 2.1 cm; a_1 is 1.9 cm, and this multiplied by 1.08 gives 2.05 cm. The difference, 0.05 cm, is within the experimental error of measurement of the deflection, and therefore no correction is necessary.

As a check on the accuracy of the method the computations summarized in table 1 were made. The voltage across the gap is found by multiplying the deflection at a by the deflection constant of the oscillograph, which is 180 v/cm, and by the reduction factor K of the voltage divider, which is 13.3. The breakdown voltage is therefore 5,000 v. Current maxima (table 1, column 8) are computed from eq 4. Finally, the average power during each cycle is computed (column 9). From this the total energy expended is found to be 0.0023 j, while the amount originally stored in the capacitor was 0.0025 j. These results are in sufficiently close agreement, especially when it is realized that a small amount of energy may still be left in the capacitor when the discharge ceases.

(b) MEASUREMENTS ON TYPICAL IGNITION CIRCUIT

Figure 7 is an oscillogram of a spark discharge through the longest lead (about 6 ft) of a shielded ignition harness, using the measuring circuit whose calibration is discussed above. One end of the lead was connected to the magneto and the other end to a spark plug. The spark plug was screwed into a bomb and the electrodes surrounded by an atmosphere of CO_2 gas at 105-lb/in.^{2} pressure. The L_1 inductor was connected in the discharge circuit on the grounded side of the spark plug, and the oscillations of voltage across this coil were superposed on the timing wave. The timing wave was spread out across the photographic film by using the varying magnetic field of 60-c current, this field deflecting the beam from left to right in figure 7, at a rate of about 3.6×10^4 cm/s.

The frequency in this discharge was 5.9 Mc/s. The capacitance, measured with current of 2,000-c frequency, was 200 $\mu\mu$f. The corresponding inductance is therefore $L=1/\omega^2C=3.6$ μh.

Since both positive and negative turning points are visible the double amplitudes were measured, and are tabulated in table 2, column 2. The smooth curve through the plotted turning points (plot 2(a), fig. 10) gives the adjusted amplitudes in column 3, and from these are computed the decrements shown in plot 2(b). The adjusted decrement for each cycle is obtained from the smooth curve through these points, and from these the effective resistance shown in column 8 are obtained. Both positive and negative maximum currents were measured, and the total energy obtained as before. This is 0.0135 j.

The breakdown voltage of the gap may be computed from the total energy. The agreement, for the previous case, between the energy computed from the oscillogram and the initial energy in the capacitor indicates the reliability of this method. From $CV^2/2=0.0135$ j, the voltage $V=11{,}600$ v.

TABLE 2.—*Analysis of spark discharge from oscillogram of figure 7*

$$I_n=\frac{V_n}{\omega L_1}=\frac{13.3\times180\times\text{amplitude}}{2\pi\times5.9\times10^8\times1.15\times10^{-6}}=56.2\times\text{amplitude}.$$

$$R_n=\frac{\delta_n}{\pi\omega C}=42.9\delta_n.$$

$$W=\frac{159600}{2\times5.9\times10^8}=0.0135\ \text{j}.$$

1	2	3	4	5	6	7	8		9		10
Oscillation number	Measured double amplitude	Double amplitude from plot 2 (a), fig. 10	Ratio, $\frac{I_n}{I_{n+1}}$	Decrement	Decrement from plot 2 (b), fig. 10	Effective resistance	Amplitude		Crest current		PR
							Left	Right	Left	Right	
	cm					*ohms*	cm	cm	amp	amp	w
1	2.80	2.80	1.27	0.24	0.234	10.0	1.31	1.49	73	84	61,000
2	2.20	2.20	1.29	.26	.248	10.6	1.03	1.17	58	65	40,000
3	1.70	1.70	1.31	.27	.260	11.2	0.79	.91	44	51	22,000
4	1.30	1.30	1.30	.26	.272	11.6	.61	.69	34	38	15,000
5	1.00	1.00	1.33	.29	.286	12.2	.46	.54	26	30	9,000
6	0.75	0.75	1.36	.31	.298	12.8	.35	.40	20	22	5,000
7	.55	.55	1.38	.32	.312	13.4	.25	.30	14	17	2,000
8	.40	.40	1.33	.29	.324	13.9	.18	.22	10	12	1,400
9	.30	.30			.336	14.4	.14	.16	8	9	800
Total											159,000

2. SPARK CHARACTERISTICS BY MEASUREMENT OF MAGNETIC DEFLECTION

(a) MEASUREMENTS ON TYPICAL IGNITION CIRCUIT

The circuit on which measurements were made by the measurement of voltage across inductance was also used as an example in the method of magnetic deflection. Suitable deflection coils were made and placed in such a position adjacent to the deflection tube that the discharge current produced the oscillogram shown in figure 8. The frequency is in this case 6.6 Mc/s. The deflection constant for the coils in this position was subsequently found to be 15.5 amp/cm., so that the crest current is approximately 84 amp. Table 3 with plot 3 Figure 11 gives the results of measures on this oscillogram.

(b) CALIBRATION

The standard discharge circuit was used to determine the deflection constant of the oscillograph with the deflection coils in the position they occupied during measurements on the typical ignition circuit. The three-turn coil was used in series with the deflection coils, and the total inductance of the circuit was measured by the method described in section IV, 1 (b), page 407. This was 1.95 μh. The capacitance C was 200 $\mu\mu$f. The current in the standard discharge circuit is shown in the oscillogram of figure 9. The frequency was 7.9 Mc/s.

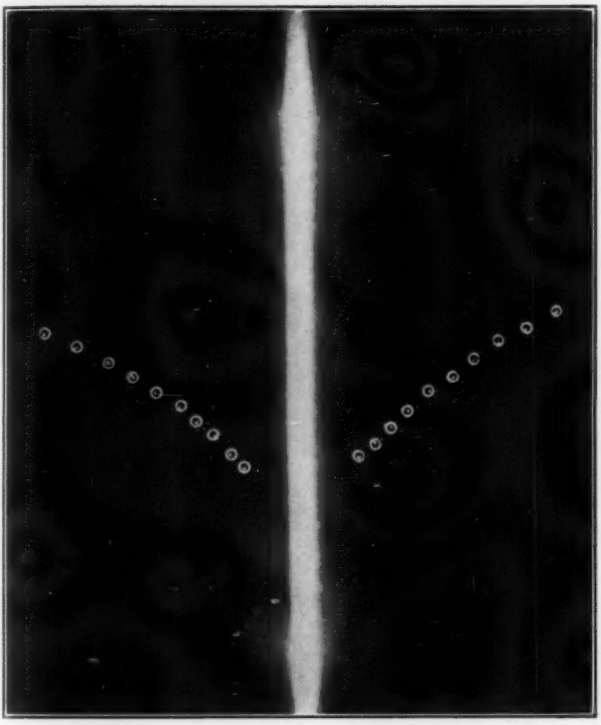

FIGURE 9.—*Oscillogram of spark discharge, obtained for calibration of the oscillograph for measurement of current by magnetic deflection.*

UNIV. OF MICH.

TABLE 3.—*Analysis of spark discharge from oscillogram of figure 8*

$I_n = 15.5 \times$ amplitude.

$W = \frac{158900}{2 \times 6.6 \times 10^6} = 0.0120$ j.

1	2	3	4	5	6	7	8	9	10
Oscillation number	Measured double amplitude	Double amplitude from plot 3 (a), fig. 11	Ratio, $\frac{I_n+I'_n}{I_{n+1}+I'_{n+1}}$	Decrement	Amplitude	Resistance	Resistance, average for half-cycle from plot 3(b) fig. 11	Crest current	I^2R
	cm				cm	*Ohms*	*Ohms*	amp	w
1	10.8	10.80	1.27	0.24	5.4	9.2	9.2	84	65,000
2	8.4	8.50	1.29	.25	4.2	9.8	9.2	65	39,000
3	6.6	6.60	1.29	.25	3.2	9.8	9.2	50	23,000
4	5.1	5.10	1.26	.23	2.4	8.9	9.3	37	12,800
5	4.0	4.05	1.29	.25	1.9	9.8	9.6	29	8,100
6	3.1	3.15	1.31	.27	1.4	10.4	10.4	25	5,000
7	2.3	2.40	1.41	.34	1.0	13.2	11.4	16	2,900
8	1.7	1.70	1.42	.35	0.8	13.5	12.8	12	1,800
9	1.2	1.20	1.50	.40	.5	15.6	14.6	8	900
10	0.8	0.80			.3		16.6	5	400
Total									158,900

The coils were then removed and by measuring the voltage across L_1 in another discharge it was found that the crest current was 53 amp, which corresponds to the maximum deflection of 3.4 cm in figure 9. The deflection constant is therefore $53/3.4 = 15.5$ amp/cm. Table 4 gives the results of measurements made on the oscillogram of figure 9, for which actual measurements are shown on plot 4, figure 11.

TABLE 4.—*Analysis of spark discharge from oscillogram of figure 9*

$I_n = 15.5 \times$ amplitude.

$W = \frac{47200}{2 \times 7.9 \times 10^6} = 0.0024$ j.

1	2	3	4	5	6	7	8	9	10
Oscillation number	Measured double amplitude	Double amplitude from plot 4(a), fig. 11	Ratio, $\frac{I_n+I'_n}{I_{n+1}+I'_{n+1}}$	Decrement	Amplitude	Resistance	Resistance, average for half-cycle, from plot 4(b), fig. 11	Crest current	I^2R
	cm				cm	*Ohms*	*Ohms*	amp	w
1	6.80	6.80	1.13	0.12	3.4	3.8	3.7	53	10,400
2	6.00	6.02	1.14	.13	3.0	4.0	3.9	46	8,300
3	5.20	5.26	1.16	.15	2.6	4.6	4.2	40	6,700
4	4.50	4.53	1.16	.15	2.3	4.6	4.5	36	5,800
5	3.95	3.90	1.18	.17	2.0	5.1	4.9	31	4,700
6	3.30	3.30	1.17	.16	1.7	4.8	5.3	26	3,600
7	2.80	2.81	1.21	.19	1.4	5.9	5.7	22	2,800
8	2.30	2.33	1.24	.22	1.2	6.6	6.2	19	2,200
9	1.90	1.87	1.25	.22	1.0	6.9	6.6	16	1,700
10	1.50	1.50			0.8		7.1	12	1,000
Total									47,200

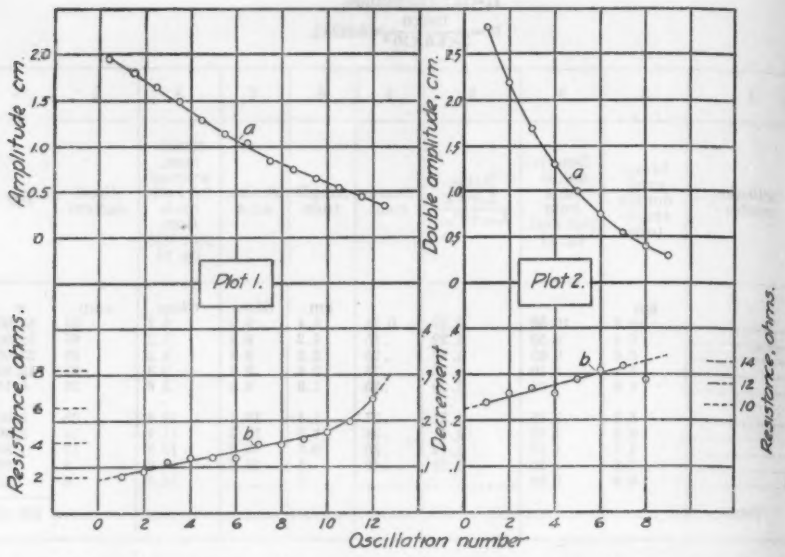

FIGURE 10.—*Measurements of amplitude, decrement, and resistance, from oscillograms shown in figures 6 and 7.*

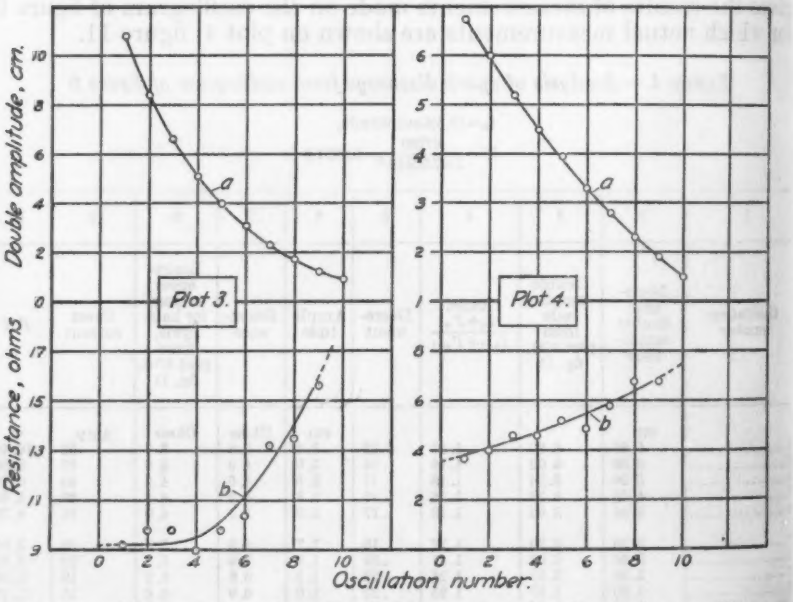

FIGURE 11.—*Measurements of amplitude, decrement, and resistance from oscillograms shown in figures 8 and 9.*

VII. DISCUSSION OF RESULTS

The sources of accidental error in making current or voltage measurements lie chiefly in the measurements of deflection and in determining the sensitivity of the oscillograph. The uncertainty of the values given in the tables for voltage and current from measurements made on the oscillograms is difficult to determine, especially when the cathode beam is deflected so rapidly that no well-defined trace is left on the film.

It is possible to correct the measured values of current for the presence of the measuring circuit. Thus, in the case of the circuit for which measurements are given in table 2, the omission of the L_1 inductor would deduct 1.15 μh from the total inductance of the circuit, leaving 2.45 μh. The crest current of the discharge would be approximately 20 percent greater than that measured. The total energy remains the same.

It will be noted that energy is being dissipated at the rate of 60 kw at 6.5 Mc/s. It is also probable that there are present in the discharge, especially at its beginning, still more powerful transient phenomena, of too high speed to be recorded by the oscillograph. In particular the discharge of the capacitance of the spark plug through the low inductance of the spindle shank may give rise to exceedingly high currents of very short duration. For example, the inductance of the spindle shank of a typical mica spark plug computed from its dimensions is about 0.04 μh, and the measured capacitance ranges from 15 $\mu\mu$f for unshielded plugs to 50 $\mu\mu$f for shielded plugs. Using these values, the natural frequency of the discharge of the plug itself would range from 100 to 200 Mc/s (wave length 3 to 1.5 m), and the crest currents for an initial voltage of 5,000 v would range from 100 to 175 amp. Radiation at these frequencies, as well as at the lower frequency, say 6 Mc/s (wave length 50 m), of the main capacitive part of the ignition circuit, might cause interference with reception in aircraft or automobile radio receivers.

Not all of the energy available in the secondary winding of the magneto or other source of high voltage is stored in the first charge in the capacitance of the circuit. At the end of the capacitive component of the discharge the energy remaining in the winding, or part of it, may appear as an inductive component, in which a unidirectional current of a small fraction of an ampere flows through the circuit for a relatively long time, compared with the time elapsed during the capacitive component. This inductive component is not observable with the high-voltage oscillograph, as the sensitivity of this type of oscillograph is too low. It has, however, been observed with the vibrating-string type of oscillograph [3], and with the low-voltage, hot-cathode type of cathode-ray oscillograph [4].

The "spark" occurring in the secondary circuit of a spark generator on interrupting the primary current usually consists of a number of separate discharges, each of which may consist of a capacitive and an inductive component. In each discharge the decay of the current in the inductive component, if such a component is present, is followed by the rapid rise of resistance of the gap, whereupon the capacitance is again charged to such voltage that the discharge is repeated. The spark ends when there is no longer sufficient energy in the secondary winding to charge the capacitance to the breakdown voltage.

VIII. REFERENCES

[1] BS J. Research **9**, 81 (1932) RP460.
[2] Cir. NBS 74.
[3] Ntl. Advisory Comm. Aeron. Rept. 58 (1920).
[4] Proc. Phys. Soc. (London) **45**, 288 (1933).
[5] Fleming, Principles of Electric Wave Telegraphy and Telephony, 3d ed. (Longmans & Co., London, 1916).
[6] BS Sci. Pap. **17**, 407 (1922) S424.

APPENDIX A

DERIVATION OF EXPRESSION FOR VOLTAGE ACROSS CAPACITANCE OF OSCILLOGRAPH CIRCUIT

In measuring the voltage across a portion of the inductance of the discharge circuit, the oscillograph and connecting leads constitute a circuit coupled inductively with the discharge circuit. The voltage across the deflection plates can be found by mathematical methods usually applied to such circuits. Consider the closed circuit $L_1L'C'R'$ of figure 1. If, as has been assumed, the discharge itself is not appreciably affected by the presence of the measuring circuit, the electromotive force introduced into this circuit in a spark discharge is given by eq 2, viz:

$$v_{L_1}=\frac{V_oL_1}{\omega L}\sqrt{\alpha^2+\omega^2}e^{-\alpha t}\cos(\omega t+\theta) \tag{1a}$$

Applying Kirchhoff's law to this circuit, the resulting equation is

$$(L_1+L')\frac{di_2}{dt}+R'i_2+v_C=v_{L1} \tag{2a}$$

where i_2 is the instantaneous current in the oscillograph circuit, and v_C is the instantaneous voltage across the capacitance in this circuit.

Since

$$i_2=C'\frac{dv_C}{dt} \tag{3a}$$

eq 2a may be written

$$\frac{d^2v_C}{dt^2}+\frac{R'}{(L_1+L')}\frac{dv_C}{dt}+\frac{v_C}{(L_1+L')C'}= \tag{4a}$$
$$\frac{V_oL_1}{\omega L(L_1+L')C'}\sqrt{\alpha^2+\omega^2}e^{-\alpha t}\cos(\omega t+\theta)$$

Writing $\lambda=R'/2(L_1+L')$ and $\beta^2=1/C'(L_1+L')$, this becomes

$$\frac{d^2v_C}{dt^2}+2\lambda\frac{dv_C}{dt}+\beta^2v_C=\frac{\beta^2V_oL_1}{\omega L}\sqrt{\alpha^2+\omega^2}e^{-\alpha t}\cos(\omega t+\theta) \tag{5a}$$

The general solution of this equation is the sum of a particular integral and a complementary function. The latter is of the form $(Ae^{-m_1t}+Be^{-m_2t})$, where m_1 and m_2 are the roots of the auxiliary equation

$$m^2+2\lambda m+\beta^2=0 \tag{6a}$$

The particular integral may be found by the usual method of factorizing the left-hand side of eq 5a and finding the integrating factors of the resulting first-order equations. The complete solution is

$$v_C=\frac{V_0L_1}{P\omega L}\sqrt{\alpha^2+\omega^2}e^{-\alpha t}\cos(\omega t+\theta+\psi)$$
$$+A_1e^{-(\lambda-\sqrt{\lambda^2-\beta^2})t}+A_2e^{-(\lambda+\sqrt{\lambda^2-\beta^2})t} \tag{7a}$$

Here λ and β have the meanings given above,

$$\beta\psi=\tan^{-1}2\omega(\alpha-\lambda)/(\alpha^2+\beta^2-2\alpha\lambda-\omega^2), \text{ and}$$

$$P^2=1+\frac{2(\alpha^2-2\alpha\lambda-\omega^2)}{\beta^2}+\frac{4\lambda}{\beta^4}(\lambda-\alpha)(\alpha^2+\omega^2)+\frac{(\lambda^2+\omega^2)^2}{\beta^4}$$

The integration constants A_1 and A_2 may be determined, if desired, from the initial conditions.

The first term on the right-hand side of the equation represents a forced oscillation in the measuring circuit, and it is this quantity which is to be measured. The second and third terms represent parasitic transients, and it is desirable that these be damped out very quickly. To do this, λ should be made large compared with β, by including resistance in the oscillograph circuit. If $\beta>\lambda$ the transients will be oscillatory rather than aperiodic, and eq 7a then takes the form which represents two superimposed oscillations in the measuring circuit, well known in the theory of spark telegraphy and the theory of the induction coil [5, 6].

It is desirable that P in eq 7a be approximately equal to unity and that the angle ψ be small, but the experimental limitations in the choice of C' and L' may sometimes mean that these desiderata cannot be obtained.

The correction factor to be applied to the observed voltage v_C across the capacitance of the oscillograph circuit to find the voltage v_{L_1} across L_1 is obtained by comparing the maximum voltage V_n of the nth cycle derived from eq 1a, with $(V_C)_n$ derived from eq 7a.

Thus

$$V_n=\frac{V_0L_1}{\omega L}\sqrt{\alpha^2+\omega^2}e^{-\frac{\alpha}{\omega}(n\pi-\theta)} \tag{8a}$$

and

$$(V_C)_n=\frac{V_0L_1}{P\omega L}\sqrt{\alpha^2+\omega^2}e^{-\frac{\alpha}{\omega}(n\pi-\theta-\psi)} \tag{9a}$$

assuming that the second and third terms on the right-hand side of eq 7a have become negligibly small.

Dividing eq 8a by eq 9a,

$$Q=\frac{V_n}{(V_C)_n}=Pe^{-\frac{\alpha\psi}{\omega}} \tag{10a}$$

The quantity Q is found experimentally by method described in section IV, 2, page 407.

APPENDIX B

DISPLACEMENT OF LINE OF ZERO VOLTAGE ON AN OSCILLOGRAM

It sometimes occurs, as in figure 6, that when the voltage being measured becomes zero the cathode beam of the oscillograph remains deflected away from its position for zero voltage on the deflection plates. This is due to the action of the capacitance voltage divider. It commonly occurs when recurrent voltage impulses are applied to the oscillograph, between which impulses the voltage is constant or decays slowly, so that a charge remains on the high-tension circuit at the beginning of the next discharge.

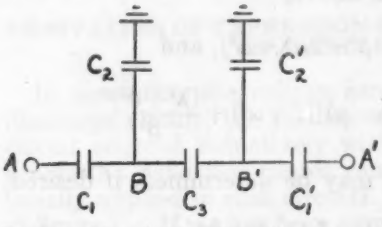

FIGURE 12.—*Schematic diagram of capacitance voltage divider.*

Figure 12 shows the divider circuit, with C_3 representing the deflection plates of the oscillograph. Suppose a constant potential $\overline{V}_A$ is applied to A until leakage reduces the potential at B and B' to zero. A' is assumed to be at zero potential. Since $\overline{V}_B=\overline{V}'_B=0$, the cathode beam is not deflected. The charge which has leaked onto B is $\overline{V}_AC_1$. If the voltages at A and A' are suddenly changed to values V_A and V'_A, respectively, the potentials of conductors B and B' take corresponding values V_B and V'_B. Before appreciable leakage has taken place the total charge on B is

$$-\overline{V}_AC_1=(V_B-V_A)C_1+(V_B-V'_B)C_3+V_BC_2 \tag{1b}$$

Since the charge on B' remains zero

$$0=(V'_B-V_B)C_3+(V'_B-V'_A)C'_1+V'_BC'_2 \tag{2b}$$

Solving eq 1b for V_A,

$$V_A=V_B\left(1+\frac{C_2}{C_1}+\frac{C_3}{C_1}\right)-V_B\frac{C_3}{C_1}+\overline{V}_A \tag{3b}$$

In a similar manner V'_A is obtained from eq 2b,

$$V'_A=V'_B\left(1+\frac{C'_2}{C'_1}+\frac{C_3}{C'_1}\right)-V_B\frac{C_3}{C'_1} \tag{4b}$$

Subtracting eq 4b from eq 3b and putting $C_2/C_1=C'_2/C'_1$, which is a necessary operating condition for the voltage divider [1], and

$$K=1+\frac{C_2}{C_1}+C_3\left(\frac{1}{C_1}+\frac{1}{C'_1}\right)$$

the result is

$$V_A-V'_A=(V_B-V'_B)K+\overline{V}_A, \text{ or } V_B-V'_B=\frac{V_A-V'_A}{K}-\frac{\overline{V}_A}{K} \tag{5b}$$

The presence of the term $\overline{V}_A/K$ shows that a deflection proportional to this quantity is added to the deflection in one direction and subtracted in the opposite direction. This is equivalent to a displacement of the zero line in an oscillogram of alternating voltage. It can be prevented by reducing $\overline{V}_A$ to zero in the interval between sparks, either by means of a shunting resistance of the proper value or by momentarily grounding the circuit.

WASHINGTON, July 23, 1937.

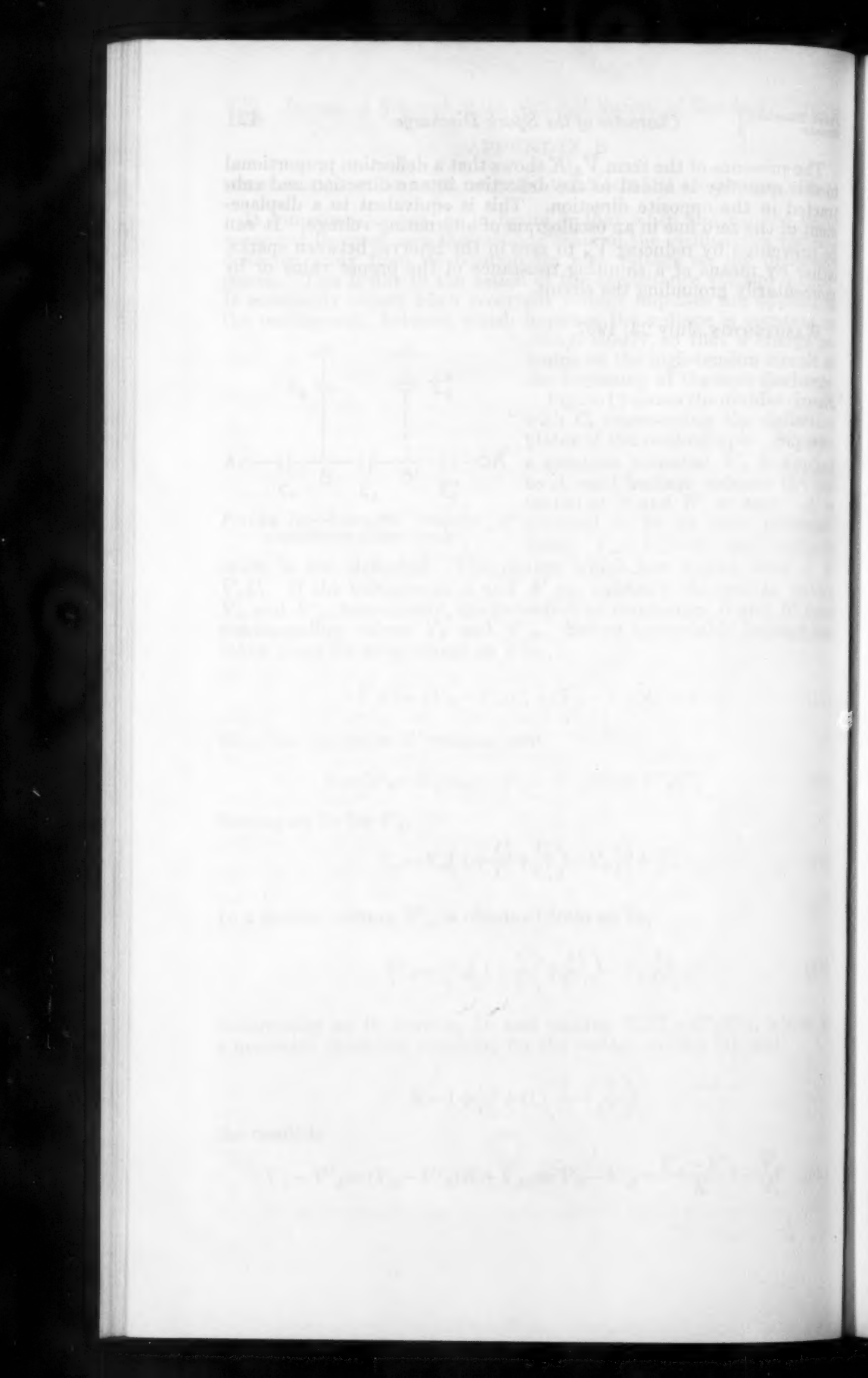

U. S. Department of Commerce National Bureau of Standards

RESEARCH PAPER RP1033

Part of Journal of Research of the National Bureau of Standards, Volume 19, October 1937

SEPARATION OF THE THREE METHYLOCTANES FROM MIDCONTINENT PETROLEUM [1]

By Joseph D. White [2] and Augustus R. Glasgow, Jr.[2]

ABSTRACT

The complex methyloctane fraction of an Oklahoma petroleum has been successfully separated into its constituent hydrocarbons. The isolation of three of its seven components, 2-, 3-, and 4-methyloctane, by alternating distillation with extraction and crystallization is described. The three, in the order named, are present in petroleum in the proportion of 3, 1, and 1; the total methyloctane content of the crude oil being about 0.3 percent.

The boiling point, freezing point, density, refractive index, and critical solution temperature in aniline have been determined for each compound.

CONTENTS

	Page
I. Introduction	423
II. Procedure	424
1. Preliminary fractionation	424
2. Isolation of 2-methyloctane	426
3. Isolation of 3-methyloctane	427
4. Isolation of 4-methyloctane	430
III. Properties of the isolated compounds	432
IV. Content of the methyloctanes in the petroleum	434
V. References	435

I. INTRODUCTION

The presence of the methyloctane fraction in an Oklahoma petroleum [3] became apparent when, a few years ago, the material boiling normally between 140 and 145° C was redistilled after first removing the aromatic hydrocarbons by extraction [1].[4] More recently, Tongberg, Fenske, and Nickels [2] have encountered the same fraction in petroleum from the Yates field in Texas. Besides *o*-xylene, which was extracted, not less than six hydrocarbons are present in the fraction from Oklahoma petroleum, namely, two naphthenes and four isomeric nonanes. It is not surprising, therefore, to find so little recorded concerning the composition of the corresponding fractions in other petroleums.

Separation of the methyloctane fraction into its constituent hydrocarbons is not an easy task. There is no record that it has been done previously. To carry out the separation successfully has required the judicious use of distillation, extraction, absorption, and crystallization, with the aid of modern and efficient fractionating equipment.

[1] Financial assistance has been received from the research fund of the American Petroleum Institute. This work is part of Project 6, The Separation, Identification, and Determination of the Constituents of Petroleum. This paper was presented before the American Chemical Society meeting in Rochester, September 1937.

[2] Research Associate at the National Bureau of Standards, representing the American Petroleum Institute.

[3] A description of the oil is given in BS J. Research **2**, 469, table 1 (1929) RP45, and in J. Research NBS **15**, 212 (1935) RP824.

[4] Numbers in brackets throughout the text indicate references listed at the end of the paper.

II. PROCEDURE

1. PRELIMINARY FRACTIONATION

After extracting the xylenes with liquid sulphur dioxide, the material was systematically distilled at a pressure of 215 mm through a 30-plate column equipped with bubbling caps. Results of the distillation are shown in figure 1. The lower graph gives the volume of distillation fractions boiling successively in intervals of 0.5° C. In all, nearly 17 liters (representing 2,250 liters of crude oil) distilled within the range 98 to 104° C, which corresponds approximately to 140.5 to 146° C at normal pressure. The upper graph of unshaded lines shows the refractive index [5] of each half-degree fraction of distillate. The range in index indicates, in the absence of more than small amounts of aromatic hydrocarbons, that the distillate was composed of a mixture of some of the nonanaphthenes and isononanes known to boil in this region of temperature.

Nitration tests indicated that on the average the material contained about 2 mole percent of aromatic hydrocarbons. To free the distillate from these constituents, all fractions boiling between 98 and 103.5° C were filtered through columns of silica gel. The procedure has been described elsewhere [3]. Briefly, fractions of distillate with narrow boiling ranges were filtered through glass columns, 3 by 50 cm, filled with gel of 40- to 200-mesh obtained from the Silica Gel Corporation, of Baltimore. The effect of the filtration was, by adsorption of the aromatic constituents, to lower somewhat the refractive index of the filtrate. When the index of the latter began to rise towards that of the material being filtered, the gel was considered saturated and was replaced with a fresh supply. On refiltering the oil, its refractive index remained unchanged. The index of the filtrate was now lower by 0.0001 than that of the material which had been treated with nitrating mixture. From these facts it was concluded that the aromatic constituents had been effectively removed. Adsorbed oil was recovered from the spent gel by displacing with water, either by leaching or distilling with steam. The results of the filtration are shown in table 1.

TABLE 1.—*Volumes and refractive index of the distillation fractions before and after filtering through silica gel*

Boiling range at 215 mm before filtering	Volume				Refractive index		
	Before filtering	After filtering		Lost by filtering	Before filtering, n_D^{25}	After filtering	
		Filtrate	Adsorbed			Filtrate, n_D^{25}	Adsorbed, n_D^{25}
°C	ml	ml	ml	ml			
98 to 100.5	5,230	4,905	210	115	1.415	1.4125	1.445
100.5 to 102.0	5,850	5,380	360	110	1.4125	1.4115	1.425
102.0 to 103.5	5,660	5,150	460	50	1.418	1.416	1.433

The refractive index of the filtrate is shown in more detail in the graph of shaded lines in the upper part of figure 1. Both refractive-index graphs show that, whereas each of the half-degree fractions

[5] All refractive indices recorded in this paper are for n_D^{25} unless specified otherwise. Those obtained for the purpose of routine analysis were determined at 25° C. The indices of the final purified products were determined at 20° C.

boiling below 100.5° C was filtered separately, the fractions boiling between 100.5 and 102° C and between 102 and 103.5° C were mixed before filtering. Arrows in the lower part of the figure show the boiling range of the mixtures; dotted lines in the upper part show

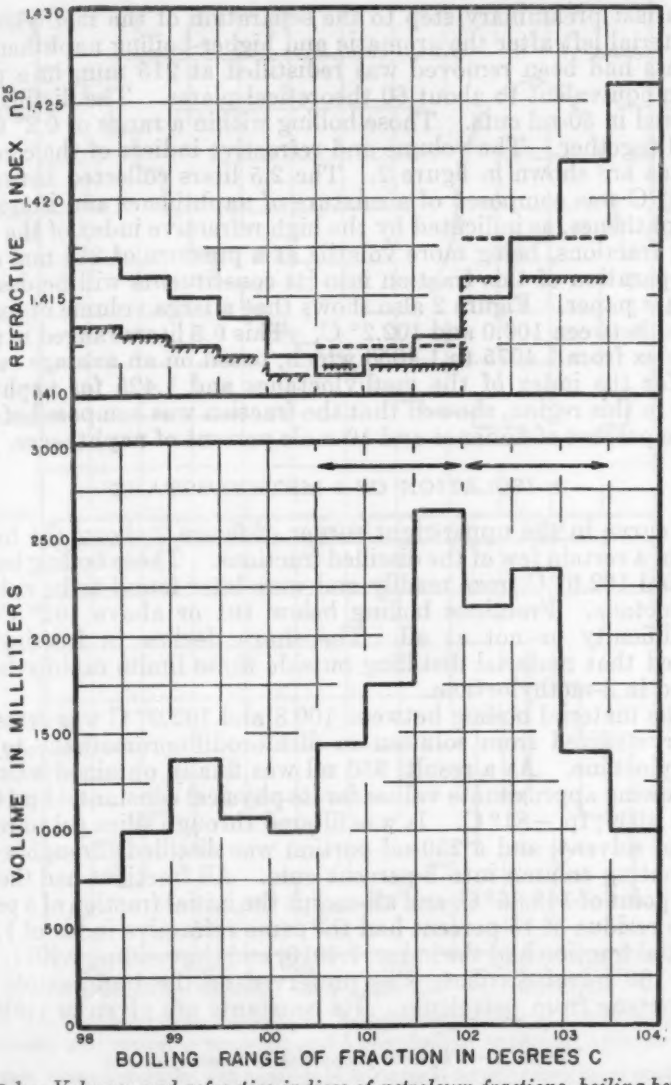

FIGURE 1.—*Volumes and refractive indices of petroleum fractions, boiling between 98 and 104° C at 215 mm, after extraction with sulphur dioxide and redistillation.*

Lower graph, volume distribution with respect to boiling range; upper unshaded graph, refractive indices; upper shaded graph, refractive indices after filtration through silica gel. For explanation of arrows and dotted lines, see text.

their refractive indices before filtering. The mixing was done in order to expedite filtration of fractions requiring a subsequent distillation with glacial acetic acid to remove the higher-boiling more-refracting naphthenes present [4, 5]. Of the total 15.5 liters of fil-

trate, 10.5 liters which boiled between 100.5 and 103.5° C (142.5 and 145.5° C at 760 mm) was distilled with acetic acid with the result that about 4 liters, enriched in naphthenes boiling normally at 146° C or above, was displaced, leaving a 6.5-liter fraction in which isononanes alone were concentrated.

As a last preliminary step to the separation of the methyloctanes, all material left after the aromatic and higher-boiling naphthene constituents had been removed was redistilled at 215 mm, in a packed column equivalent to about 60 theoretical plates. The distillate was recovered in 50-ml cuts. Those boiling within a range of 0.2° C were poured together. The volume and refractive indices of the combined fractions are shown in figure 2. The 2.5 liters collected between 98 and 99° C was composed of a mixture of naphthenes and isononanes, the naphthenes, as indicated by the high refractive index of the lower-boiling fractions, being more volatile at a pressure of 215 mm of Hg. The separation of this fraction into its constituents will be described in a later paper. Figure 2 also shows that a large volume of material distilled between 100.0 and 102.2° C. This 6.5 liters ranged in refractive index from 1.4075 to 1.4050 which, based on an average value of 1.403 for the index of the methyloctanes and 1.425 for naphthenes boiling in this region, showed that the fraction was composed of about 90 mole percent of nonanes and 10 mole percent of naphthenes.

2. ISOLATION OF 2-METHYLOCTANE

The curve in the upper-right corner of figure 2 shows the freezing points of a certain few of the distilled fractions. Those boiling between 101.0 and 102.0° C froze readily and were later found to be rich in 2-methyloctane. Fractions boiling below 101 or above 102° C froze with difficulty or not at all. The sharp decline in freezing point indicated that material distilling outside these limits rapidly became depleted in 2-methyloctane.

All the material boiling between 100.8 and 102.0° C was systematically crystallized from solution in dichlorodifluoromethane to yield 2-methyloctane. As a result, 350 ml was finally obtained which had the following approximate values for its physical constants: bp 143.35° C; n_D^{25} 1.4009; fp −81° C. It was filtered through silica gel to remove traces of solvent, and a 250-ml portion was distilled through a small fractionating column into 5-percent cuts. All fractions had the same boiling point of 143.35° C, and all except the initial fraction of 5 percent and the residue of 15 percent had the same refractive index of 1.4008. The initial fraction had the index, 1.4010, and the residue, 1.4011. The middle 100 ml of distillate was preserved as the best sample of 2-methyloctane from petroleum. Its constants are given in table 2.

TABLE 2.—*Physical properties of 2-methyloctane*

Sample	Normal boiling point	Freezing point	Specific gravity, d_4^{20}	Refractive index n_D^{20}	cst in aniline	Combustion analysis
	°C	°C			°C	*Moles* H_2O / *Moles* CO_2
From Oklahoma petroleum	[a] 143.255	−80.49±.02	[b] 0.7134	1.4032	77.5±0.5	1.111±.005
Whitmore and Southgate	[c] 142.80	[c] −80	[c] .7107	[c] 1.40285		

[a] Determined by E. R. Smith of this Bureau. dt/dp=0.0495.
[b] Determined by the Division of Weights and Measures of this Bureau.
[c] Private communication from H. A. Southgate and F. C. Whitmore, Pennsylvania State College.

3. ISOLATION OF 3-METHYLOCTANE

After a process of interlocking distillation with crystallization to remove effectively the 2-methyloctane, all mother liquors which

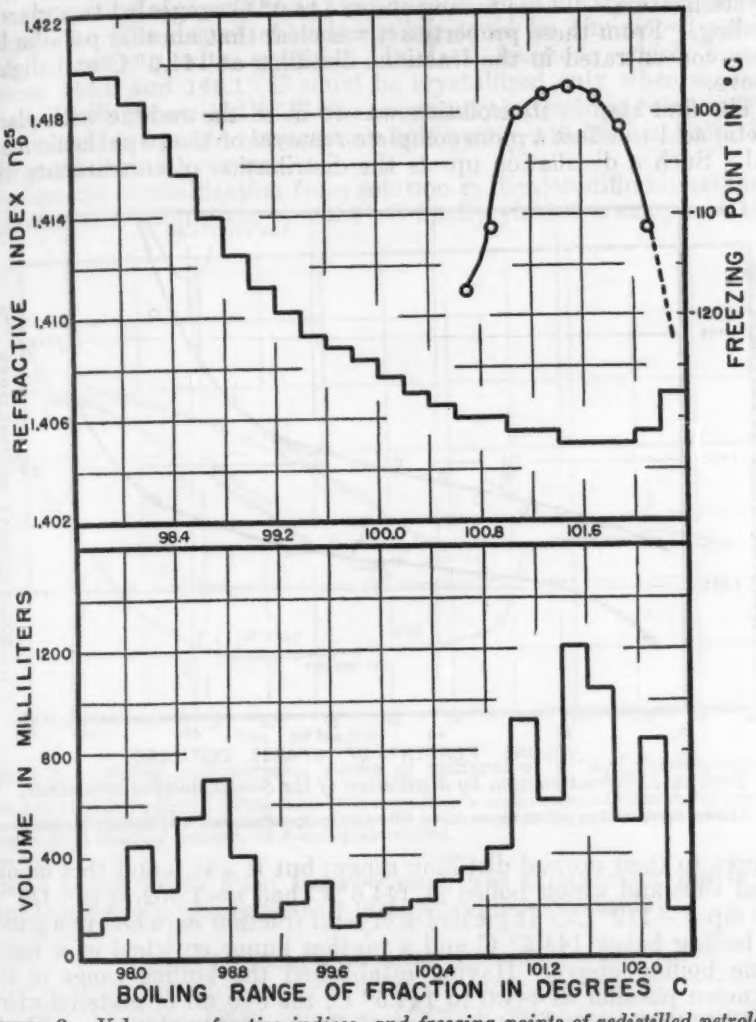

FIGURE 2.—*Volumes, refractive indices, and freezing points of redistilled petroleum fractions after removing aromatic and higher-boiling naphthene hydrocarbons.*

Lower graph, volume distribution with respect to boiling range at 215 millimeters; upper graph, refractive indices; curve at upper right, freezing points

boiled above 143.6° C, together with the distillation stock boiling up to 144.4° C (102.4° C at 215 mm), were redistilled into 50-ml fractions. About 500 ml of distillate and 600 ml of still residues were obtained. The distillate boiled between 143.8 and 144.2° C, ranged in refractive index from 1.404 to 1.405 and, from combustion analysis, contained 5

percent of naphthenes.[6] The residue boiled at 144.6° C and contained about 20 percent of naphthenes. Fractions boiling at 144.0° C froze at −117° C but did not fractionate on crystallization. Those boiling below 144.0° C froze above −117° C and yielded 2-methyloctane on crystallization. Those boiling above 144.0° C congealed to a glass on cooling. From these properties it was clear that another paraffin had been concentrated in the fractions distilling at 144.0° C and slightly above.

The first step in its isolation was to distil the residue with glacial acetic acid to effect a more complete removal of the naphthenic material. Such a distillation upsets the distribution of constituents with

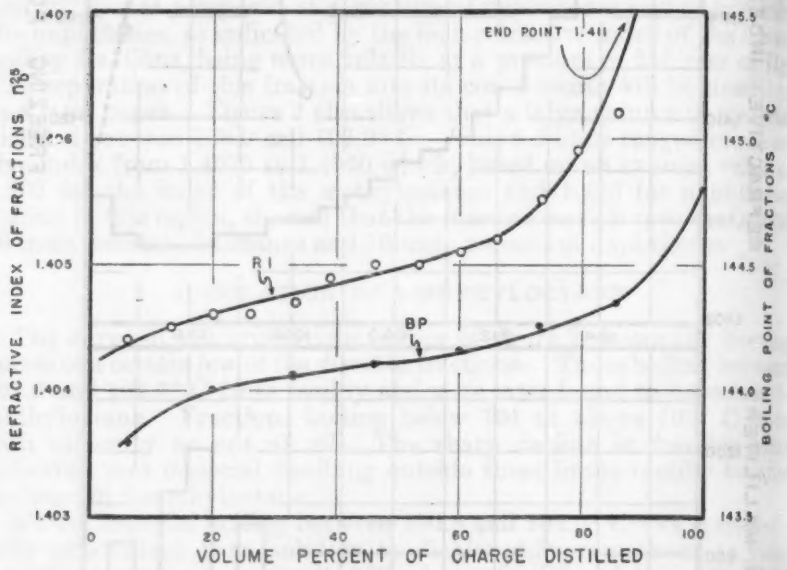

FIGURE 3.—*Fractionation by distillation of the 3-methyloctane concentrate.*

Lower curve, boiling points; upper curve, refractive indices of successive distillation fractions.

respect to their normal distilling range; but it was found that oil distilled thus and which boiled at 144.6° C had $n=1.409$, fp = −116° C and mp = −112° C. It yielded a crystal fraction enriched in a paraffin boiling below 144.5° C and a mother liquor enriched in a naphthene boiling above. Having established the boiling range of the unknown paraffin as 144.0 to 144.5° C, the 800 ml of material which boiled within these limits was carefully fractionated at atmospheric pressure. The results are shown in figure 3. The cooling and warming curve of a 50-ml cut, taken after 60 percent of the charge had been distilled, is shown in curve *I* of figure 4. The cut boiled at 144.2° C, had nearly the formula C_9H_{20}, a refractive index of 1.4052, froze at −114.0° C and melted at −111.5° C. A mixture of the sample with an equal amount of 2-methyloctane boiled at 143.85° C. Its cooling and warming curves are shown as curve *II* in figure 4. The initial freezing point of −90° C is that of excess 2-methyloctane.

[6] The combustion analyses of the paraffin-naphthene hydrocarbon mixtures studied in this work are made by determining the ratio of moles H_2O/moles CO_2 with an average deviation of ±0.0005. This enables one to express the composition of the mixture in moles percent of naphthenes and nonanes to within about 0.5 percent. For the method of combustion used, see Rossini, BS J. Research 8, 121 (1932) RP405.

The eutectic halt occurred at −114.5° C. Extrapolation of the melting curve indicated that the eutectic point was near −113.5° C. A property of the distilled fraction was its tendency to undercool greatly before crystallizing. The undercooling of 15° C and the prolonged induction period of crystallizing are typical of all of the fractions shown in figure 3. The degree of undercooling could be diminished somewhat by seeding with crystals.[7] In fact, fractions which boiled between 144.0 and 144.1° C could be crystallized only when seeded. Material boiling near 144.0° C was apparently eutectic in composition as indicated by a single temperature halt near −113.5° C in both the cooling and warming curves.

Systematic crystallization from solution in dichlorodifluoromethane of all distillate boiling above 144.1° C finally yielded a sample of the

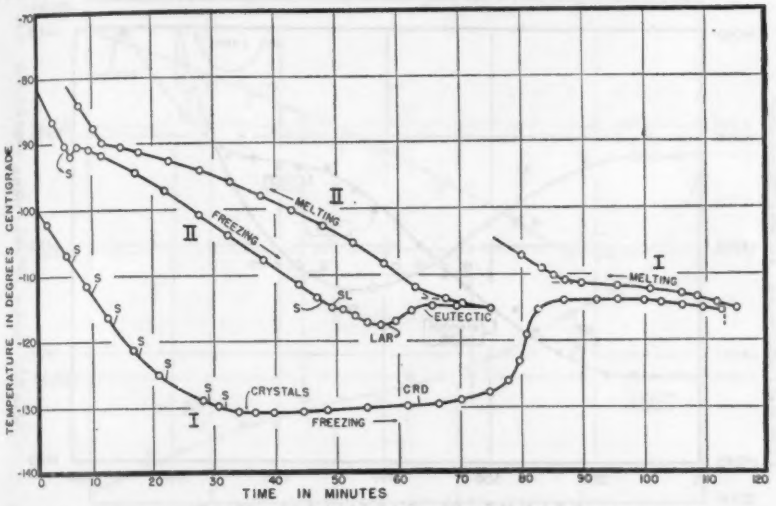

FIGURE 4.—*Cooling and warming curves of mixtures of 2- and 3-methyloctane.*

Curve *I*, for a distillation fraction boiling at 144.2° C; curve *II*, for a mixture of equal volumes of the sample used for curve *I* and of 2-methyloctane. *S*, stirred with a cold rod to induce crystallization; *SL*, stirrer labored; *LAR*, liquid air removed; *CRD* cooling rate reduced.

nonane which, when freed from solvent, was of sufficient purity to identify it from its properties as 3-methyloctane. See table 3.

TABLE 3.—*Physical properties of 3-methyloctane*

Sample	Normal boiling point	Melting point	Specific gravity, d_4^{20}	Refractive index, n_D [3]	cst in aniline	Combustion analysis
	°C	°C			°C	*Moles* H_2O / *Moles* CO_2
From Oklahoma petroleum	[a] 144.180	−108.00 ±.05	[b] 0.7210	1.4065	75.0 ±0.5	1.1095 ±.0004
Synthetic (*l*-form)	[c] 143 to 144		[d] .720	[e] 1.4075		

[a] Determined by E. R. Smith of this Bureau. $dt/dp = 0.0495$.
[b] Determined by the Division of Weights and Measures of this Bureau.
[c] Levene and Marker, J. Biol. Chem. 91, 101 (1931).
[d] Calculated from value given for 27° C.
[e] Calculated from value given for 25° C.

[7] Crystals for seeding were obtained by cooling a small portion of the fraction mixed with dichlorodifluoromethane to reduce its viscosity.

4. ISOLATION OF 4-METHYLOCTANE

Figure 5 shows the results of distilling the lower-boiling residues from the fractional crystallization of 2-methyloctane. The lower curve in the figure reveals two boiling-point plateaus, one at 142.4° C, the other near 143.4°. Freezing points of fractions boiling at these temperatures are shown by the numbers in the boxes. Material boiling at the higher temperature crystallized readily to yield 2-methyloctane. Fractions boiling at 142.4° C would freeze while those boiling near 142.7° C would not. They became very viscous at −130° C and congealed to glasses on further cooling. The constant-boiling nature, the freezing behavior, and low refractive index of the distillate which boiled at 142.4° C indicated that it was a concentrate of another paraffin hydrocarbon. To obtain more of the compound, all distilla-

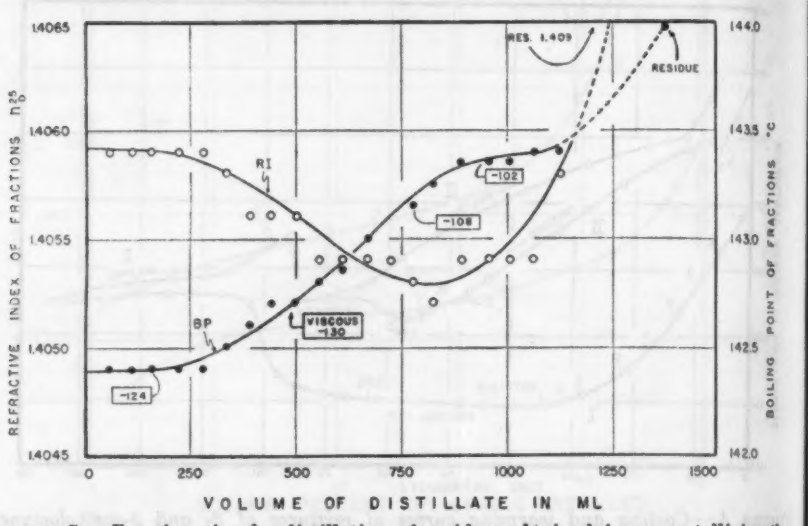

FIGURE 5.—*Fractionation by distillation of residues obtained from crystallizing the 2-methyloctane concentrate.*

Black circles indicate boiling points, white circles indicate refractive indices of successive distillation fractions. Numbers in the boxes indicate freezing points.

tion stock boiling normally between 141 and 143° C was first distilled at 215 mm to remove the lower-boiling naphthenes. Subsequently, the material obtained by this procedure which boiled between 142 and 143° C was distilled with acetic acid to separate higher boiling naphthenes. As a result, 2 liters was obtained which boiled within the range 141.5 to 143.4° C. The material ranged in refractive index from 1.410 to 1.404 and, from combustion analysis, varied in naphthene content from 20 to 5 mole percent. Assuming the refractive index of the naphthenic material to be 1.425, the paraffin base of the distillate was calculated to vary in refractive index from 1.406 to 1.403. The range could be explained by assuming that the detected paraffin boiling near 142.4° C was mixed with a lower-boiling paraffin having a higher refractive index and with 2-methyloctane with a lower index. Further analysis proved this assumption to be correct. A systematic distillation at normal pressure of the 2-liter fraction yielded at last 1 liter of distillate boiling between 142.0 and 143.0° C. The results of the final

distillation are shown in figure 6. The boiling-point curve shows, as did the curve in figure 5, a region of minimum slope centering on 142.4° C. Apparently the distillation did not improve the concentration of the detected compound. It did reveal, none the less, that the compound was present in limited quantities and that the composition of the material, which originally distilled between 141.5 and 143° C, was quite complex. Additional evidence indicated that the material contained at least five compounds. Of the final distillate, 250 ml, representing the middle portion, was subjected to further fractionation by crystallization. The 50-ml distillation cuts comprising this fraction contained on the average 10 mole percent of naphthenes and probably a greater amount of paraffinic constituents other than the one

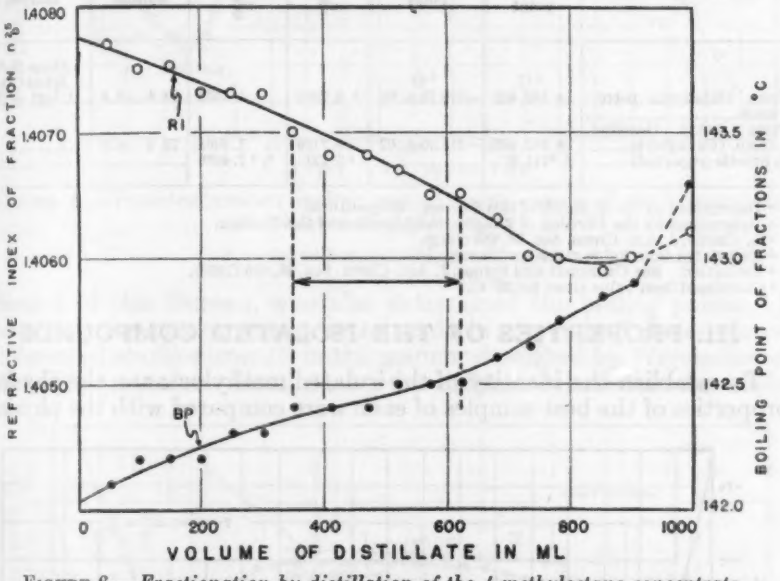

FIGURE 6.—*Fractionation by distillation of the 4-methyloctane concentrate.*

Lower curve, boiling points; upper curve, refractive indices of successive distillation fractions. The arrow indicates the portion of the distillate subsequently subjected to fractional crystallization.

being concentrated. The cuts were, however, largely composed of the desired component. None of them showed a normal cooling behavior. Between −125 and −130° C each became suddenly viscous and thereupon produced a temperature halt which in all respects resembled true crystallizing behavior, with the exception that no definitely visible crystals were formed. At this stage the samples were faintly turbid and had the consistency of stiff glue.

Crystallization of the 250-ml fraction from a solution in propane and methane by the method described by Leslie [6] yielded a 70-ml sample of hydrocarbon which, when freed from solvent, boiled at 142.4° C, had a refractive index of 1.4055, and melted at −119° C. By combustion it was found to be composed of 5.7 mole percent of naphthenes and 94.3 percent of isononanes. Of the latter, 4-methyloctane (see table 4) and 3-ethylheptane [8] boil, respectively, at

[8] A sample of 3-ethylheptane was lent to us by F. C. Whitmore and H. P. Orem, of the Pennsylvania State College.

142.5 and 143.1° C. Since the petroleum fraction had a lower boiling point and a lower refractive index than 3-ethylheptane, and since there is no evidence that this petroleum contains 3-ethylheptane in more than negligible amounts, if at all, it was concluded that the sample of petroleum in question was a concentrate of 4-methyloctane. Confirmatory evidence of this was obtained from the slight elevation of the melting point when 5 percent of synthetic 4-methyloctane was added to the sample.

TABLE 4.—*Properties of 4-methyloctane*

Sample	Normal boiling point	Melting point	Specific gravity, d_4^{20}	Refractive index, n_D^{20}	cst in aniline	Combustion analysis
	°C	°C				*Moles* H_2O / *Moles* CO_2
From Oklahoma petroleum	[a] 142.433	−119.13±.05	[b] 0.7245	1.4078	73.4 ±0.5	1.1047 ±.0005
From Ethyl Gasoline Corp. (Calingaert)	[a] 142.485	−113.30±.02	[b] .7199	1.4061	74.5 ±.5	
Synthetic (reported)	[c, d] 141.3		[c] 0.721	[c, f] 1.4050		

[a] Determined by E. R. Smith of this Bureau. $dt/dp=0.0492$.
[b] Determined by the Division of Weights and Measures of this Bureau.
[c] L. Clarke, J. Am. Chem. Soc. **34**, 683 (1912).
[d] Calculated from value given for 771 mm.
[e] Estimated. See Calingaert and Soroos, J. Am. Chem. Soc. **58**, 635 (1936).
[f] Calculated from value given for 25° C.

III. PROPERTIES OF THE ISOLATED COMPOUNDS

To establish the identity of the isolated methyloctanes, the physical properties of the best samples of each were compared with the physical

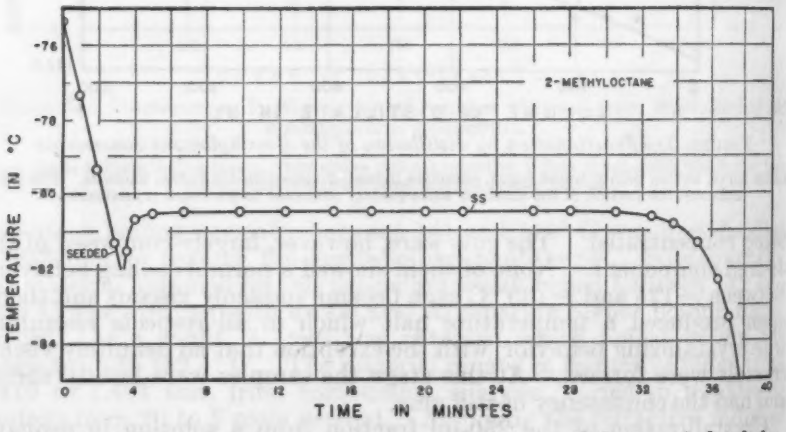

FIGURE 7.—*Time-temperature cooling curve of the 2-methyloctane isolated from petroleum.*

properties reported for the corresponding synthetic compound. In cases where the reported densities showed large discrepancies, values were computed from the molecular volume data correlated by Calingaert and Hladky [7]. Results of the comparisons are given in tables 2, 3, and 4. The errors indicated are average deviations. A similar comparison was made, in the case of 4-methyloctane, with a sample

of high purity lent to us by Dr. Calingaert of the Ethyl Gasoline Corporation in Detroit (see table 4). Ebulliometric tests of purity were made on the samples by E. R. Smith of the Physical Chemistry

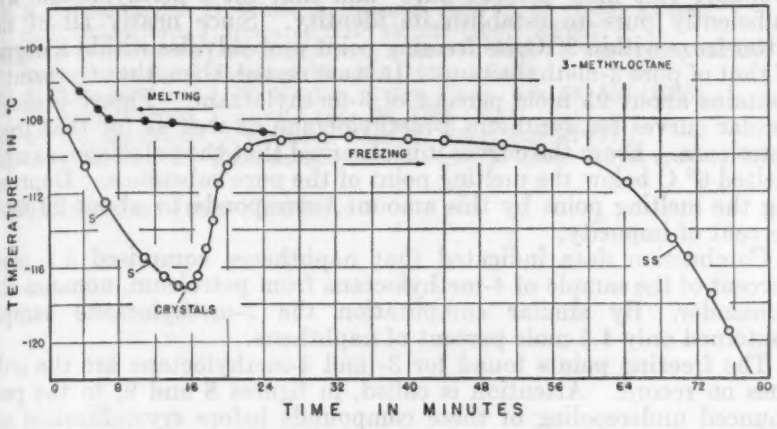

FIGURE 8.—*Time-temperature cooling and warming curves of the 3-methyloctane isolated from petroleum.*

S, seeded with crystals; *SS*, stirrer stopped.

Section of this Bureau, who also determined the boiling points. In each case the measurements were made in a standard Świętosławski differential ebulliometer [8] in the manner described by Wojciechowski [9]. The tests were based on Δt, the difference between the boiling

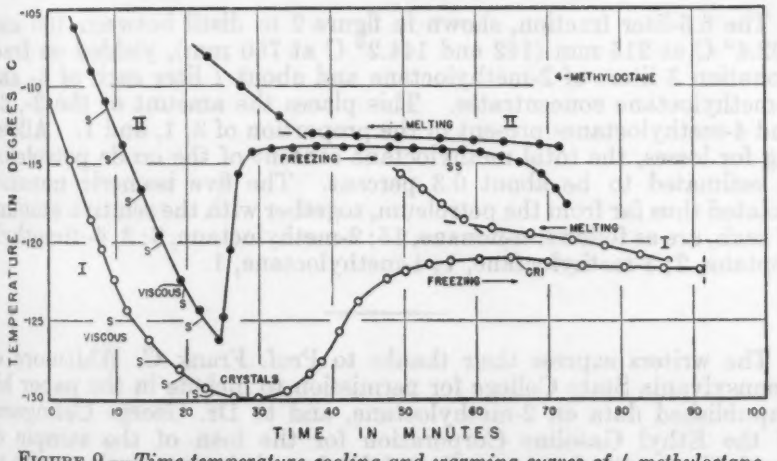

FIGURE 9.—*Time-temperature cooling and warming curves of 4-methyloctane.*

Curve *I*, from petroleum; curve *II*, from the Ethyl Gasoline Corporation.
S, seeded with crystals; *CRI*, cooling rate increased, *SS*, stirrer stopped.

and condensation points. Although the magnitude of the difference depends upon the nature of the impurity as well as the amount, a relative idea of purity is thus obtained. The values found for Δt were all small, 0.015° C for 2-methyloctane, 0.028° C for 3-methyloctane, and 0.036° C for 4-methyloctane.

As a further test of purity, the behavior of the samples during cooling and warming was observed. The freezing and melting curves shown in figures 7 and 8 indicate that the sample of 2-methyloctane was probably 99.9 mole percent pure [9] and that the 3-methyloctane was sufficiently pure to establish its identity. Since nearly all of the latter froze within 2° C, its freezing point probably lies within a degree of that of pure 3-methyloctane. It is estimated, then, that the sample contains about 95 mole percent of 3-methyloctane. Figure 9 shows similar curves for synthetic 4-methyloctane as well as for that from petroleum. From the curves it is observed that the petroleum sample melted 6° C below the melting point of the pure substance. Depressing the melting point by this amount corresponds to about 20 mole percent of impurity.

Combustion data indicated that naphthenes comprised 5.7 mole percent of the sample of 4-methyloctane from petroleum, nonanes the remainder. By similar computation the 3-methyloctane sample contained only 1.5 mole percent of naphthene.

The freezing points found for 3- and 4-methyloctane are the only ones on record. Attention is called, in figures 8 and 9, to the pronounced undercooling of these compounds before crystallization set in. Parks, Thomas, and Light associate the phenomenon with optical isomerism [10]. These authors state that in *dl* mixtures, especially *dl* mixtures of hydrocarbons, the presence of two varieties of molecules with equal intermolecular forces strongly militates against crystallization.

IV. CONTENT OF THE METHYLOCTANES IN THE PETROLEUM

The 6.5-liter fraction, shown in figure 2 to distil between 100 and 102.4° C at 215 mm (142 and 144.2° C at 760 mm), yielded on fractionation 3 liters of 2-methyloctane and about 1 liter each of 3- and 4-methyloctane concentrates. This places the amount of the 2-, 3-, and 4-methyloctanes present in the proportion of 3, 1, and 1. Allowing for losses, the total methyloctane content of the crude petroleum is estimated to be about 0.3 percent. The five isomeric nonanes isolated thus far from the petroleum, together with the relative amount of each, are as follows: *n*-nonane, 15; 2-methyloctane, 3; 2, 6-dimethylheptane, 2; 3-methyloctane, 1; 4-methyloctane, 1.

The writers express their thanks to Prof. Frank C. Whitmore of Pennsylvania State College for permission to include in the paper his unpublished data on 2-methyloctane, and to Dr. George Calingaert of the Ethyl Gasoline Corporation for the loan of the sample of synthetic 4-methyloctane. Grateful acknowledgment is also made to Prof. M. R. Fenske and H. P. Orem of Pennsylvania State College and to Dr. F. D. Rossini of the National Bureau of Standards, for their aid in placing valuable data on the isomeric nonanes at our disposal, and to S. T. Schicktanz, F. W. Rose, Jr., and other members of the staff of Project 6 for superintending the distillation of the petroleum.

[9] Calculated from a computed depression of the freezing point of 0.01° C and an estimated heat of fusion of 4.0±0.5 Kcal/mole.

V. REFERENCES

[1] J. D. White and F. W. Rose, Jr. BS J. Research **9**, 711 (1932) RP501.
[2] C. O. Tongberg, M. R. Fenske, and J. E. Nickels, Ind. Eng. Chem. **29**, 70 (1937).
[3] B. J. Mair and J. D. White, J. Research NBS **15**, 59 (1935) RP809.
[4] S. T. Schicktanz, J. Research NBS **18**, 129 (1937) RP967.
[5] J. D. White and F. W. Rose, Jr., J. Research NBS **17**, 943 (1936) RP955.
[6] R. T. Leslie, BS J. Research **10**, 609 (1933) RP552.
[7] G. Calingaert and J. W. Hladky, J. Am. Chem. Soc. **58**, 153 (1936).
[8] W. Świetosławski, J. Phys. Chem. **38**, 1169 (1934).
[9] M. Wojciechowski, J. Research NBS **17**, 453 (1936) RP921.
[10] G. S. Parks, S. B. Thomas, and D. W. Light, J. Chem. Phys. **4**, 64 (1936).

WASHINGTON, JULY 17, 1937.

U. S. Department of Commerce National Bureau of Standards

RESEARCH PAPER RP1034

Part of Journal of Research of the National Bureau of Standards, Volume 19, October 1937

GRAPHICAL COMPUTATION OF STRESSES FROM STRAIN DATA

By Ambrose H. Stang and Martin Greenspan

ABSTRACT

The arithmetic involved in the use of the analytical solution for principal stresses in terms of strains on four intersecting gage lines 45° apart is very tedious if these stresses are computed at many locations. This paper presents graphs which materially reduce the time and labor necessary for such computations. There are presented, also, graphs by means of which normal and shearing stresses on oblique planes are readily obtained from principal stresses. The use of the various graphs is illustrated by numerical examples.

The time required to compute principal stresses, and other normal stresses and shearing stresses, from strain data, in the case of plane stress, may be considerably reduced through use of graphs. Such graphs are presented in this paper, and numerical examples illustrating their use are given.

Figure 1 shows a plate under the action of loads on its boundary. Suppose it is required to determine the state of stress at any location 0. The lines U and V are the directions of the maximum and of the minimum principal stresses, respectively. The lines 1, 2, 3, and 4 are the directions of gage lines intersecting at 45° as shown, along which strain readings are taken. Let ϵ_1, ϵ_2, ϵ_3, and ϵ_4 be the components of strain along these gage lines. Then with the value for Poisson's ratio of 1/3, which probably is adequate for most structural materials, the principal stresses are given by the formulas:[1]

$$\sigma_u=\frac{3}{8}E\left[\epsilon_1+\epsilon_2+\epsilon_3+\epsilon_4+\sqrt{(\epsilon_1-\epsilon_3)^2+(\epsilon_2-\epsilon_4)^2}\right] \quad (1)$$

for the maximum principal stress, and

$$\sigma_v=\frac{3}{8}E\left[\epsilon_1+\epsilon_2+\epsilon_3+\epsilon_4-\sqrt{(\epsilon_1-\epsilon_3)^2+(\epsilon_2-\epsilon_4)^2}\right] \quad (2)$$

for the minimum principal stress, where E is Young's modulus of elasticity.

These equations may be put in the form

$$\sigma_u=\frac{3}{8}E(A+B), \quad (3)$$

$$\sigma_v=\frac{3}{8}E(A-B), \quad (4)$$

where

$$A=\epsilon_1+\epsilon_2+\epsilon_3+\epsilon_4, \quad (5)$$

$$B=\sqrt{(\epsilon_1-\epsilon_3)^2+(\epsilon_2-\epsilon_4)^2}. \quad (6)$$

[1] W. R. Osgood, *Determination of principal stresses from strains on four intersecting gage lines 45° apart.* J. Research NBS 15, 579 (1935) RP851.

The directions of the principal stresses are given by the relation[2]

$$\tan 2\theta = -\frac{\epsilon_2 - \epsilon_4}{\epsilon_1 - \epsilon_3}, \tag{7}$$

where θ (fig. 1) is the angle measured positive counterclockwise from the direction of σ_u to gage line 1.

The quantity A of equation 5 is obtained directly by addition of the measured strains ϵ_1, ϵ_2, ϵ_3, and ϵ_4.

The quantity B of equation 6 and the angle θ of equation 7 can be obtained graphically from figure 2 as follows. Find the point the rectangular coordinates of which are $|\epsilon_1 - \epsilon_3|$ and $|\epsilon_2 - \epsilon_4|$.[3] The polar coordinates of this point are B[4] and $|\theta|$. The value of B may be read on either of the scales for the rectangular coordinates by following a circle from the point to either of the axes. The value of $|\theta|$ may be read on one of the two scales for θ. The table at the top of figure 2, read vertically, indicates for the various combinations of signs of $\epsilon_1 - \epsilon_3$ and $\epsilon_2 - \epsilon_4$ whether the inside scale, θ_i, or the outside scale, θ_o, is to be used, and gives the sign of θ.

Figure 3 is a nomograph for determining the principal stresses, σ_u and σ_v, after the values A and B have been determined, for the case $E=28{,}600$. Similar graphs may be drawn corresponding to any value of E. The maximum principal stress, σ_u, is obtained in the following way. Locate $A\times 10^5$ on the left-hand scale, $B\times 10^5$ on the upper half (marked "*FOR* σ_u") of the right-hand scale, and connect the two points on the scales with a straight line. This line intersects the middle scale at the value of σ_u. The minimum principal stress, σ_v, is obtained in the same way, except that $B\times 10^5$ is located on the lower half (marked "*FOR* σ_v") of the right-hand scale.

There are several ways to construct one nomograph which will give σ_u and σ_v for all values of E, but it is more convenient to construct a separate nomograph, such as is shown in figure 3, for each value of E. A nomograph for a definite value of E can be made as follows. Axes for A, B, and σ are drawn parallel to each other, the axes of A and B on opposite sides of the axis of σ and equidistant from it. Zeros for the three axes are laid off on the same straight (horizontal) line. The graduations on all three scales are uniform and the same on the A and B scales. These scales are laid off with 100 graduations on each side of their zeros. Since the σ scale is also uniformly graduated, it is necessary to locate only one point other than the zero on the σ axis. This may be done by solving equation 3 for A, with $A=B$, E equal to the desired value of the modulus of elasticity, and σ_u chosen equal to any convenient value. A line connecting the values of A and B ($A=B$), thus computed, intersects the σ axis at the chosen value of σ_u and thus locates the necessary point for graduating the σ scale.

Suppose, for example, it were desired to regraduate the σ scale of figure 3 to adapt it for $E=30{,}000$. To locate the value $\sigma=10$ on the scale, we substitute $\sigma_u=10$, $A=B$, and $E=30{,}000$ in equation 3 and solve for A, getting $A=B=44.4\times 10^{-5}$. A line connecting 44.4 on

[2] See footnote 1.

[3] $|\epsilon_1-\epsilon_3|$ and $|\epsilon_2-\epsilon_4|$ are first multiplied by some power of 10 (the same for each) to bring the values within the range of the scales. The value of B, subsequently read from the chart, must be divided by this same power of 10.

[4] See footnote 3.

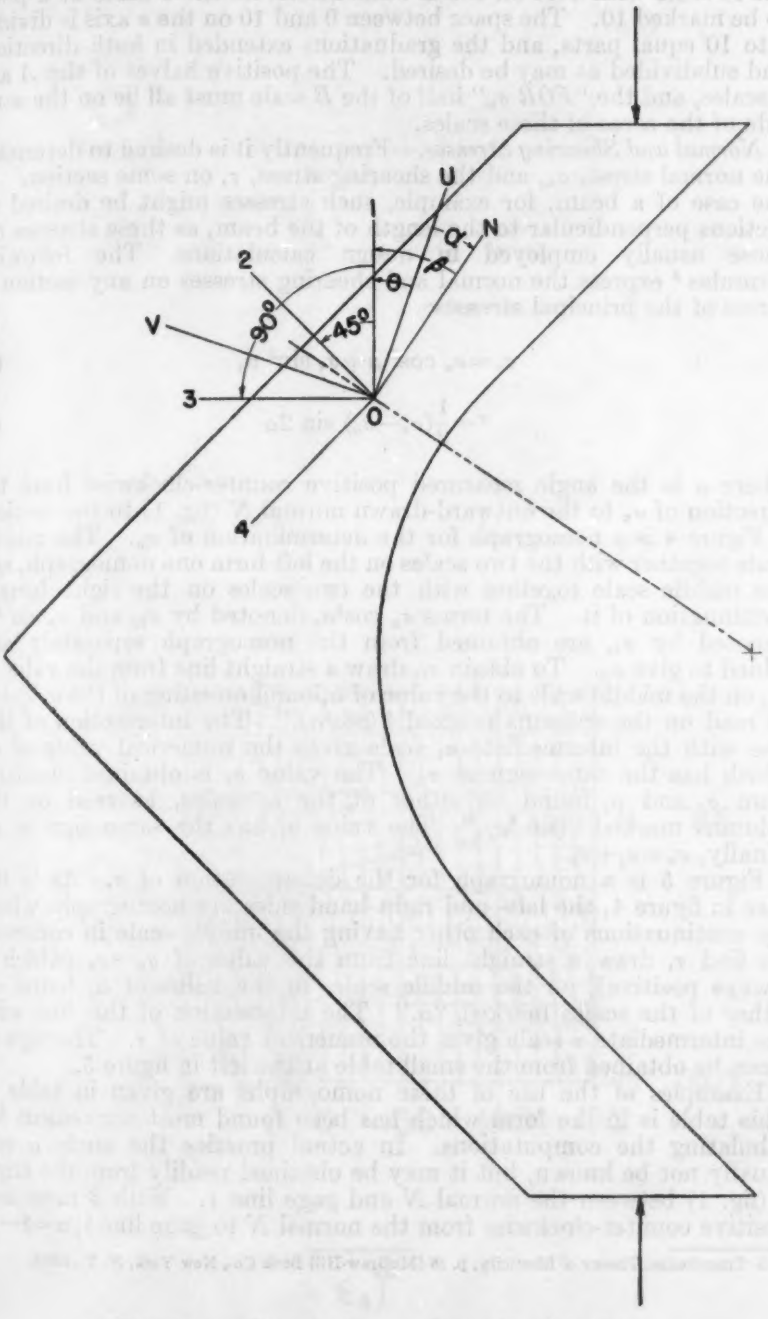

FIGURE 1.—*Example of a member under plane stress.*

Four gage lines (1, 2, 3, 4), intersecting at O. Directions (U, V) of principal stresses, and direction (N of normal to any section. As shown above, the angle α is negative, the angles β and θ, positive

the A scale with 44.4 on the B scale intersects the σ scale at a point to be marked 10. The space between 0 and 10 on the σ axis is divided into 10 equal parts, and the graduations extended in both directions and subdivided as may be desired. The positive halves of the A and σ scales, and the "*FOR* σ_u" half of the B scale must all lie on the same side of the zeros of these scales.

Normal and Shearing Stresses.—Frequently it is desired to determine the normal stress, σ_n, and the shearing stress, τ, on some section. In the case of a beam, for example, such stresses might be desired on sections perpendicular to the length of the beam, as these stresses are those usually employed in design calculations. The following formulas [5] express the normal and shearing stresses on any section in terms of the principal stresses:

$$\sigma_n=\sigma_u \cos^2 \alpha+\sigma_v \sin^2 \alpha, \tag{8}$$

$$\tau=\frac{1}{2}(\sigma_v-\sigma_u) \sin 2\alpha \tag{9}$$

where α is the angle measured positive counter-clockwise from the direction of σ_u to the outward-drawn normal N (fig. 1) to the section.

Figure 4 is a nomograph for the determination of σ_n. The middle scale together with the two scales on the left form one nomograph, and the middle scale together with the two scales on the right form a continuation of it. The terms $\sigma_u \cos^2\alpha$, denoted by σ_1, and $\sigma_v \sin^2\alpha$, denoted by σ_2, are obtained from the nomograph separately and added to give σ_n. To obtain σ_1, draw a straight line from the value of σ_u, on the middle scale to the value of α, found on either of the α scales, as read on the columns marked "$(\cos^2\alpha)$." The intersection of this line with the intermediate σ_1 scale gives the numerical value of σ_1, which has the same sign as σ_u. The value σ_2 is obtained similarly from σ_v and α, found on either of the α scales, as read on the columns marked "$(\sin^2\alpha)$." The value σ_2 has the same sign as σ_v. Finally, $\sigma_n=\sigma_1+\sigma_2$.

Figure 5 is a nomograph for the determination of τ. As is the case in figure 4, the left- and right-hand sides are nomographs which are continuations of each other having the middle scale in common. To find τ, draw a straight line from the value of $\sigma_u-\sigma_v$ (which is always positive), on the middle scale, to the value of α, found on either of the scales marked "α." The intersection of this line with the intermediate τ scale gives the numerical value of τ. The sign of τ can be obtained from the small table at the left in figure 5.

Examples of the use of these nomographs are given in table 1. This table is in the form which has been found most convenient for tabulating the computations. In actual practice the angle α will usually not be known, but it may be obtained readily from the angle β (fig. 1) between the normal N and gage line 1. With β measured positive counter-clockwise from the normal N to gage line 1, $\alpha=\theta-\beta$.

[5] S. Timoshenko, Theory of Elasticity, p. 16 (McGraw-Hill Book Co., New York, N. Y., 1934).

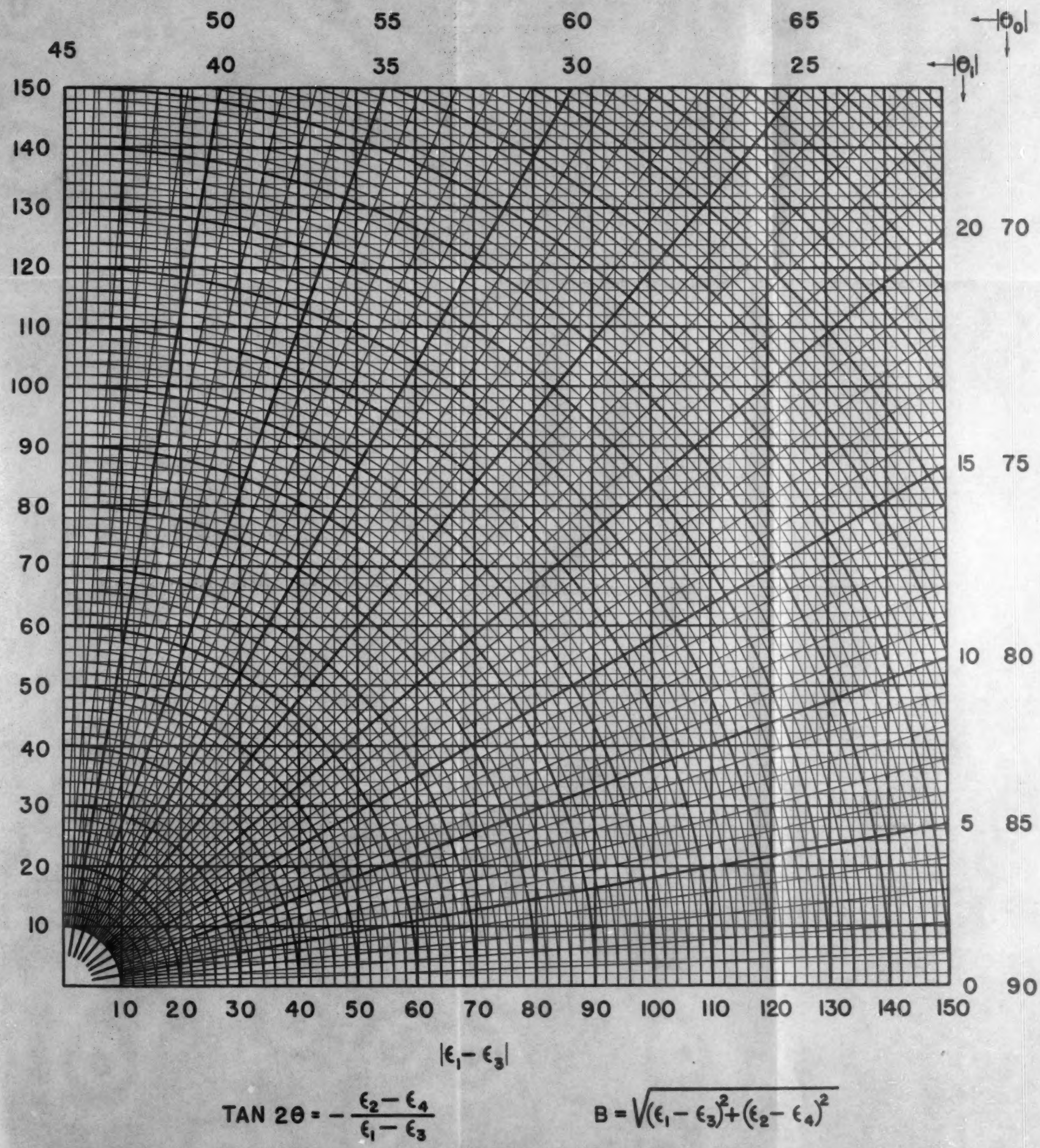

$$\text{TAN } 2\theta = -\frac{\epsilon_2-\epsilon_4}{\epsilon_1-\epsilon_3} \qquad B=\sqrt{(\epsilon_1-\epsilon_3)^2+(\epsilon_2-\epsilon_4)^2}$$

FIGURE 2.—*Graph for* $B=\sqrt{(\epsilon_1-\epsilon_3)^2+(\epsilon_2-\epsilon_4)^2}$ *and for* θ.

UNIV. OF MICH.

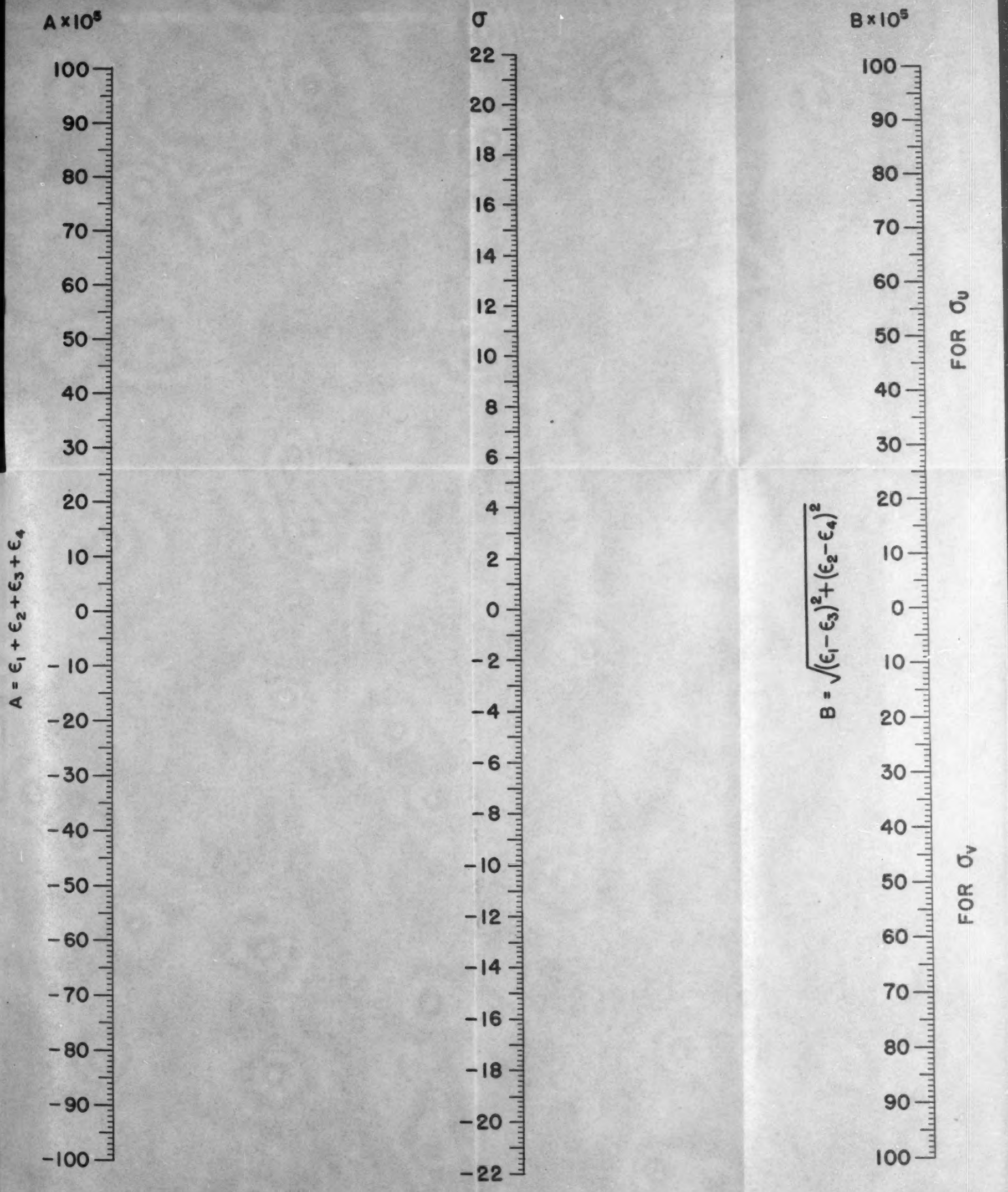

FIGURE 3.—*Graph for principal stresses, σ_u and σ_v.*

UNIV. OF MICH.

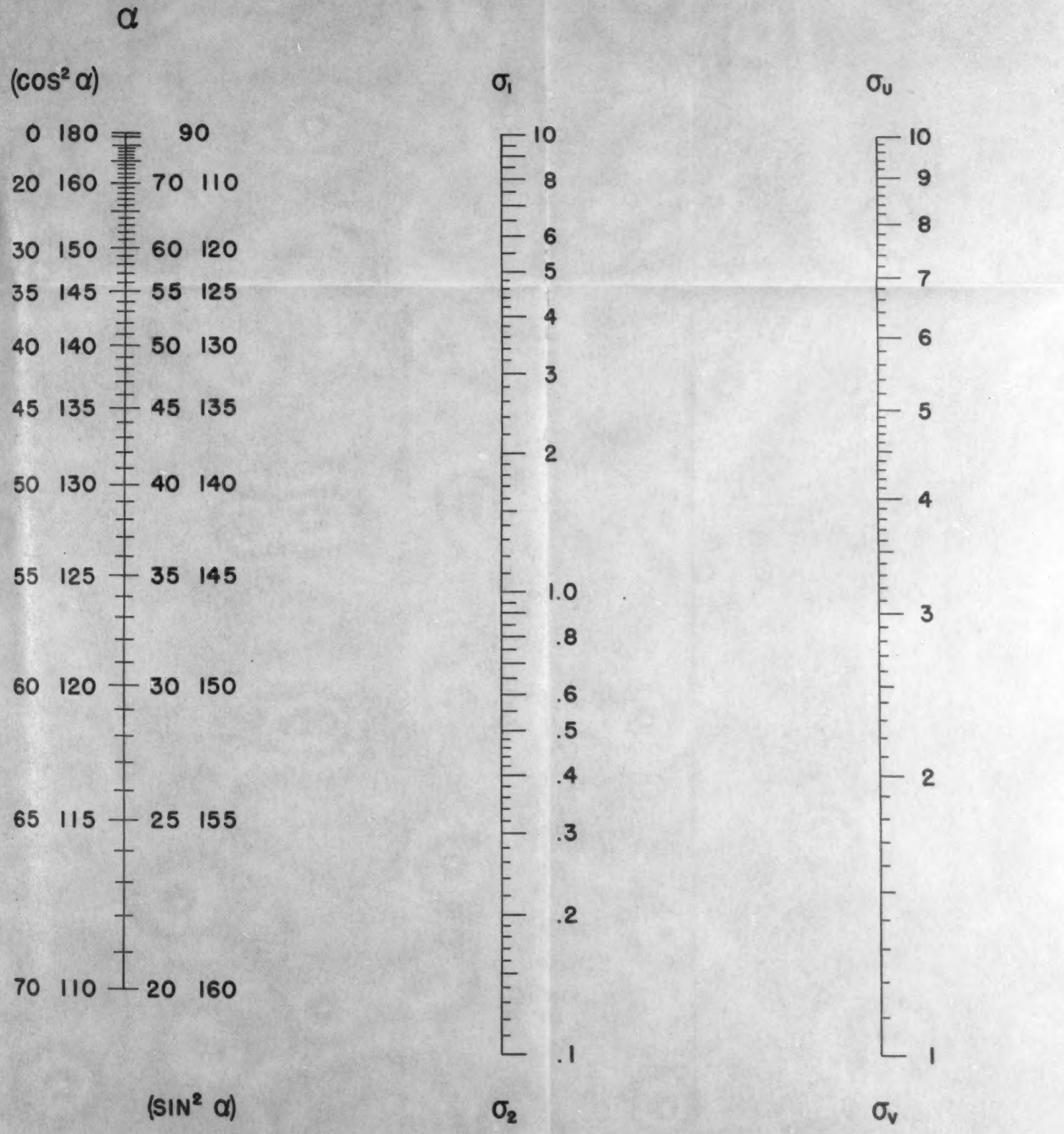

$$\sigma_N = \sigma_U \cos^2\alpha + \sigma_V \sin^2\alpha = \sigma_1 + \sigma_2$$

FIGURE 4.—*Graph for normal stress* σ_n.

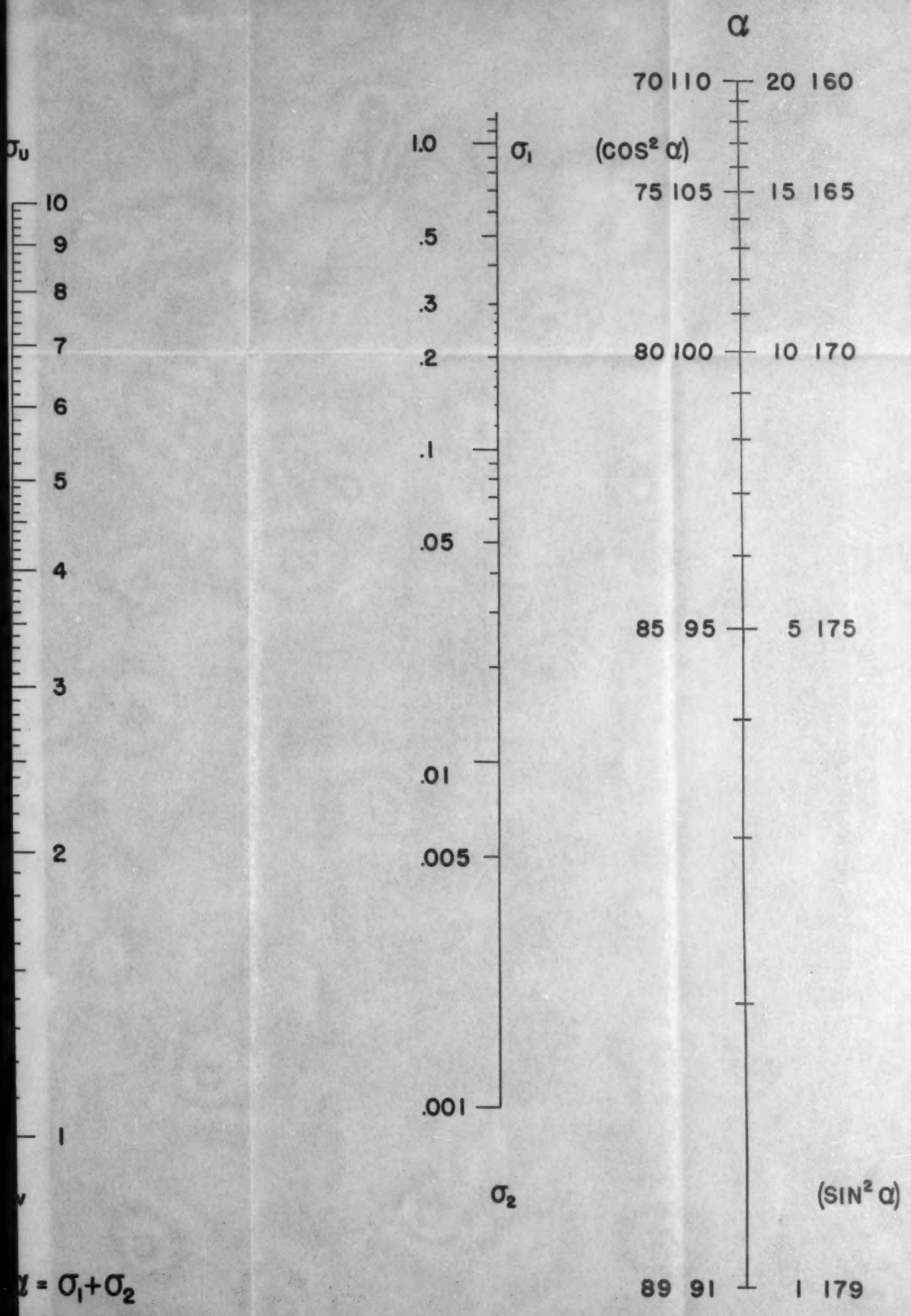

raph for normal stress σ_u.

UNIV. OF MICH.

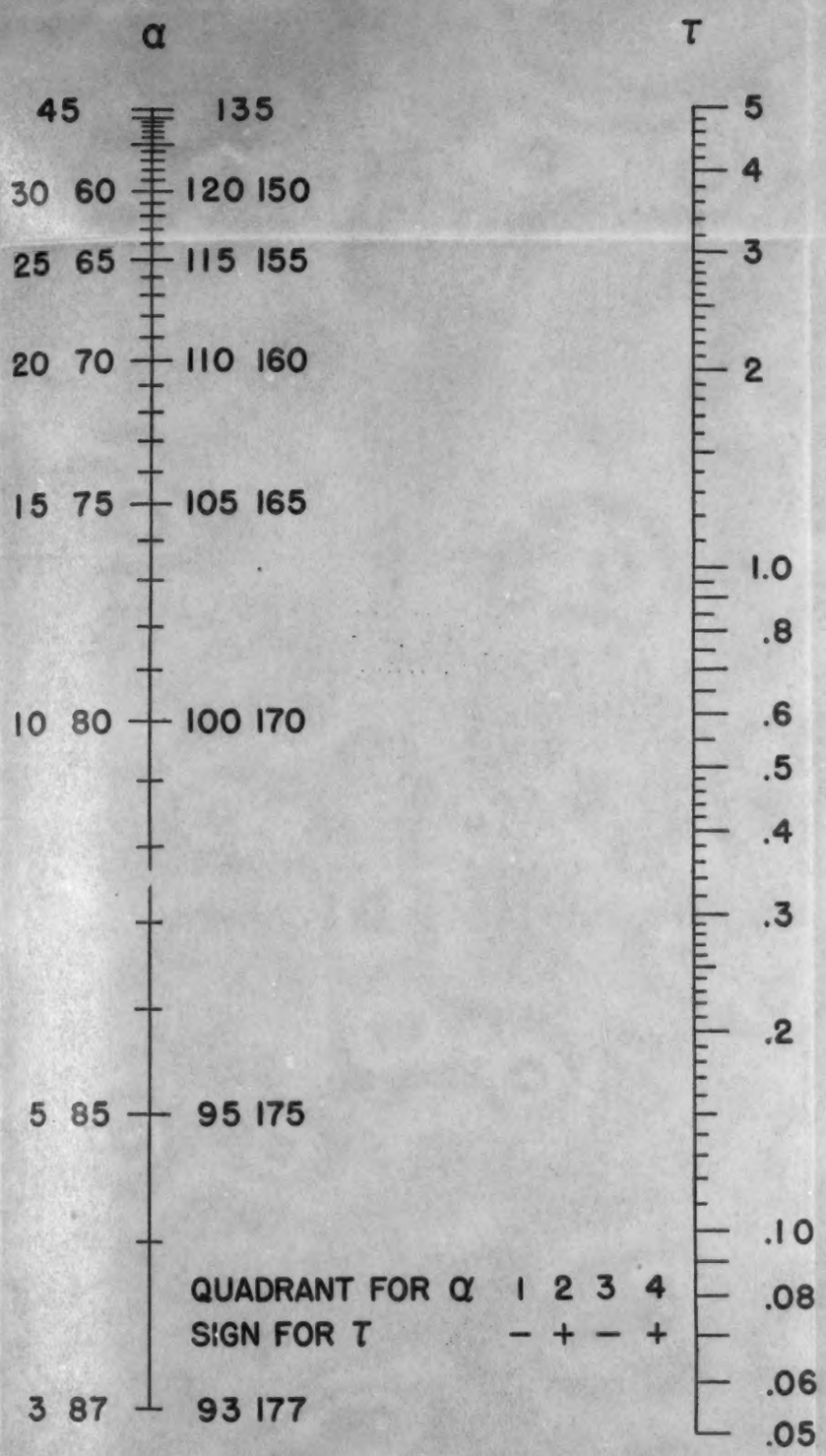

FIGURE 5.—*Graph for shearing stress τ.*

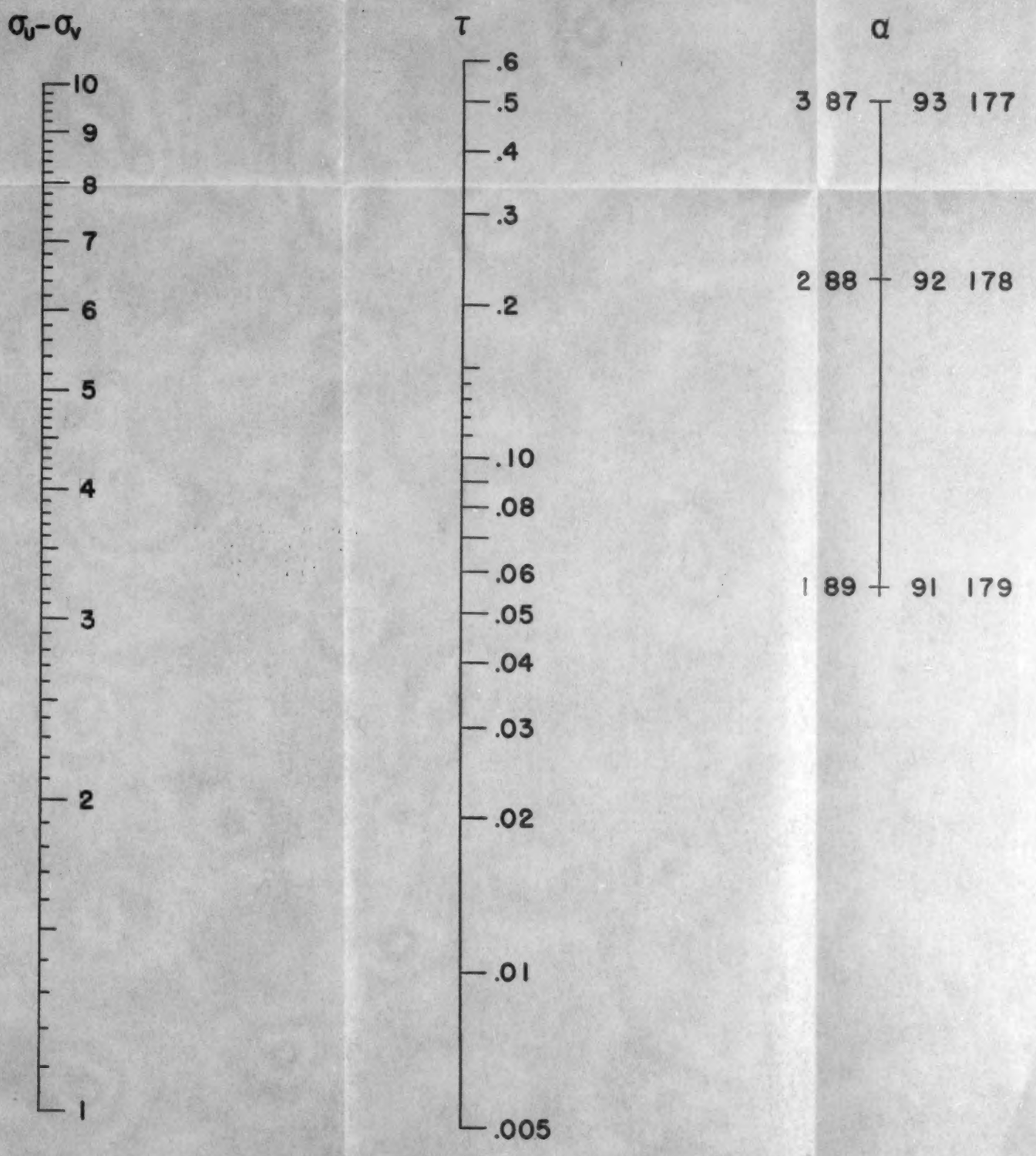

$$\tau = \frac{1}{2}(\sigma_v - \sigma_u) \sin 2\alpha$$

FIGURE 5.—*Graph for shearing stress* τ.

UNIV. OF MICH.

FIGURE 5.—Graph for shearing stress τ.

TABLE 1.—*Examples of calculations of stresses from strain data by means of the charts*

[E=28,600 kips/in.^{2}]

Quantity \ Example→	1	2	3	4
ϵ_2 (observed)	+0.00017	+0.00038	−0.00031	−0.00039
ϵ_3 (observed)	+.00008	−.00003	−.00016	+.00021
ϵ_4 (observed)	−.00027	−.00034	+.00044	−.00007
ϵ_1	−.00017	+.00007	+.00028	−.00065
$\epsilon_3-\epsilon_4$	+.00044	+.00072	−.00075	−.00032
$A=\epsilon_1+\epsilon_2+\epsilon_3+\epsilon_4$	+.00025	−.00010	−.00044	+.00086
B (fig. 2)	−.00019	+.00008	+.00025	−.00090
σ_u, kips/in.^{2} (fig. 3)	.00051	.00073	.00087	.00092
σ_v, kips/in.^{2} (fig. 3)	+3.4	+8.7	+12.0	+.1
$\sigma_u-\sigma_v$	−7.5	−7.0	−6.7	−19.5
$\tau_{max}=\frac{1}{2}(\sigma_u-\sigma_v)$ kips/in.^{2}	10.9	15.7	18.7	19.6
θ, degrees (fig. 2)	5.4	7.8	9.3	9.8
β (from layout), degrees	−14.8	+4.0	+74.8	−55.2
$\alpha=\theta-\beta$, degrees	+45.0	+45.0	+45.0	+122.0
σ_1, kips/in.^{2} (fig. 4)	−59.8	−41.0	+29.8	−177.2
σ_2, kips/in.^{2} (fig. 4)	+.9	+5.0	+9.0	+.1
$\sigma_3=\sigma_1+\sigma_2$, kips/in.^{2}	−5.6	−3.0	−1.7	0
τ, kips/in.^{2} (fig. 5)	−4.7	+2.0	+7.3	+.1
	+4.7	+7.7	−8.1	−.9

WASHINGTON, August 10, 1937

U. S. Department of Commerce National Bureau of Standards

RESEARCH PAPER RP1035

Part of Journal of Research of the National Bureau of Standards, Volume 19, October 1937

MUTAROTATION OF *l*-SORBOSE

By William Ward Pigman and Horace S. Isbell

ABSTRACT

Optical-rotation measurements are reported on carefully purified *l*-sorbose at 0.4 and 20° C. In contradiction of the statements in various periodicals and text books, the results show that this sugar exhibits a small complex mutarotation.

Since the ketohexose, *l*-sorbose, has become of commercial importance, particularly as an intermediate in the synthesis of ascorbic acid, an accurate knowledge of its physical and chemical properties is desirable. The optical rotation of *l*-sorbose was studied by Lobry de Bruyn and Van Ekenstein,[1] who reported that no mutarotation was observable. Although the effect of temperature, concentration, and other factors on the equilibrium specific rotation have been studied,[2] it has been generally assumed, except for a statement by Riiber,[3] that the sugar does not mutarotate or else that the mutarotation is too rapid to be detected.[4]

We have made a number of measurements of the optical rotatory power of pure samples of anhydrous *l*-sorbose [5] in water solution and have found that neither of the earlier assumptions is correct, since the sugar exhibits a definite mutatotation in which the optical rotation increases slightly at first and then decreases, so that the initial and final rotations are not widely different. The observed change (about 0.7° S) is undoubtedly real and is not due to accidental impurities, because samples of the sugar which had been purified and then recrystallized 2, 3, 5, and 6 times from water gave the same characteristic mutarotation. On account of its complex character the mutarotation cannot be represented by the usual first-order equation but requires an equation containing two exponential terms. The measurements and equations representing the reactions at both 20 and 0° C are given in table 1.

[1] M. M. C. A. Lobry de Bruyn and W. A. Van Ekenstein, Rec. trav. chim. **19**, 6 (1900).
[2] R. H. Smith and B. Tollens, Ber. deut. chem. Ges. **33**, 1285 (1900).
[3] C. N. Riiber, Saertrykk av Tidsskrift for kjemi og bergvesen, no. 10, p. 16 (1932).
[4] Tollens-Elsner, Kurzes Handbuch der Kohlenhydrate, p. 383 (Johann Ambrosius Barth, Leipzig, 1935).
[5] The material used was furnished through the courtesy of the Bureau of Chemistry and Soils, U. S. Department of Agriculture.

TABLE 1.—*Mutarotation of l-sorbose in water* [1]

Time	Observed rotation	$m_1 \times 10^3$	Deviation	$m_2 \times 10^3$
	11.3 g per 100 ml at 20.0° C in a 4-dm tube. $°S = -1.13\times10^{-.0404t} + .77\times10^{-.324t} - 56.77$ $[\alpha]_D^{20} = -.86\times10^{-.0404t} + .59\times10^{-.324t} - 43.4$			
Minutes	°S			
0	(−57.124)	----------	(0.772)	----------
1.75	−57.446	----------	.282	290
2.69	−57.498	----------	.150	210
4.06	−57.451	----------	----------	----------
6.33	−57.404	----------	----------	----------
9.37	−57.246	----------	----------	----------
12.37	−57.129	----------	----------	----------
15.32	−57.049	37	----------	----------
19.64	−56.953	40	----------	----------
23.09	−56.898	41	----------	----------
26.14	−56.864	42	----------	----------
34.76	−56.801	----------	----------	----------
120	−56.768	----------	----------	----------
Average	----------	40	----------	250
	11.6 g per 100 ml at 0.4° C in a 4-dm tube $°S = -.74\times10^{-.0355t} + .40\times10^{-.030t} - 58.0$ $[\alpha]_D^{0.4} = -.55\times10^{-.0355t} + .30\times10^{-.030t} - 43.3$			
0	(−58.341)	----------	(0.400)	----------
4.66	−58.409	----------	.200	----------
9.16	−58.447	----------	.213	31
14.02	−58.461	----------	.159	28
19.93	−58.477	----------	.098	31
29.91	−58.478	----------	(.029)	----------
40.95	−58.429	----------	----------	----------
50.11	−58.407	----------	----------	----------
60.12	−58.365	----------	----------	----------
70.83	−58.301	----------	----------	----------
81.35	−58.265	5.2	----------	----------
89.88	−58.231	6.0	----------	----------
105.99	−58.190	5.6	----------	----------
205.08	−58.061	5.1	----------	----------
1,350	−57.998	----------	----------	----------
Average	----------	5.5	----------	30

[1] The equations and values for mutarotation constants, m_1, and m_2, are determined by the method described by Isbell and Pigman, J. Research NBS 18, 156 (1937) RP969. Each observed rotation represents the average of 10 consecutive readings.

The smallness of the mutarotation might arise from one of two possibilities: (1) Equilibrium might be established between isomers having only slightly different optical rotatory values, in which case the equilibrium solution would contain considerable quantities of these isomers, or (2) the known modification might greatly predominate in the equilibrium state and other modifications be present only in small quantities. In order to decide between these possibilities, solubility measurements were made of *l*-sorbose in water at 0° C. An excess of finely powdered *l*-sorbose was shaken with ice water for 3 minutes and filtered; after standing until equilibrium was reached, the solution read −127.52° S in a 4-dm tube. A solution allowed to reach equilibrium at 0° C in the presence of an excess of *l*-sorbose read −128.63° S in a 4-dm tube. The small difference (0.87 percent) between the two values indicates that the equilibrium solution of

l-sorbose is composed almost exclusively of that isomer which is known in the crystalline state.

The specific rotations for *l*-sorbose in water were found to be $[\alpha]D^{0.4}=-43.3$ and $[\alpha]D^{20}=-43.4$ (12 g. of *l*-sorbose in 100 ml). The equilibrium appears to be only slightly affected by temperature. This behavior resembles that of glucose, as might be expected from the analogous structures of the two sugars. The equilibrium specific rotation in 50-percent (in volume) ethyl alcohol was found to be $[\alpha]D^{20}=-43.4$ (0.6067 g made up to 25 ml read $-12.18°$ S in a 4-dm tube).

WASHINGTON, August 10, 1937.

12341—37——5

U. S. Department of Commerce National Bureau of Standards

RESEARCH PAPER RP1036

Part of Journal of Research of the National Bureau of Standards, Volume 19, October 1937

RECOMBINATION OF IONS IN THE AFTERGLOW OF A CESIUM DISCHARGE

By Fred L. Mohler

ABSTRACT

A discharge through a 500-cm³ bulb is short-circuited by a motor-driven commutator and the radiation and electrical characteristics of the afterglow are studied. Radiation at a definite time interval after the cutoff was observed by means of a sectored disk on the commutator shaft, while electrical measurements were made by closing a probe circuit momentarily by means of a second commutator.

The afterglow fades at a rate which decreases with increasing pressure up to 46μ and remains nearly constant (the half value time for a 6-amp. discharge is 1.5×10^{-3} sec) in the pressure range 46 to 110 μ. The spectral-intensity distribution of the continuous recombination spectrum indicates a much-lower electron temperature than in the discharge, decreasing with time from 1,360° K at 0.9×10^{-3} sec to 1,200° K at 1.7×10^{-3} sec.

The number of ions at any time during the afterglow is measured by the positive-ion current to a negative probe, and the flow of ions to the wall is measured by the current to a collector against the bulb wall. The difference between the change in number of ions in the bulb and the flow of ions to the wall gives the number recombining in the space. From this is derived a recombination coefficient of 3.4×10^{-10} in the pressure range 10 to 30 μ.

CONTENTS

		Page
I.	Introduction	447
II.	Apparatus and methods	448
III.	Visual-intensity measurements	449
IV.	Spectrophotometric measurements	451
V.	Electrical measurements	452
VI.	Discussion	455

I. INTRODUCTION

The rate of recombination of positive and negative ions in air and the common gases at pressures of the order of 1 atmosphere is known from many experiments.[1] For the usual case where the number of positive and negative ions is equal,

$$dn/dt=-\alpha n^2, \tag{1}$$

where n is the number of ions of either sign per cubic centimeter and α is the recombination coefficient. For the common gases at a pressure of 1 atmosphere, α is of the order of 10^{-6}. It decreases with decreasing pressure, probably in proportion to the pressure, though there is conflicting evidence on this point. The evidence supports Thomson's

[1] Loeb, Kinetic Theory of Gases, p. 583 (McGraw-Hill Book Co., New York, N. Y., 1934), gives a good summary on the subject.

theory that recombination is the result of a three-body collision between ions of molecular mass and a neutral molecule. The usual experimental technique is not applicable at pressures much less than 0.1 atmosphere, but it is to be expected that with decreasing pressure the three-body process will become negligible and two-body recombination of positive ions and electrons with emission of radiation will become predominant. The observation of a continuous spectrum extending from a series limit to shorter wave lengths gives evidence for the existence of spontaneous two-body recombination. Boeckner and the author have measured the rate of recombination into a few quantum states by measuring the number of quanta of radiation emitted.[2] In this way it was found that the recombination coefficient for recombination into the 6P state of cesium is 6×10^{-14} for an electron temperature of 3,500° K. The method gives no indication of the total recombination into all possible quantized states. There are also difficulties in evaluating theoretically the contribution of all levels for recombination with electrons with a temperature distribution.

The only important contribution on the rate of recombination in a low-pressure discharge is a study by Kenty of the decrease in electron concentration in the afterglow of an argon discharge.[3] By means of a double commutator he measured by a probe wire the number of electrons per cubic centimeter at various time intervals after the discharge was cut off. Assuming that diffusion to the walls was negligible, he obtained a value of $\alpha=2\times10^{-10}$ (with a fivefold uncertainty, because of difficulties with the probe measurements) for an electron temperature of 3,100° K and a gas pressure of 0.8 mm. His paper includes qualitative evidence that the loss of ions by wall diffusion is small. Miss Hayner [4] had previously shown that the plasma condition which exists in the discharge persists after the discharge is cut off. That is the space maintains a positive charge with respect to the walls so that the rate at which electrons reach the walls is limited to the rate at which the heavy positive ions can diffuse. Because of this phenomenon the study of recombination at low pressures is practicable.

As the rate of recombination is a fundamental atomic constant, the author has tried to eliminate some of the uncertainties in previous work. The cesium discharge has been used and this study includes visual photometric measurements of the rate of decay of the afterglow, some spectrophotometric measurements, and probe measurements of the change in electron concentration and diffusion of ions to the walls. The visual measurements were an essential preliminary to see under what range of conditions the afterglow could be considered as a uniformly ionized volume.

II. APPARATUS AND METHODS

To reduce the effect of ion diffusion to the walls it is desirable to use a large bulb, though the size will be limited by the discharge current available. In most of this work the discharge tube has been a 500-cm³ bulb with cathode and anode in diametrically opposite side tubes. The discharge was operated on direct current and interrupted by a commutator running at a speed of about 1,200 rpm. There are

[2] F. L. Mohler and C. Boeckner, BS J. Research **2**, 489 (1929) RP46. F. L. Mohler, BS J. Research **11**, 771 (1933) RP565 and correction noted in J. Research NBS **17**, 849 (1936) RP948.
[3] Kenty, Phys. Rev. **32**, 624 (1928).
[4] Hayner, Z. Phys. **35**, 365 (1925).

obvious advantages in short-circuiting the discharge rather than breaking the circuit, as the instant of cutoff is then perfectly definite and all sparking occurs at the time when the discharge comes on. The cesium discharge operates at about 10 v, and by running the discharge on a 100-v battery with series resistance, a discharge of 6 amp could be interrupted without destructive arcing.

The commutators were copper segments set flush in the edge of a fiber disk and contact was made by carbon brushes. For the intensity measurements there were four segments on the commutator and a disk with four 1-cm sectors cut in it was mounted on the same shaft as the commutator to permit viewing the afterglow at known time intervals after the cutoff. A long slit immediately in front of the discharge was focused on the plane of the sectored disk, and by looking through the disk the afterglow was viewed stroboscopically at a time after the cutoff determined by the angular separation between the sector and the image at the instant of cutoff, and the motor speed. Each flash lasted 0.0007 sec at 1,200 rpm. The intensity was measured by a simple photometer. A white surface extending into the image of the discharge was illuminated by a headlight lamp with a yellow filter in front of it and intensity was matched by changing the distance of the lamp and by interposing neutral screens.

To photograph the spectrum of the afterglow the stroboscopic image was focused on the slit of a spectrograph. As a basis for intensity measurements, there was included on each plate a series of exposures to a calibrated strip lamp placed back of the sectored disk.

For the electrical measurements, two commutators with two segments on each were used. One of these short-circuited the discharge for about 0.004 sec and the other put the probe or disk electrode into the circuit for about 0.001 sec at an adjustable time interval after the cutoff. The probe electrodes consisted of a disk 3 cm in diameter against the wall of the bulb to measure the flow of ions to the wall and a wire 0.5 mm in diameter extending radially with an exposed surface 6 cm long. This was operated at a negative voltage to measure the positive-ion current. This current is proportional to the electron concentration at a given pressure, and the method of determining the proportionality factor is described later.

There is a small potential drop across the commutator when the current is short-circuited and this modifies somewhat the conditions in the afterglow. A low-resistance potential divider has been put in the discharge circuit to balance this potential difference.

III. VISUAL INTENSITY MEASUREMENTS

The appearance of the discharge undergoes an abrupt change at the instant of the cutoff and then fades relatively slowly. At low pressure the discharge is a purplish pink color which fills the bulb and the afterglow is pale yellow. With increasing pressure the color change becomes less marked but the intensity distribution changes. In the discharge the intensity becomes concentrated near the cathode and anode, while in the afterglow the glow is fairly uniform but brightest near the center of the bulb. At vapor pressures greater than 100 μ of mercury the glow expands from the center during the afterglow period. The dark period described by Miss Hayner [5] and

[5] Hayner, Z. Phys. 35, 365 (1925).

Dr. Kenty [6] is not conspicuous in the cesium discharge. In the spectrum of the afterglow the higher series lines and continuous bands beyond the series limits are relatively intense and the appearance supports the view of Miss Hayner and Dr. Kenty that the glow is predominantly a recombination spectrum. It is known that the electron temperature drops very rapidly after the cutoff,[7] and it seems safe to assume that excitation drops essentially to zero in the short transition period before the uniform glow fills the bulb.

If it is assumed that the intensity, j, comes entirely from recombination, then j is proportional to n^2, that is,

$$n=kj^{1/2}$$

where k is an arbitrary constant which changes rather slowly with the electron temperature. With this limitation $j^{1/2}$ is a measure of the electron concentration without any assumption that the change in n comes entirely from spontaneous recombination. For the case that the change comes entirely from recombination, an integration of equation 1 over the time interval t_1 to t_2 gives

$$\frac{1}{n_2}-\frac{1}{n_1}=\alpha(t_2-t_1) \tag{2}$$

and using intensity as a measure of electron concentration

$$\frac{1}{j_2^{1/2}}-\frac{1}{j_1^{1/2}}=k\alpha(t_2-t_1) \tag{3}$$

A plot of $j^{-1/2}$ versus time will then give a straight line if volume recombination is predominant, but because of wall recombination, the observed curves will in general be steeper and concave upwards.

Measurements of intensity as a function of time after the cutoff have been plotted on this scale to see if the time variation of intensity is consistent with the assumption that volume recombination is predominant. Figure 1 gives a typical group of measurements based on intensity at a time t after cutting off a 5.8-ampere discharge. The curves start out nearly straight and curve upward at an increasing rate. With increasing pressure up to 21 μ the slope near the origin rapidly decreases, presumably because of decreasing diffusion to the walls. In the pressure range 40 to 110 μ there is a nearly constant minimum slope and at higher pressures the slope again increases. It is to be expected that α will increase with the pressure, but as it appears that the distribution of ionization is less uniform at high pressure, the evidence for a real change in α is uncertain. Since diffusion to the walls will decrease with increasing pressure, the results indicate that as pressures increase above 21 μ volume recombination becomes predominant.

An approximate numerical value of the constant k in equation 3 can be obtained with the assumption that the intercept at $t=0$ is proportional to $1/n_0$, where n_0 is the number of electrons per cubic centimeter in the steady discharge. A similar bulb with a probe surface midway between the wall and the center of the bulb gave a

[6] Kenty, Phys. Rev. **32**, 624 (1928).
[7] Randall and Webb, Phys. Rev. **48**, 544 (1935).

mean value $n_0=1.9\times10^{12}$ in the pressure range 46 to 110 μ.[8] The slope of the curve of figure 1 obtained in this pressure range gives a value $\alpha=3.5\times10^{-10}$ on the assumption that diffusion to the walls is negligible.

IV. SPECTROPHOTOMETRIC MEASUREMENTS

The spectrum of the cesium afterglow has been briefly described by Boeckner and the author.[9] At a pressure of 100 μ the line-intensity distribution is much like that of the discharge, but the continuous spectrum decreases beyond the series limit much faster than in the

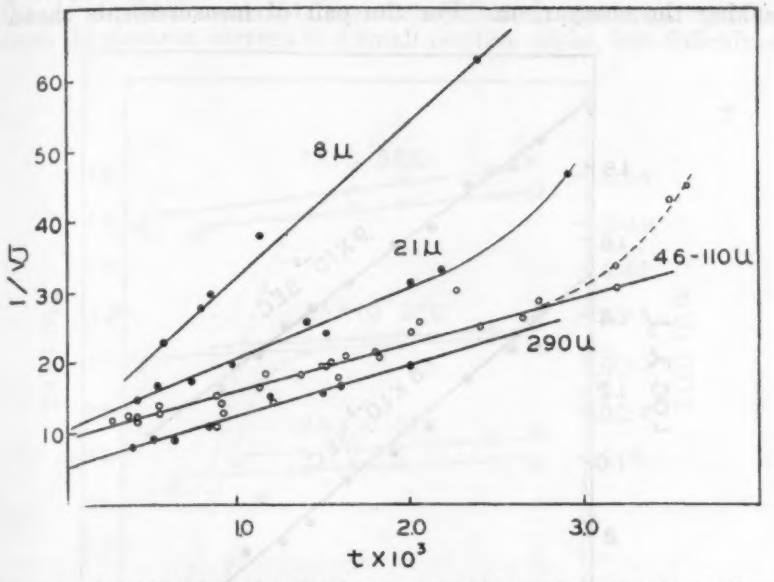

FIGURE 1.—*Intensity, j, of the afterglow as a function of time after the cutoff on a scale of $1/j^{1/2}$ in arbitrary units versus time.*

Vapor pressure in microns of mercury is indicated on each curve.

discharge. This indicates that the electron temperature is much lower in the afterglow and the measurement of the intensity distribution offers a good method of measuring the instantaneous values of the electron temperature in the afterglow. The intensities at two wave lengths, λ_1 and λ_2, at intervals V_1 and V_2, in electron volts beyond the series limits are related to the electron temperature by the equation[10]

$$T_e=5040\frac{V_2-V_1}{\log\lambda_1 j_1-\log\lambda_2 j_2} \tag{4}$$

Figure 2 gives a plot based on measurements of the band beyond the $6P$ limit in the wave-length range 5000 to 4600 A. Measurements were made at time intervals of 0.90×10^{-3} sec and 1.80×10^{-3} sec

[8] This figure for n_0 involves a large and rather uncertain correction factor for the effect of vapor pressure on the probe current. Mohler, J. Research NBS 17, 849 (1936) RP948.
[9] F. L. Mohler and C. Boeckner, BS J. Research 2, 489 (1929) RP46.
[10] F. L. Mohler, BS J. Research 10, 771 (1933) RP565.

after short-circuiting a 5.8-amp discharge at a pressure of 68 μ. The slopes of the curves leadto values of1,350 and 1,200° K for the electron temperatures at these two times. The electron temperature during the discharge is about 2,700° K. A second experiment at a pressure of 85 μ gave temperatures of 1,360 and 1,200° K at intervals of 0.87×10^{-3} and 1.63×10^{-3} sec after the cutoff.

It has been attempted to compare the absolute intensities at the limit with the recombination spectrum of the cesium positive column at low pressure[11] as a basis for measuring the number of electrons per cubic centimeter in the afterglow.

It is assumed that the intensity at the limit is proportional to $T_e^{-3/2}$. There are experimental uncertainties of perhaps 50 percent in making the comparison. For the pair of measurements shown in

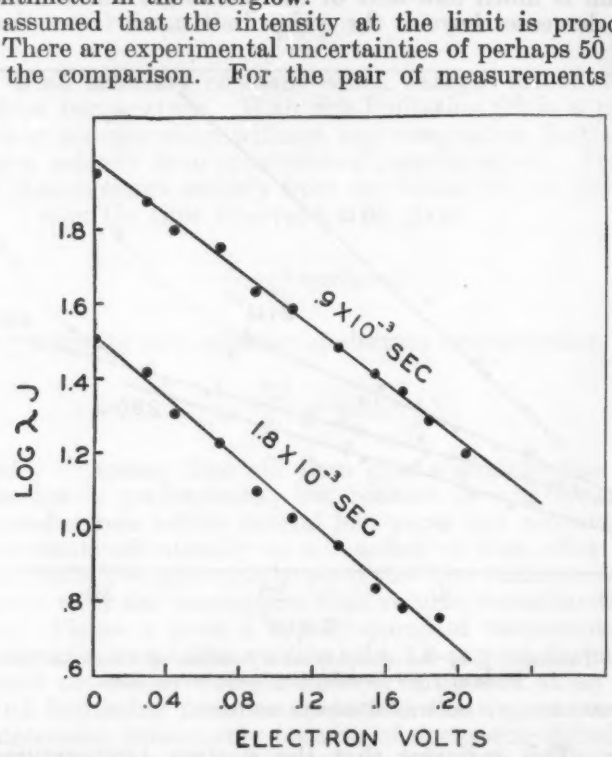

FIGURE 2.—*Semilogarithmic plot of intensity distribution in the continuous spectrum of the afterglow beyond the 6P limit on a scale to give electron temperature.*

Ordinates give log λJ in arbitrary units and abscissas give the frequency interval beyond the series limit, in units of electron volts. The slopes give electron temperatures of 1,350 and 1,200° K for the upper and lower lines, respectively.

figure 2, $n_e=1.78\times10^{12}$ and 0.95×10^{12} for the second pair referred to above $n_e=1.45\times10^{12}$ and 0.98×10^{12}. Again assuming that wall recombination is negligible, these values in equation 2 give values of

$$\alpha=5.5\times10^{-10} \text{ and } 4.3\times10^{-10}$$

V. ELECTRICAL MEASUREMENTS

The change in the total number of ions ΔN in the bulb in any interval Δt after the cutoff is equal to the number of ions flowing to the wall, plus the number recombining in the space. This assumes, as seems

[11] F. L. Mohler, BS J. Research **10**, 771 (1933) RP565.

reasonable, that there is no production of ions in the afterglow period. With the approximation that the distribution of ions is uniform and that the current density to the walls is uniform

$$\frac{\Delta N}{\Delta t}=\frac{4\pi r^2 i_w}{e}+\frac{4}{3}\pi r^3\,\alpha n^2, \tag{5}$$

where r is the radius of the bulb, i_w/e the number of ions flowing to the wall per unit area, and αn^2 the number recombining per unit volume. The current density of positive ions to the wall is found by measuring the ion current to the disk at negative potentials and extrapolating to the potential of zero current.

The conventional method of measuring electron concentration is to measure the electron current to a small positive probe, but difficulties

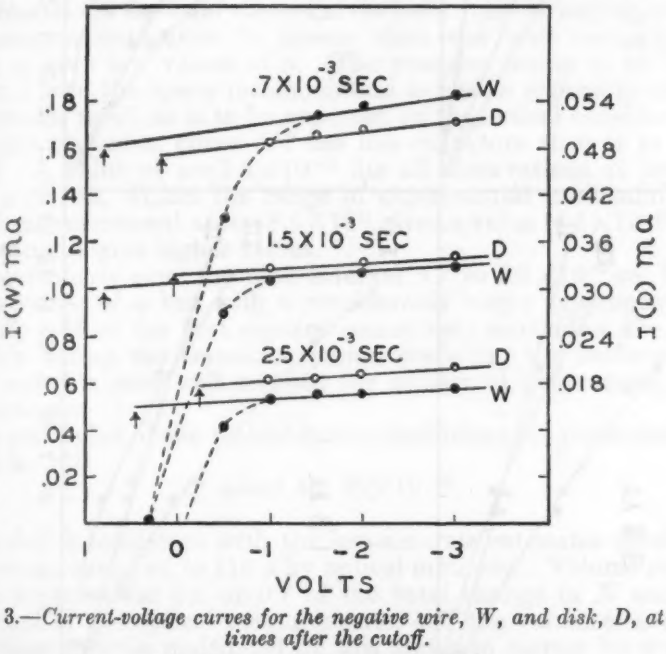

FIGURE 3.—*Current-voltage curves for the negative wire, W, and disk, D, at various times after the cutoff.*

Currents are plotted on two different scales.

were encountered in obtaining reproducible results and the method was adopted of measuring the positive current to a large negative probe. This gives very good precision, but it is essential to find the proportionality factor between ion current and ion concentration. This factor was found from the condition that in equation 5 at low currents the term on the right is negligible. That is, by setting $\Delta N=ki_+$ the factor k is found which satisfies the equation. The method is not very accurate, but it happens that for the higher discharge currents the value of α is quite insensitive to the absolute value of n. As the use of equation 5 involves double differences it is more important to have precise relative values.

Figure 3 gives typical current-voltage curves at various time intervals after cutting off a 6-amp discharge in cesium at a pressure

of 13 μ. Curves *D* give the plate current and curves *W* the current to the wire probe. The figure indicates how the curves are extrapolated to the space potential and wall potential for the wire and disk, respectively. The slope of the plate current-voltage curve comes from a capacity effect. The change in the current to the wire

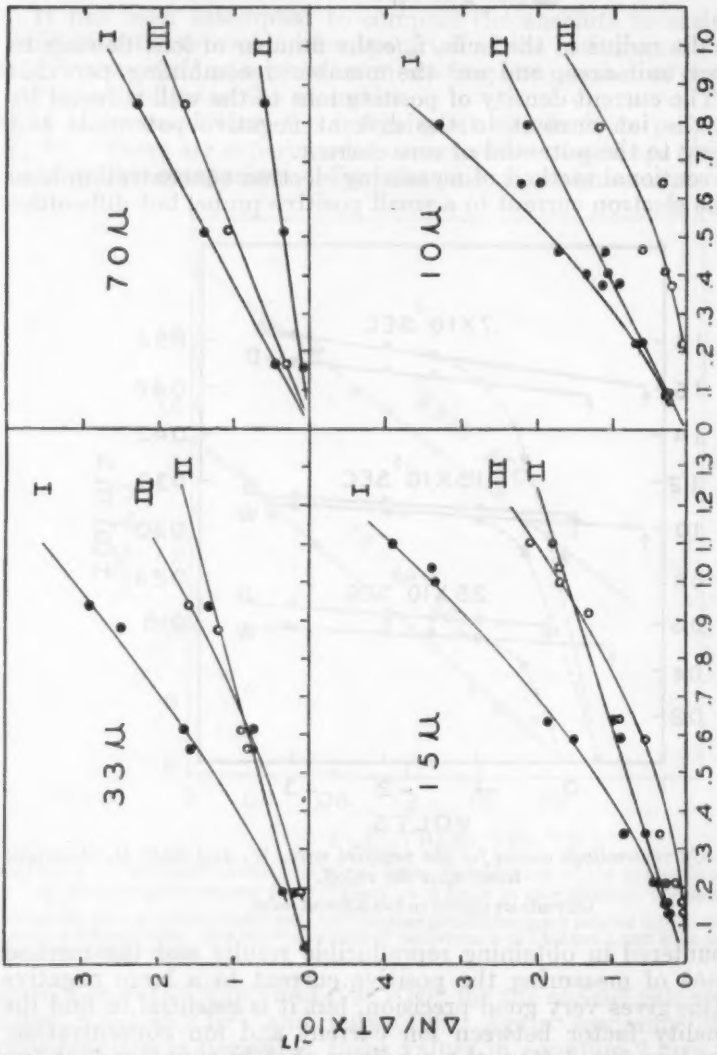

FIGURE 4.—*Curves I, rate of change in the number of ions in the bulb; II, the rate at which they flow to the wall; III, the rate at which they recombine in the space, expressed as a function of the number of electrons per cubic centimeter.*

can be accounted for by the change in area of the space-charge sheath. In some cases the space-charge equation has been used to compute the current at the space potential, but the simple linear extrapolation gives nearly the same result. It is evident that the time change in the probe current is slightly greater than that in the plate

current, which shows that the concentration of ions changes faster at the center than at the wall. With the proportionality factor between ion current and ion concentration found from similar low-current measurements, the data of figure 3 give $\Delta N/\Delta t$ and i_w at various times. In figure 4, curves *I*, $\Delta N/\Delta t$ is plotted as a function of the mean value of n over the time interval Δt for four different pressures. Each curve gives values obtained with different values of the current for the time interval 1.5×10^{-3} to 2.5×10^{-3} sec. after the cutoff.

Curves *II* give the mean values of the wall current in ions per second for the same conditions. At each pressure it is a nearly linear function of n and it decreases with increasing pressure. For small values of n, curve *II* approaches curve *I*, that is, the wall current accounts for nearly the entire change in the number of ions. Curves *III* give the difference between curves *I* and *II*, which is the space recombination in the total volume of the bulb. At the higher pressures the space recombination is greater than the wall recombination, except at very low values of n. The precision seems to be best at 15 μ and here the space recombination is within experimental error proportional to n^2, as is to be expected on theoretical considerations. At higher pressures, curve *III* has less curvature than is to be expected. A value of $\alpha=3.4\times10^{-10}$ fits all observations at pressures of 30 μ or less, within the range of experimental uncertainty. At 70 μ the measurement at $n=8.5\times10^{11}$ gives a value of 4×10^{-10}, while lower currents give higher values.

Measurements over the time interval 0.7 to 1.5×10^{-3} sec lead to similar values of α but with a considerably larger experimental uncertainty. Here the first contact comes very soon after the cutoff, probably during the transition period preceding the uniform afterglow, and this may well account for accidental fluctuations in the measurements.

The best value of the recombination coefficient for pressures of 30 μ or less is

$$\alpha=(3.4\pm.5)\times10^{-10}$$

This value is consistent with the less-accurate estimates obtained in the pressure range 46 to 110 μ by optical methods. Volume recombination accounts for 0.6 or 0.7 of the total change in N under the conditions of the optical measurements, and the values of α derived from them must be multiplied by this factor to correct for wall loss. The spectrophotometric measurements give a corrected value of

$$\alpha=3.6\times10^{-10}.$$

VI. DISCUSSION

The value of the recombination coefficient found here agrees with the value obtained by Kenty in the argon discharge well within his estimated range of uncertainty. The value of 3.4×10^{-10} was found for an electron temperature of about 1,200° *K*. The value probably varies inversely as the first or a higher power of the temperature, and a value of less than 2×10^{-10} is to be expected in the cesium discharge. The relative importance of volume recombination in a columnar discharge can be estimated on this basis. For a 4-amp current at a pressure of 15 μ in a tube 1.8 cm in diameter, the flow of ions to the

walls is 10^{18} ions per second per centimeter of tube, while the volume recombination is less than $1.\times10^{17}$. At 290 μ the flow to the walls is about 5×10^{17} and the volume recombination nearly an equal amount. It is concluded that volume recombination in a columnar discharge is certainly negligible at the lower pressures. Whether or not it becomes important between 100 and 300 μ cannot be asserted definitely until more is known concerning the pressure and temperature variation of the recombination coefficient.

WASHINGTON, July 9, 1937.

U. S. DEPARTMENT OF COMMERCE NATIONAL BUREAU OF STANDARDS

RESEARCH PAPER RP1037

Part of Journal of Research of the National Bureau of Standards, Volume 19, October 1937

JOURNAL-BEARING DESIGN AS RELATED TO MAXIMUM LOADS, SPEEDS, AND OPERATING TEMPERATURES [1]

By Samuel A. McKee

ABSTRACT

This paper outlines briefly a method suggested as a basis for journal-bearing design more especially for applications where the loads and speeds are variable and may reach relatively high values. This method is based upon two primary considerations; first, that the bearing shall operate in the region of stable lubrication, and second, that the operating temperature of the bearing shall not exceed some fixed value.

Equations are derived for the rate of heat generation and for the rate of heat dissipation in terms of factors of construction and operation. Equating the rates of heat generation and dissipation yields an approximate relation between the construction and operation factors and the rise in temperature of a bearing above its surroundings when operating in the region of stable lubrication. The product of the maximum allowable pressures and speeds at which a bearing will operate under the conditions prescribed for safety is obtained by substituting in the above relation permissible values for the temperature rise and the generalized operating variable ZN/P, where Z is the viscosity of the oil, N the speed of the journal, and P the bearing pressure.

In a numerical example to illustrate the application of the method, individual values for the maximum permissible pressure and speed for a given bearing when using a given lubricant are obtained from the equation for the product of the speed and pressure and the minimum permissible value of ZN/P for stable lubrication.

CONTENTS

		Page
I.	Introduction	457
II.	Heat generated in bearing	459
III.	Heat dissipated	459
IV.	Application to design	461
V.	Numerical example	461
VI.	Conclusion	464
VII.	Symbols	465
VIII.	References	465

I. INTRODUCTION

The past decade has seen a considerable advance in the science of journal-bearing lubrication. A number of mathematical and analytical treatments have extended the knowledge of the mechanics of the load-carrying oil film, and experimental investigations have justified the concept of such a film as a basis for design and have also provided correction factors for use in applying theoretical relations. The problem of bearing design, however, is complicated by the fact that a

[1] Presented at the General Discussion on Lubrication and Lubricants, London, England, Oct. 13 to 15 1937, of The Institution of Mechanical Engineers.

journal bearing not only is required to support its load under all conditions of operation, but also in many applications must provide means for dissipating the heat generated in shearing the film of lubricant.

With bearings operating at moderate loads and speeds, the heat generated in the bearing usually is small in comparison with the capacity of the bearing for heat dissipation, and the prime consideration in design is to insure that the bearing shall operate with a complete film of lubricant between the surfaces.

Rational methods [1, 2] [2] for the design of bearings operating under constant moderate loads and speeds have been described in the literature, and it is unnecessary to discuss them in detail at this time. Two methods for assuring conditions for "thick-film" or stable lubrication have been suggested. One is based upon the evaluation of the minimum thickness of the oil film by means of theoretical hydrodynamical relations involving the bearing dimensions and the assumed operating conditions. The other is based upon dimensional analysis and involves the choice of a suitable value for the generalized operating variable ZN/P, the product of the viscosity of the lubricant by the speed of the journal divided by the load per unit projected area. This variable is of particular significance in that it determines the value of both the coefficient of friction and the relative film thickness for a given bearing whenever conditions are such that the bearing is operating in the region of stable lubrication. By its use experimental data may be so correlated as to be directly applicable to design computations. It has been customary to assume a reasonable operating temperature as a basis for a first computation and by methods of successive approximations based on the relations between the heat generated, viscosity, and temperature rise, determine the operating temperature of the bearing. Recently, however, Hersey [3] has suggested a three-dimensional graphical method for the simultaneous solution of the equations involving the three variables. The final computation, of course, is accurate only to the extent that the relations between the three variables are known.

The present-day trend toward the speeding up of all types of machinery has resulted in the use of higher speeds and loads with journal bearings. In a number of applications this has reached the point where the factors affecting bearing temperature are as important as those relating to proper film formation. Many applications also involve wide variations of load and speed. In such cases the designer possibly is more interested in the extreme conditions of load and speed at which a given bearing will operate successfully than he is in its performance at normal running conditions. From this standpoint a rational basis for design would seem to be the determination of the maximum allowable loads and speeds predicated upon two primary considerations: first, that the bearing shall always operate in the region of stable lubrication, and second, that the operating temperature of the bearing shall never exceed some fixed value.

The rise in temperature accompanying the operation of a journal bearing at a given load and speed with a given lubricant decreases the viscosity, and in the region of stable lubrication will result in a decrease in the rate of heat generation. Furthermore this rise in temperature increases the rate of heat dissipation. A bearing operating in the

[2] Figures in brackets here and elsewhere in the text correspond to the numbered references at the end of this paper.

stable region therefore will tend to reach a condition of equilibrium at some temperature where the rate of heat generation is equal to the rate of heat dissipation. Hence, if the equilibrium operating temperature is to be used as a basis for design a knowledge of the factors affecting both the rate of heat generation and the rate of heat dissipation is essential.

II. HEAT GENERATED IN BEARING

Using the nomenclature given in the list of symbols, the rate of heat generation may be expressed as

$$H=k_1F\pi DN, \tag{1}$$

which may also be written as

$$H=k_1\pi fPLD^2N \tag{2}$$

Values for f, the coefficient of friction, for a given bearing at various operating conditions may be computed from theoretical hydrodynamical equations or obtained directly from experimental data. For small-bore full-journal bearings friction data obtained at the National Bureau of Standards are available. In one investigation [4] the effects of changes in the length-diameter and clearance-diameter ratios were determined over a wide range of operating conditions. The results indicated that an equation of the form

$$f=k_2(ZN/P)(D/C)+\Delta f \tag{3}$$

is reasonably accurate for the practical determination of friction losses in bearings of this type when operating in the stable region. In this equation k_2 is equal to 473×10^{-10} when the units given in the list of symbols are employed.[3] Δf is a correction for changes in the length-diameter ratio. The values to be used for various L/D ratios are shown in figure 1.

Substituting equation 3 in equation 2 yields,

$$H=k_1PND[k_2(ZN/P)(D/C)+\Delta f]\pi LD \tag{4}$$

III. HEAT DISSIPATED

In self-cooled bearings the heat is dissipated to the surroundings by a combination of radiation, convection, and conduction. Some heat also is carried away by the oil flowing through the bearing. The influence of these factors will vary with different types of bearings and different operating conditions. The available experimental data on the heat dissipation of bearings are not of such scope as to provide a rigorous evaluation of the factors involved. There is some indication [3, 5], however, that with some types of bearings the rate of heat dissipation may be approximately represented as:

$$H'=k_3A\Delta T^{1.3} \tag{5}$$

The value for the over-all coefficient of heat dissipation k_3 will depend upon many factors, including the convection currents present. Some

[3] Customary English units are employed except for Z which is expressed in centipoises following the usual practice.

data indicate that when the bearing is in a strong draft the value of k_3 may be 3 or 4 times as great as when the bearing is in still air.

Equation 5 may also be written

$$H' = k_3 k_4 \pi LD\Delta T^{1.3} \tag{6}$$

where k_4 is the ratio between the effective area for heat dissipation and the working area in the bearing. Since for equilibrium operating

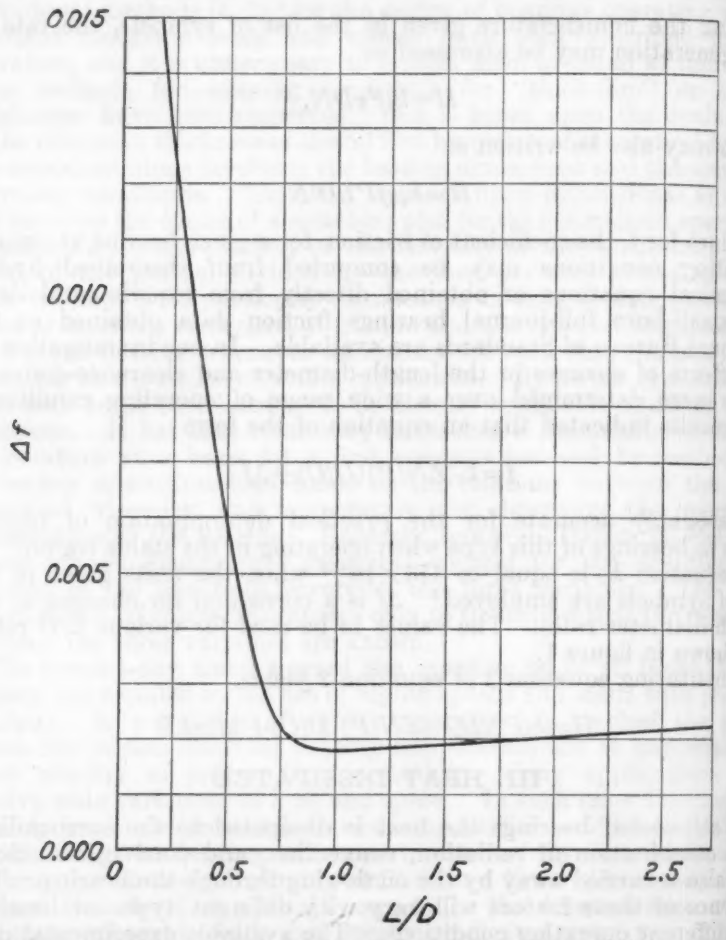

FIGURE 1.—*Values of Δf for various L/D ratios, small-bore 360° bearings.*

conditions, the rate of heat dissipation must equal the rate of heat generation, equations 4 and 6 may be combined to form

$$k_1 PND[k_2(ZN/P)(D/C)+\Delta f] = k_3 k_4 \Delta T^{1.3} \tag{7}$$

This equation indicates approximately the relation between the rise in temperature of a bearing above its surroundings and the other factors involved, when it is operating in the region of stable lubrication.

IV. APPLICATION TO DESIGN

It will be noted that equation 7 involves both the generalized operating variable ZN/P, upon which depends the relative film thickness, and the rise in temperature ΔT which determines the operating temperature of the bearing. This suggests the possibility of obtaining a basis for design as discussed previously in this paper by substituting in equation 7 a minimum limiting value of ZN/P to assure stable lubrication, and a maximum limiting value of ΔT based upon a maximum allowable bearing temperature and a maximum temperature of the surroundings. The limiting value for ZN/P could be chosen with a reasonable margin of safety above the minimum point of f-(ZN/P) curves where friction data for similar bearings are available, or it may be based upon operating experience with bearings of the same type. The limiting operating temperature would depend upon the particular application. In some cases the question of oil stability may be the deciding factor, while in others the effect of temperature upon the characteristics of the bearing metal may be of more importance. If such limiting values are substituted it is seen that for a given bearing equation 7 will assume the form

$$PN=K, \tag{8}$$

wherein K represents the product of the maximum allowable pressures and speeds at which the bearing will operate under the conditions prescribed for safety. It should be noted that this equation is not dependent upon the particular form of equations 4 and 6 but is applicable to all types of journal bearings where the heat-dissipation characteristics are independent of the speed of the journal. In some bearing applications the heat-dissipation coefficient may be dependent upon the speed of rotation. In these cases the form of equation 8, more nearly representative of actual conditions, might be $PN^c=K$, where c is less than 1.

Equation 8 may be written also as

$$PV=K' \tag{9}$$

This is a more general relation where a given value of K' is applicable to all bearings having the same C/D ratios, L/D ratios and heat-dissipation characteristics. It is of interest that equation 9 is similar in form to a relation that has been used to a considerable extent in the past as a basis for bearing design. It should be noted, however, that equation 9 is not a "blanket" relationship that is applicable to all conditions. It involves a definite relation between load, speed, viscosity of the oil, and operating temperature, as prescribed by the limits assumed for safe operation.

V. NUMERICAL EXAMPLE

To illustrate the application of equation 8, a numerical example is given in which the following assumptions are made: A 360° bearing with $D=3$ in., $L=3$ in., $C=0.004$ in., conditions for heat dissipation are such that $k_3k_4=0.00116$, minimum allowable $ZN/P=30$, maximum temperature of surroundings$=100°$ F, and maximum allowable

bearing temperature=250° F. Under these assumptions, $\Delta T=150$, $D/C=750$, and $L/D=1$, hence $\Delta f=0.0018$ (from fig. 1). By substituting the above values in equation 7 and solving for PN a value of 850,000 is obtained, which is the value of K in equation 8. Thus with this bearing under the conditions assumed to represent the limits for safe operation the product of the pressure by the speed should not exceed 850,000, or if expressed as in equation 9, PV should not exceed 667,000.

Values for the individual variables P and N, when using different lubricants, may be obtained by the simultaneous solution of the equations $PN=850{,}000$ and $ZN/P=30$ for a number of values of Z.

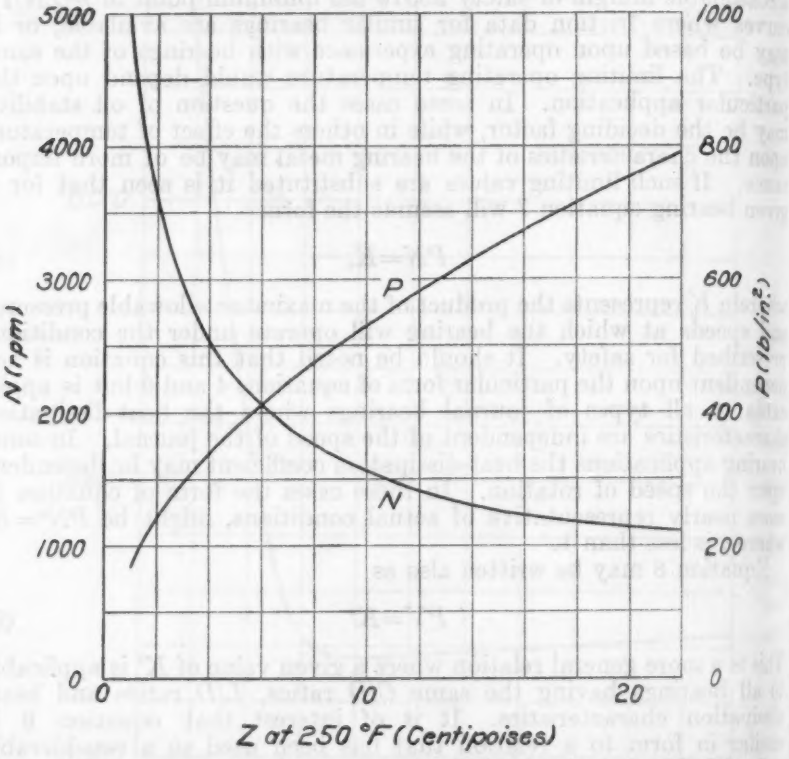

FIGURE 2.—*Pressure-viscosity and speed-viscosity curves for 3- by 3-inch bearing under assumed limiting conditions.*

The results of these computations are given by the PZ and NZ curves in figure 2. A point on the PZ curve represents the maximum pressure at which the bearing may be operated under the given limitations when using an oil having a viscosity at 250° F as indicated. The point on the NZ curve at the same viscosity indicates the speed required when operating at the maximum pressure. Suppose, for example, an oil having a viscosity of 5 centipoises at 250° F is used in this bearing. From figure 2 the values of P and N at $Z=5$ are 374 lb/in.^{2} and 2,260 rpm, respectively. Thus, if the bearing were operating with this oil at a speed of 2,260 rpm and a load such that the pressure on the projected area was 374 lb/in.^{2}, it would come to equilibrium

under the assumed conditions when the temperature reached 250° F and the value of ZN/P would equal 30. It is obvious that if N_1 and P_1 are a pair of limiting values of N and P, any value of P lower than P_1 may be combined with N_1 without reducing the value of ZN/P below the permissible limit or increasing the value of ΔT above the permissible limit, so that a bearing which can be operated at N_1P_1 can be operated safely at N_1 and any value of P below P_1. With a value of P lower than P_1 for a given oil the bearing will not be operating at

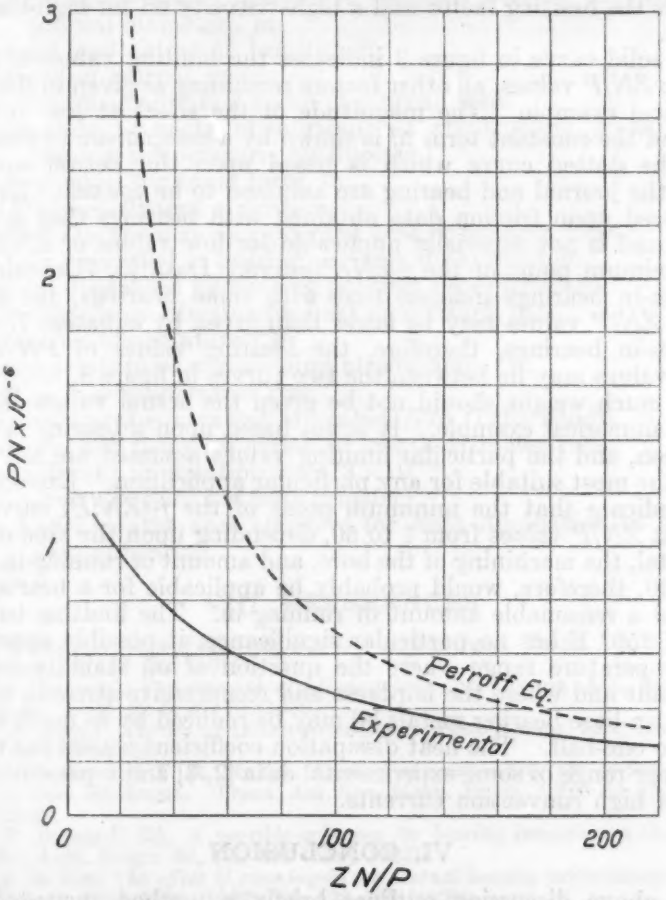

FIGURE 3.—*Curves showing effect of ZN/P value on PN relation for 3- by 3-inch bearing, under assumed limiting conditions.*

$ZN/P=30$ when the limiting temperature is reached; thus the value for PN of 850,000 no longer holds and some value of N other than N_1 becomes the limiting value. This new limiting value may be obtained by the substitution in equation 7 of the limiting value of ΔT, the value of Z at the limiting temperature and the given value of P. Equation 7 will then take on the form $aN\ [bN+\Delta f]=K''$, where a, b, Δf, and K'' are constant terms, and thus may be solved directly for N. Conversely, if the pressure is held at P_1 and N is less than

N_1, the value of PN will be lower than the limit. However, the question as to whether the value of ZN/P is within the limit depends upon whether the lower operating temperature will cause an increase in Z great enough to counteract the decrease in N and hence for a given bearing is dependent upon the viscosity-temperature relation of the particular oil used. The curves in figure 2 also provide a means for selecting a lubricant that will tend to provide maximum bearing capacity for the particular operating conditions. They indicate, for example, the desirability of the use of a low-viscosity oil where high speed is the limiting factor and a high-viscosity oil for high-load conditions.

The solid curve in figure 3 indicates the limiting values of PN at various ZN/P values, all other factors remaining as given in the above numerical example. The magnitude of the effect at low values of ZN/P of the constant term Δf is shown by a comparison of this curve with the dotted curve which is based upon the Petroff equation, where the journal and bearing are assumed to be coaxial. Equation 7 is based upon friction data obtained with bearings that were not run-in and is not especially applicable for low values of ZN/P near the minimum point of the f-ZN/P curve. Data [6, 7] obtained on well-run-in bearings indicate that with some bearings, the friction at low ZN/P values may be lower than given by equation 7. With well-run-in bearings, therefore, the limiting values of PN at low ZN/P values may lie between the two curves in figure 3.

Too much weight should not be given the actual values obtained in this numerical example. It is not based upon a bearing in actual operation, and the particular limiting values assumed are not necessarily the most suitable for any particular application. Experimental data indicate that the minimum point of the f-(ZN/P) curve may occur at ZN/P values from 1 to 50, depending upon the kind of bearing metal, the machining of the bore, and amount of running-in. The value 30, therefore, would probably be applicable for a bearing that has had a reasonable amount of running-in. The limiting temperature of 250° F has no particular significance, it possibly approaches the temperature range where the question of oil stability becomes significant and where the hardness and compressive strength of some of the tin-base bearing metals [8] may be reduced by as much as one-third to one-half. The heat dissipation coefficient chosen lies toward the upper range of some experimental data [2, 3] and represents conditions of high convection currents.

VI. CONCLUSION

The above discussion outlines briefly a method suggested as a possible basis for design more especially for heavy-duty, high-speed bearings. As outlined, the method is directly applicable to self-cooled bearings. It may be made applicable to independently cooled bearings, however, either by the insertion in equation 7 of suitable factors relating to the characteristics of the cooling system, or in its present form to indicate a limit beyond which independent cooling is necessary, and thus provide a measure of the capacity of the cooling system required. It is realized that with the data available at present it will provide only a rough approximation of bearing capacity. Further steps indicated before it could be applied more rigorously

[1]
[2]
[3]
[4]
[5]
[6]
[7]
[8]

are a complete investigation of the frictional characteristics of journal bearings at the lower values of ZN/P and a comprehensive study of the factors affecting the heat-dissipation characteristics for various types of bearing applications.

VII. SYMBOLS

D=journal diameter, in.
L=bearing length, in.
C=running clearance (difference between bearing diameter and journal diameter), in.
W=total load acting on bearing, lb.
N=speed of journal, rpm.
$V=\pi DN/12$=peripheral speed of journal, fpm.
Z=absolute viscosity of lubricant at atmospheric pressure and bearing temperature, centipoises.
F=tangential frictional force, lb.
$f=F/W$=coefficient of friction.
$P=W/LD$=pressure on projected area of bearing, lb/in.^{2}.
H=heat generated in bearing per unit time, Btu/min.
H'=heat dissipated by bearing per unit time, Btu/min.
A=bearing area effective for heat dissipation, in.^{2}.
T_b=bearing temperature, °F.
T_0=temperature of surrounding atmosphere, °F.
$\Delta T=T_b-T_0$=temperature rise.
k_1=mechanical equivalent of heat=1/778 (12)=Btu/in. lb.
Δf=correction factor, function of length-diameter ratio.
k_2=coefficient in equation 3=473×10^{-10}.
k_3=overall coefficient of heat transfer.
$k_4=A/\pi DL$=ratio area effective for heat dissipation to working area of bearing.

VIII. REFERENCES

[1] M. D. Hersey, *Laws of lubrication of journal bearings.* Trans. Am. Soc. Mech. Engrs. **37**, 167–202 (1915).
[2] G. B. Karelitz, *Performance of oil-ring bearings.* Trans. Am. Soc. Mech. Engrs. APM–52–5, 57–70 (1930).
[3] M. D. Hersey, Theory of Lubrication (John Wiley & Sons, Inc., London and New York, 1936).
[4] S. A. McKee and T. R. McKee, *Friction of journal bearings as influenced by clearance and length.* Trans. Am. Soc. Mech. Engrs. APM–51–15, 161–171 (1929).
[5] D. P. Barnard, 4th, *A possible criterion for bearing temperature stresses.* J. Soc. Auto. Engrs. **30**, 192–197 (May 1932).
[6] S. A. McKee, *The effect of running-in on journal bearing performance.* Mech. Eng. **49**, 1335–1340 (1927), **50**, 528–533 (1928).
[7] S. A. McKee and T. R. McKee, *Journal bearing friction in the region of thin film lubrication.* J. Soc. Auto. Engrs. **31**, (T) 371–377 (1932).
[8] H. K. Herschman and J. L. Basil, *Mechanical properties of white metal bearing alloys at different temperatures,* Proc. Am. Soc. Testing Materials **32**, pt. 2, 536 (1932).

Washington, July 5, 1937.

U. S. Department of Commerce National Bureau of Standards

RESEARCH PAPER RP1038

Part of Journal of Research of the National Bureau of Standards, Volume 19, October 1937

ESTIMATION OF AMINO NITROGEN IN INSOLUBLE PROTEINS

By Henry A. Rutherford, Milton Harris, and Arthur L. Smith [1]

ABSTRACT

An apparatus is described for determining the rate of evolution of nitrogen from proteins and other amino compounds during treatment with nitrous acid. Examination of the rate curves of a number of proteins indicates that there is a primary reaction with a relatively rapid evolution of nitrogen followed by a secondary reaction with a much slower evolution of nitrogen in which the rate is approximately constant. Extrapolation of the straight-line portions of the curves to zero time gives values which appear to be good estimates of the amino-nitrogen contents of the proteins.

CONTENTS

	Page
I. Introduction	467
II. Apparatus and technique of operation	469
III. Results and discussion	470
1. Decomposition of nitrous acid	470
2. Estimation of amino nitrogen	471
IV. Summary	476
V. References	477

I. INTRODUCTION

The basic amino acids, arginine, lysine, and histidine, which are of primary importance in proteins appear to be held in the protein chains by peptide linkages involving their carboxyl and α-amino groups. Presumably, the remaining basic groups are free in the native protein and as a result, they have been related to the combining of various proteins with acids, dyes, and tannins. Completely satisfactory conclusions on the nature of such combinations have not been obtained because of the lack of suitable methods for the quantitative estimation of the free-amino groups in proteins and especially those in insoluble proteins.

The Van Slyke method [1] [2] which has been used for the determination of amino nitrogen in solutions of amino acids, peptides, etc., has limitations which have frequently been discussed [2, 3]. Its application to proteins, and more especially insoluble proteins, is further limited because of the difficulty of preparing solutions of these materials without chemical degradation.

[1] Research Associates at the National Bureau of Standards, representing the American Association of Textile Chemists and Colorists. This work was aided by grants from the Textile Foundation, Inc., the Chemical Foundation, Inc., and the Eavenson and Levering Co.

[2] Numbers in brackets refer to the references at the end of the paper.

In a previous investigation, Kanagy and Harris [4] avoided such degradation by working with suspensions of powdered wool and collagen. It was shown that when these proteins are treated with nitrous acid, increasing amounts of nitrogen are evolved with increasing duration of treatment. The amount of nitrogen evolved in any arbitrary length of time does not necessarily represent the amino-nitrogen content of the protein in question. The rate of evolution of

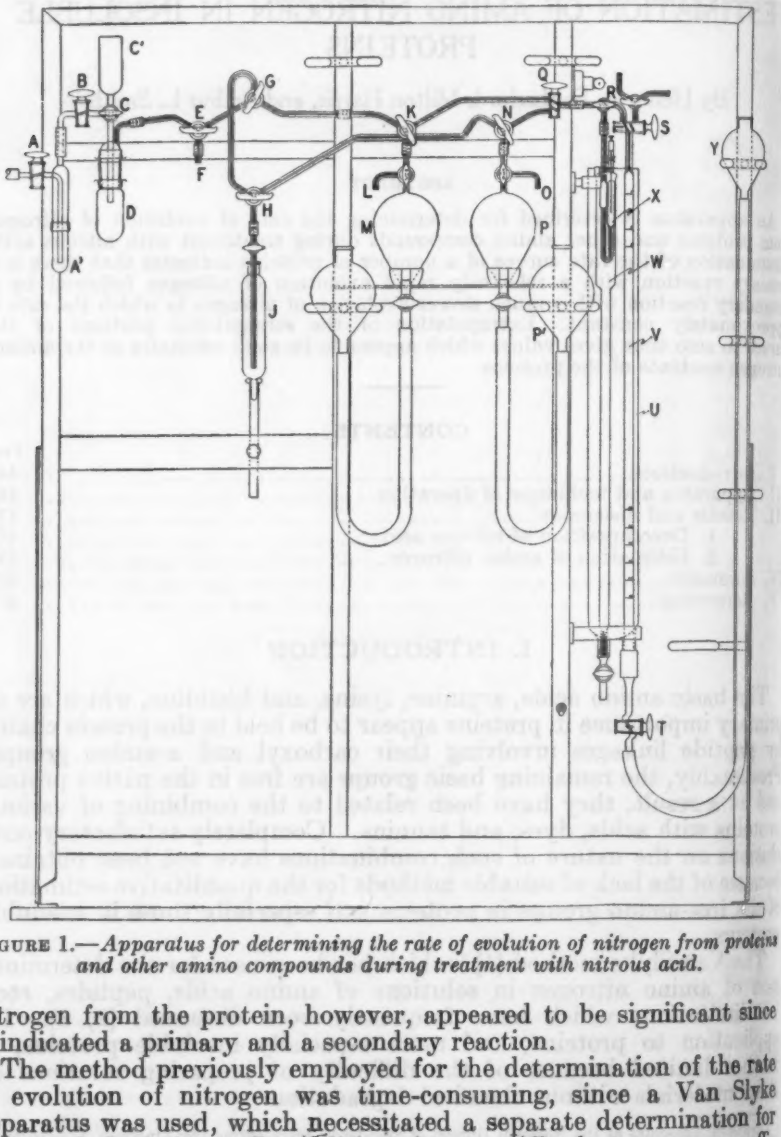

FIGURE 1.—*Apparatus for determining the rate of evolution of nitrogen from proteins and other amino compounds during treatment with nitrous acid.*

nitrogen from the protein, however, appeared to be significant since it indicated a primary and a secondary reaction.

The method previously employed for the determination of the rate of evolution of nitrogen was time-consuming, since a Van Slyke apparatus was used, which necessitated a separate determination for each period of time. In addition, it was difficult to prepare sufficiently uniform suspensions to assure the addition of an accurately known amount of protein for each determination. In order to

eliminate these objections, an apparatus which requires only one sample to obtain a curve which represents the rate of evolution of nitrogen, was developed. A description of the apparatus and a number of preliminary results obtained with it are reported in the present paper.

II. APPARATUS AND TECHNIQUE OF OPERATION

The apparatus which was developed for this investigation is shown in figure 1. An excellent, detailed description of the construction, assembly, and manipulation of the distributor *EGKQNH*, the bubbling pipette *J*, the water jacket *U*, the manometer *X*, the compensator *W*, and the burette *V* is given by Shepherd [5] in a comprehensive paper on apparatus for the analysis of gas mixtures.

The bubbling pipette *J* is filled with a saturated solution of potassium permanganate, approximately 0.5 *N* with respect to potassium hydroxide. The absorption bulb *P*, which has a capacity of 500 ml, contains 300 ml of a potassium hydroxide solution [3] (prepared by adding 3 volumes of water to 5 volumes of a saturated solution of potassium hydroxide), over mercury. The sampling bulb *M* is filled with mercury to stopcock *K*. The distributor, and the arm of the manometer *X* connected thereto, are filled with oxygen-free nitrogen [5]. The burette *V* has a capacity of 25 ml and is calibrated to 0.05 ml. Readings are readily estimated to 0.01 ml. The leveling bulb *Y* contains enough mercury to completely fill the burette and leave an excess within the bulb.

At the beginning of an analysis the entire distributor as well as approximately 10 ml of the burette is filled with nitrogen [5]. The alkaline permanganate solution in *J* is adjusted to the etch-marks on the capillary stems, the mercury in *M* to stopcock *K*, and the potassium hydroxide solution in *P* to a mark just above the bulb. The pressure within the distributor, manometer, and burette is balanced against that in the compensator [5], the volume of gas in the burette is recorded, and the temperature of the water bath surrounding the compensator and burette is noted.

The sample to be analyzed is placed in the reaction vessel *D*, which has a capacity of approximately 70 ml. Obviously, the size of the sample to be used will depend on its amino-nitrogen content and the capacity of the burette. If the material to be analyzed is water-soluble, 10 ml of the solution is taken. If the material is insoluble, a known weight is placed in the reaction flask and thoroughly wet out with 10 ml of water saturated with carbon dioxide. The ground-glass joint of the reaction vessel is properly greased [5], placed in position, and securely fastened with rubber bands. The air in the reaction vessel is swept out with pure carbon dioxide, which enters through stopcock *A*, and passes through a bubbling tube A^1 for the purpose of regulating the flow of carbon dioxide, and finally out at *F*. Ten minutes is usually ample time for removal of the air and, after this time, a sample of gas may be taken through the apparatus by the following procedure, to determine whether all of the air has been removed. The stopcocks are set so that the gas may pass from *D* to *M*, a 500-ml sample of carbon dioxide is taken into bulb *M* through *ABDGK*, and stopcock *B* is closed. The gas in *M* is then passed to

[3] Solutions were saturated with nitrogen at atmospheric pressure.

the bulb *P* through *K*, *G*, *H*, and *N*. The capillary from *K* to *N* is then swept out with nitrogen from the burette through *SRQKGHN* to the bulb *P*. Practically all of the carbon dioxide is immediately taken up by the solution of potassium hydroxide. The last traces of carbon dioxide are removed by repeated passing of the gas from *P* into the bubbling pipette *J*, and back to *P*, three such passages being sufficient to remove measurable amounts of carbon dioxide. During analyses, oxides of nitrogen are formed from the spontaneous decomposition of the nitrous acid. These are removed by the alkaline permanganate solution in *J*, five of the passages described above being used. The residual gas, which is nitrogen, is then taken into the burette. The burette is opened to the manometer, the pressure within the distributor and the burette adjusted to the pressure of the compensator [5], the temperature of the water bath noted, and the increase in volume of nitrogen is determined. As a check the gas in the burette is again passed through the potassium permanganate and potassium hydroxide solutions and the volume again determined.

The procedure outlined above is followed for a regular analysis. Since the rate of reaction is markedly affected by temperature, all experiments were done in a constant-temperature room at 22° C. The nitrous acid solution, the preparation of which is described later, is added to the sample through C^1 by opening *D* to bulb *P* and slightly lowering the level of the solution in *P*. The measurement of the amount of gas evolved at any time is accomplished as follows. One and one-half minutes before taking a sample of gas, a partial vacuum is created in the reaction flask by lowering the leveling bulb P^1. The reaction flask *D*, which is attached to the distributor by means of rubber connections, is shaken for an arbitrary [4] but definite time (45 seconds in this work). A 500-ml sample of gas is then taken by passing carbon dioxide through *D* until *M* is filled, and the amount of nitrogen is determined as previously described. The sampling, purification, and determination of the volume of the residual gas require approximately 7 minutes.

III. RESULTS AND DISCUSSION

1. DECOMPOSITION OF NITROUS ACID

As was previously pointed out [4], one of the possible sources of error in the Van Slyke method is the correction for relatively large amounts of nitrogen which may be evolved by the spontaneous decomposition of the nitrous acid. It was shown that the size of the blank depends on the age of the sodium nitrite solution, on the amount of mechanical action, and on the nature of the material being analyzed. Since the amount of free-amino nitrogen is often very small, it was particularly desirable to keep the blank corrections as small as possible.

A preliminary investigation indicated that in addition to the above-mentioned factors, the size of the blank increases considerably with decreasing pH of the solution. Furthermore when the pH of the solution of nitrous acid was increased, there was a decrease in the rate at which nitrogen was evolved from an amino compound. As a result, it was necessary to seek those conditions which would give a sufficiently rapid evolution of nitrogen and as small a blank as possible.

Sodium acetate, because of its buffering action, was found to be very effective in decreasing the size of the blanks. Raising the pH of the nitrous acid solution from pH 3.4 to pH 4 by the addition of suitable amounts of sodium acetate decreased the blank by approximately 80 percent. In order to study the effect of sodium acetate on the rate of evolution of amino nitrogen, the experiments recorded in table 1 were performed. The results show that of the combinations of nitrous acid and sodium acetate tried, that given in experiment 7 was the most effective.

The nitrous acid solution used in subsequent experiments was prepared as follows. Five ml of glacial acetic acid was mixed with 5 ml of a saturated solution of sodium acetate. Six grams of sodium nitrite was dissolved in 20 ml of water previously saturated with CO_2, the two solutions were mixed, gently stirred, and then poured into the funnel C'. Exactly 1½ minutes after mixing the two solutions, the solution is allowed to run into the reaction vessel D, as previously described.

TABLE 1.—*Rates of evolution of nitrogen from alanine in solutions in which the proportion of nitrous acid and sodium acetate were varied*

Experiment	Glacial acetic acid	Sodium nitrite	Saturated sodium acetate [b]	Water [c]	Time	Total *N* as amino nitrogen
	ml	g	ml	ml	min	*Percent*
1	3	12	10	30	15	81.2
					30	84.4
2	5	12	10	25	15	92.8
					30	97.9
3[a]	5	12	10	25	15	69.4
					30	85.4
4	5	6	10	25	15	93.7
					30	97.9
5	2.5	3	10	25	15	58.8
					30	84.3
6	2.5	3		35	15	92.8
					30	99.1
7	5	6	5	30	15	96.2
					30	101
					45	101
8	5	6		35	15	99
					30	101
					45	101

[a] Reaction flask not shaken before sampling.
[b] Saturated aqueous solution at 22° C.
[c] Volume given includes 10 ml in which alanine was dissolved.

2. ESTIMATION OF AMINO NITROGEN

An examination of the literature pertaining to the Van Slyke method and its limitations [1, 2, 3] shows that many amino acids, peptides, and related compounds give faulty values when analyzed for amino-nitrogen content. A confirmation of some of those findings was obtained during the present work with various amino acids. In view of such abnormalities, it would appear at first sight to be a discouraging task to attempt to estimate the amino-nitrogen content of an insoluble protein. Although exact mechanisms to account for the abnormal behavior of many compounds are not known, it is quite certain that in most cases, the extra nitrogen is not formed by the reaction of nitrous acid with the expected end-product of the reaction [3]. The complexity of the reactions suggests that the

extra nitrogen might be formed by a series of reactions, probably involving more than one intermediate product. From this standpoint, it appears possible that insoluble proteins may be less abnormal than the less complex soluble compounds which are free to move about in solution and enter into a number of different reactions.

Of the various amino acids which give high values for amino nitrogen, only tryptophane and arginine evolve nitrogen at an appreciable rate during their secondary reactions. The remaining amino acids exhibit a rapid primary evolution of nitrogen which gives values over 100 percent, based on the theoretical content of amino nitrogen, in 5 minutes or less. They may or may not exhibit a very small increase in the amount of nitrogen evolved after this time. Since wool and collagen contain little if any tryptophane but relatively large amounts of arginine, an attempt was made in a previous investigation [4] to relate the arginine content of the protein to the rate of evolution of nitrogen during the secondary reaction.

The reaction of arginine with nitrous acid was reinvestigated with the new apparatus. Some preliminary results are shown in figures 2 and 3. Assuming that all of the nitrogen evolved (other than that corrected for in the blank) comes from the arginine, the curve in figure 2 shows that nearly 90 percent of the total nitrogen of arginine is liberated in about 150 hours. A closer examination of the first part of the curve, as shown in figure 3, reveals that a rapid evolution of nitrogen, which is called the primary reaction, occurs in the first few minutes, followed by a much slower secondary reaction in which the rate of evolution of nitrogen is approximately constant. Extrapolation of the secondary portion of the curve (fig. 3) to zero time gives a value of 25 percent, which is equal to the α-amino-nitrogen content of arginine. When the concentration of arginine in the reaction mixture was varied, as shown in table 2, the experimental values for the α-amino-nitrogen content, obtained by extrapolation of the secondary portions of the curves, are in very good agreement with the theoretical values. It is also of interest to note that for the given concentration of nitrous acid the slopes of the curves (and the rate of evolution of nitrogen) are directly proportional to the initial concentrations of arginine. However, when the arginine content is kept constant and the concentration of nitrous acid is cut to half the usual value, the rate of evolution of nitrogen in the secondary reaction is very much lower, although the extrapolated value for amino nitrogen is the same.

In the previous investigation [4] it was suggested that the arginine content of an insoluble protein could be estimated by determining the relative rates of evolution of nitrogen from the guanidine nuclei in a protein and in arginine. If this is true, then the decrease in rate of evolution of nitrogen from a protein during the secondary reaction, with decrease in concentration of nitrous acid, should be proportional to the decrease in the rate of evolution of nitrogen from arginine under similar conditions. That this suggestion is not valid is shown in table 3. The results indicate that the agreement between the calculated values for the arginine contents of wool and collagen and those obtained by isolation methods was the result of chance coincidence.

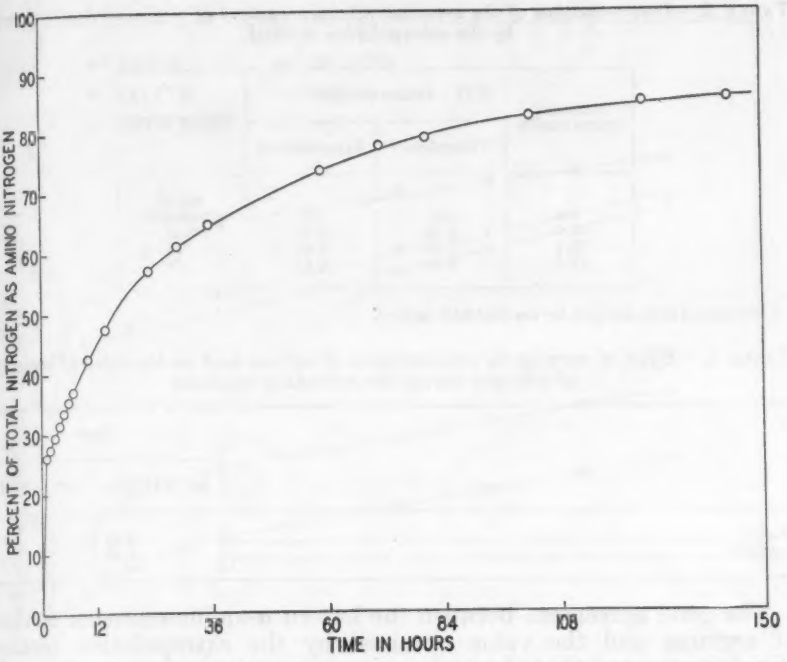

FIGURE 2.—*Rate of evolution of nitrogen during the continued treatment of arginine with nitrous acid.*

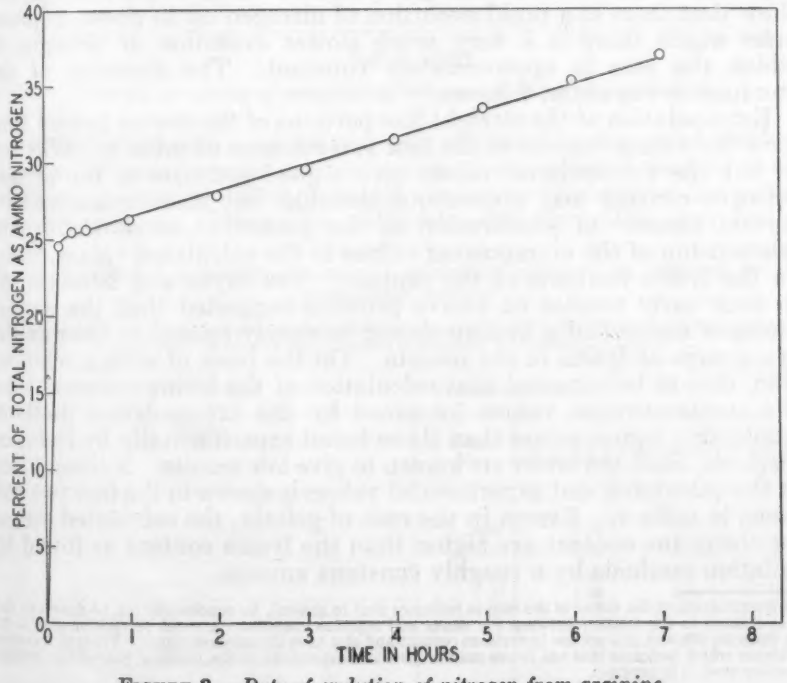

FIGURE 3.—*Rate of evolution of nitrogen from arginine.*

This is the initial portion of the curve shown in figure 2 plotted on a larger scale.

TABLE 2.—*Determination of the α-amino-nitrogen content of arginine hydrochloride by the extrapolation method.*

Arginine hydrochloride	Amino nitrogen		Slope of curve
	Theoretical *	Experimental	
mg	mg	mg	mg of nitrogen/hr
50.0	3.22	3.17	0.24
25.1	1.63	1.64	.13
12.5	0.81	0.82	.06

* Calculated from analyses by the Kjeldahl method.

TABLE 3.—*Effect of varying the concentration of nitrous acid on the rates of evolution of nitrogen during the secondary reactions*

	Slope	
	2.1 *M* HNO_2	1.05 *M* HNO_2
Wool	0.16	0.13
Arginine	1.86	.36

The good agreement between the known α-amino-nitrogen content of arginine and the value obtained by the extrapolation method (fig. 3) suggested that the amino-nitrogen content of a protein might also be estimated by that method. The results of determinations of the rates of evolution of nitrogen from a number of proteins (fig. 4) show that there is a rapid evolution of nitrogen up to about 2 hours, after which there is a very much slower evolution of nitrogen in which the rate is approximately constant. The duration of the treatments was about 7 hours.

Extrapolation of the straight line portions of the curves to zero time gave the values [4] shown in the first two columns of table 4. Whether or not the extrapolated values give a good estimate of the amino-nitrogen content may appear questionable, but there seems to be a certain amount of justification in the procedure as shown by the relationship of the extrapolated values to the calculated values, based on the lysine contents of the protein. Van Slyke and Birchard [6] in their early studies on native proteins suggested that the amino-nitrogen content of a protein should be closely related to the number of ε-groups of lysine in the protein. On the basis of such a relationship, it is to be expected that calculation of the lysine contents from the amino-nitrogen values (obtained by the extrapolation method) would give higher values than those found experimentally by isolation methods, since the latter are known to give low results. A comparison of the calculated and experimental values is shown in the last two columns in table 4. Except in the case of gelatin, the calculated values for the lysine content are higher than the lysine content as found by isolation methods by a roughly constant amount.

[4] Examination of the slopes of the curves indicates that in general, no conclusions can be drawn at this time relative to the relation between the slopes and arginine contents. A rough correlation is evident: for example, silk and zein are low in arginine content and also have the smallest slopes. There is, however, evidence which indicates that the slopes may be partially dependent on the physical state of the protein. Further work is in progress.

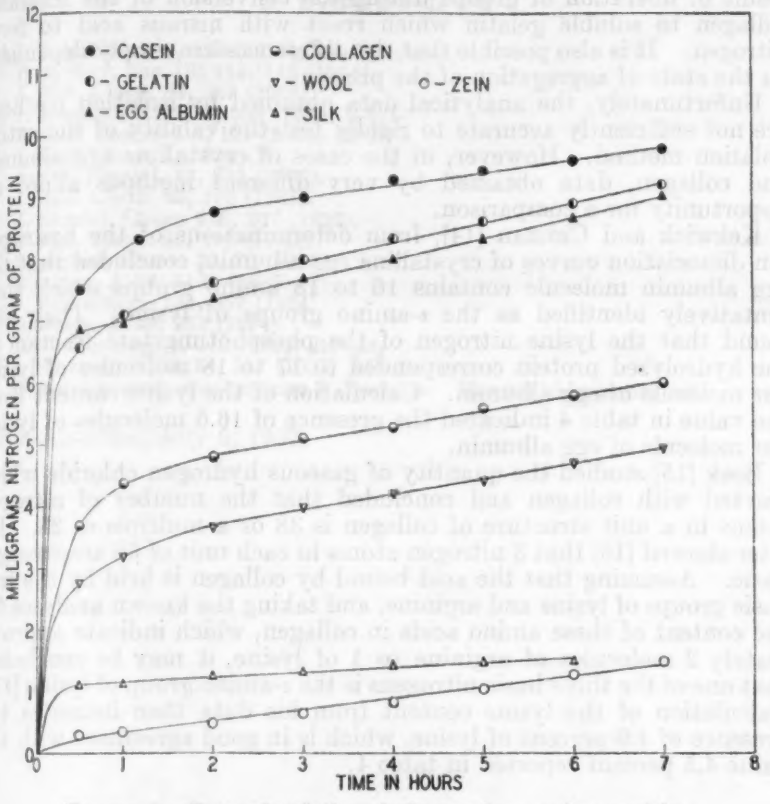

FIGURE 4.—*Rates of evolution of nitrogen from various proteins.*

Although collagen and gelatin are presumably the same protein (the gelatin was prepared from a sample of the collagen used for these analyses), they give different values for amino nitrogen by the extrapolation method. The higher value obtained for gelatin may be the

TABLE 4.—*Free a mino-nitrogen content of various proteins as obtained by the extrapolation method*

[The values for lysine in the last two columns represent those calculated from the amino-nitrogen contents and those recorded in the literature as obtained by isolation methods.]

Protein	Free amino-nitrogen		Lysine	
	% of total N	mg of N/gm of protein	Calculated	Literature
			%	%
Zein	0.68	0.12	0.12	0.0 [7]
Silk	.56	1.05	1.10	0.25 [8] / 0.85 [9]
Wool	1.94	3.16	3.3	2.3 [10]
Collagen	2.37	4.26	4.5	2.75 [11]
Egg albumin	4.50	6.75	7.1	4.97 [12]
Gelatin	4.67	7.03	7.3	2.75 [11]
Casein	5.68	8.36	8.7	6.5 [13]

result of liberation of groups during the conversion of the insoluble collagen to soluble gelatin which react with nitrous acid to form nitrogen. It is also possible that the differences are simply dependent on the state of aggregation of the protein.

Unfortunately, the analytical data obtained by isolation methods are not sufficiently accurate to rigidly test the validity of the extrapolation method. However, in the cases of crystalline egg albumin and collagen, data obtained by very different methods afford an opportunity for a comparison.

Kekwick and Cannan [14], from determinations of the hydrogen ion dissociation curves of crystalline egg albumin, concluded that the egg albumin molecule contains 16 to 18 amino groups which they tentatively identified as the ϵ-amino groups of lysine. They also found that the lysine nitrogen of the phosphotungstate fraction of the hydrolyzed protein corresponded to 17 to 18 molecules of lysine per molecule of egg albumin. Calculation of the lysine content from the value in table 4 indicated the presence of 16.6 molecules of lysine per molecule of egg albumin.

Beek [15] studied the quantity of gaseous hydrogen chloride which reacted with collagen and concluded that the number of nitrogen atoms in a unit structure of collagen is 38 or a multiple of 38. He later showed [16] that 3 nitrogen atoms in each unit of 38 are strongly basic. Assuming that the acid bound by collagen is held by the free basic groups of lysine and arginine, and taking the known analyses for the content of these amino acids in collagen, which indicate approximately 2 molecules of arginine to 1 of lysine, it may be concluded that one of the three basic nitrogens is the ϵ-amino group of lysine [17]. Calculation of the lysine content from his data then indicates the presence of 4.9 percent of lysine, which is in good agreement with the value 4.5 percent reported in table 4.

IV. SUMMARY

An apparatus for determining the rate of evolution of nitrogen from proteins and other amino compounds during treatment with nitrous acid is described. Examination of the rate curves of a number of proteins indicates that there is a primary reaction with a relatively rapid evolution of nitrogen, followed by a secondary reaction with a much slower evolution of nitrogen in which the rate is approximately constant. Extrapolation of the straight line portions of the curves to zero time gives values which appear to be good estimates of the amino-nitrogen contents of the proteins. In the case of crystalline egg albumin and collagen, the extrapolated values are in good agreement with values obtained by other methods. No conclusions relative to the significance of the slopes of the curves are drawn at this time.

The authors are indebted to Martin Shepherd for assistance in designing the apparatus used in this work and for many helpful suggestions relative to its operation.

V. REFERENCES

[1] J. Biol. Chem. **9,** 185 (1911); **12,** 275 (1912).
[2] Proc. Roy. Soc. [B] **115,** 142 (1934).
[3] J. Biol. Chem. **82,** 587 (1929).
[4] J. Research NBS **14,** 563 (1935) RP787.
[5] B. S. J. Research **6,** 121 (1931) RP266.
[6] J. Biol. Chem. **16,** 539 (?).
[7] Am. J. Physiol. **17,** 231 (1906).
[8] J. Biol. Chem. **93,** 105 (1931).
[9] Z. physiol. Chem. **120,** 207 (1922).
[10] J. Biol. Chem. **86,** 107 (1930).
[11] Z. physiol. Chem. **35,** 70 (1902).
[12] Biochem. J. **26,** 1101 (1932).
[13] J. Biol. Chem. **105,** 667 (1934).
[14] Biochem. J. **30,** 235 (1934).
[15] BS J. Research **8,** 549 (1932) RP434.
[16] J. Research NBS, **14,** 217 (1935) RP765.
[17] Personal communication from J. Beek, Jr. Results to be published.

WASHINGTON, July 6, 1937.

12341—37——8

U. S. Department of Commerce National Bureau of Standards

RESEARCH PAPER RP1039

Part of Journal of Research of the National Bureau of Standards, Volume 19, October 1937

X-RAY DIFFRACTION PATTERNS OF SOL, GEL, AND TOTAL RUBBER WHEN STRETCHED, AND WHEN CRYSTALLIZED BY FREEZING AND FROM SOLUTIONS

By George L. Clark,[1] Enno Wolthuis,[2] and W. Harold Smith

ABSTRACT

Total, sol, and gel rubber were prepared under conditions which were selected to avoid oxidation and structural changes. Total rubber when stretched and exposed to an X-ray beam produced the characteristic crystal fiber pattern. Stretched sol rubber produced no evidence whatever of this pattern even at 1,000 percent elongation. With stretched gel rubber, the pattern was formed above 100 percent elongation, and at 200 percent was sharp and intense. A large interplanar spacing of 54 A, found in the unstretched gel, was absent in the sol. The patterns obtained with stretched gel, with frozen sol, gel, and total rubber, and with gel crystals produced from an ethereal solution were measured and analyzed. The crystals produced by all of these methods are similar. The measurements agree excellently with those reported recently by Lotmar and Meyer, and by Barnes.

CONTENTS

	Page
I. Introduction	479
II. Materials and methods	481
III. Experimental results	484
1. Behavior of sol, gel, and total rubber when stretched	484
2. Large interplanar spacing in gel rubber	485
3. Diffraction patterns of stretched gel rubber	486
4. Diffraction patterns of frozen sol, gel, and total rubbers	487
5. Comparison between stretched rubber and frozen rubber, and the assignment of crystal indices	488
6. Sol and gel rubber crystallized from solutions	490
IV. Summary	491

I. INTRODUCTION

When unstretched rubber is examined by X-rays, it produces a blurred ring, the halo which is typical of the amorphous or liquid state. Its behavior when stretched was first reported by Katz,[3] who observed interference spots at 80 percent elongation. Their intensity increased with increasing elongation and at 400 percent a definite fiber diagram was observed. Consequently, rubber, when extended, was considered to be crystalline, and the Joule effect to result from an actual formation of crystals. When Katz heated stretched rubber, the interference spots vanished. Vulcanized rubber produced inter-

[1] Professor, University of Illinois.

[2] Graduate Student, University of Illinois. A part of the material in this paper was presented as a thesis by Enno Wolthuis in May 1937, to the Faculty of the Graduate School of the University of Illinois, represented by Dr. George L. Clark, in partial fulfillment of the requirements for the degree of Doctor of Philosophy.

[3] J. R. Katz, Kolloid Z. **36**, 300; **37**, 19 (1925).

ferences, but the spots were weaker than those obtained with unvulcanized rubber. The identity period along the direction of stretch was 8 A and the dimensions assigned to the unit cell were $8\times6.5\times6.5$ A, with a volume of 338 A^3.

The behavior of stretched rubber between 80 and 1,000 percent elongations was investigated by Hauser and Mark,[4] who made a more accurate study of the positions and intensities of the interferences. The positions of the interferences were found to be independent of the degree of stretching, but their intensities increased proportionally with it. The position of the amorphous ring remained unchanged during extension, but its intensity decreased with continued elongation. Therefore, an amorphous or liquid phase in unstretched rubber was supposed to be changed to a crystalline phase when it was stretched. The positions of the interferences, which depend on the dimensions of the unit cell, did not change with continued stretch and consequently a definite space lattice was indicated. Other evidence showed that new crystalline units were constantly produced during elongation, and that the major axis of the crystalline phase was oriented parallel to the direction of stretch. The interferences in stretched rubber disappeared at 60° C. When rubber was maintained in an extended condition for some time, the interference spots vanished. If rubber was milled or swollen by solvents before stretching, the interference spots did not appear. An orthorhombic configuration was assigned to the unit cell, but the possibility of a monoclinic structure was admitted. Its dimensions, $8.0\times8.6\times7.68$ A, correspond to a cell volume of 529 A^3. There were 4.12 molecules of C_5H_8 per unit cell.

The interferences obtained by Mark and von Susich [5] were better defined, and better measurements were possible. A rhombic cell was assumed and the dimensions given to it were $8.3\times8.1\times12.3$ A ±0.1 A. The volume of the unit cell was reported to be 830 ± 30 A^3, with 7.1 molecules and not 8, presumably because of poor density values. With the Weissenberg apparatus, Mark and von Susich proved that the indices (111) and (200) of Hauser and Mark are really (100) and (010). They observed that very thin specimens of rubber showed fibering and also three-dimensional orientation. So a distribution of carbon atoms was proposed which aims to reconcile the orientation of the primary valence chains in the direction of stretch, atomic spacings for single and double-linked carbon atoms, and the observed intensities. By topochemical reactions, they attempted to convert stretched rubber into derivatives retaining the structure, but X-ray patterns of the derivatives indicated an amorphous condition.

On the basis of a single experiment, Ott [6] assigned a volume of 259 A^3 to the largest possible cell. Using the values of Bragg for the radius of carbon, 0.77 A, and of hydrogen, 0.73 A, and assuming close packing, the volume of C_5H_8 was computed to be 43.1×10^{-24} ml or 43.1 A^3. On these assumptions, the maximum number of C_5H_8 groups in Ott's cell is six.

A recent paper by Lotmar and Meyer [7] reports accurate measurements of the structure of crystallized rubber. The unit cell was

[4] E. A. Hauser and H. Mark, Kolloidchem. Beihefte **22**, 63 (1926).
[5] H. Mark and G. von Susich, Kolloid Z. **46**, 11 (1928).
[6] E. Ott, Naturwissenschaften **14**, 320 (1926).
[7] W. Lotmar and K. H. Meyer, Monatsh. **69**, 115 (1936).

derived by the graphical method of Sauter, is monoclinic, and has the following axes:

$a = 8.54 \pm 0.05$ A
$b = 8.20 \pm 0.05$ A (fiber axis)
$c = 12.65 \pm 0.05$ A
$\beta = 83°20'$
Volume of unit cell = 880 A^3, approximately.

They report 7.6 molecules per unit cell and this value is based on the highest value of density, 0.965, reported in the literature.[8] Eight molecules are assumed to be present. By an elimination of possible space groups, there remains the probable one, C^5_{2h}, and the chains are presumed to have the symmetry of a twofold screw axis. The crystallite is said to be a molecular racemate of right and left spiral molecules.

Subsequent to the work of Lotmar and Meyer, Barnes [9] examined two samples of frozen crude rubber, one of which had remained frozen for 22 years, and the other for at least 11 and probably for 30 years. They lost their opacity at approximately 41° C. The measurements of Barnes agree excellently with those reported by Lotmar and Meyer for stretched rubber. Identical patterns were obtained from each specimen.

Crystal interferences in frozen, unstretched smoked sheet were found by Hauser and Rosbaud.[10] They were indicated by Debye-Scherrer rings. Later, von Susich [11] constructed a melting curve from the behavior of patterns of frozen rubber at different temperatures. With unstretched rubber, the powder pattern disappeared completely at approximately 35° C, and with stretched rubber at about 90° C. Above 90° C the pattern was that of an amorphous material. Indices were assigned to four rings in the frozen-rubber pattern, but no spacings or calculations were mentioned.

In the present investigation the work of Lotmar and Meyer is checked with stretched gel rubber, which yields a sharper and more intense diffractive pattern than is obtained with the total rubber. The powder patterns of frozen sol, gel, and total rubbers are compared as to their interplanar spacing and the intensity of their interferences, and an examination is made of the sol and gel fractions crystallized from an ethereal solution at low temperature.

II. MATERIALS AND METHODS

The rubber hydrocarbon used in this investigation was obtained from the latex of *Hevea brasiliensis*, the source of the principal rubber of commerce. It was prepared at the National Bureau of Standards from latex supplied by the United States Department of Agriculture, and was studied by X-rays at the University of Illinois.

The preparation of pure sol, gel, and total rubber hydrocarbons, and the formation of discrete crystals of sol and gel rubber from solution, have been discussed in previous issues of this journal.[12] Similar

[8] H. Mark and G. von Susich, footnote 5.
[9] William H. Barnes, Can. J. Research 15, 156 (1937).
[10] E. A. Hauser and P. Rosbaud, Kautschuk 3, 17 (1927).
[11] G. von Susich, Naturwissenschaften 18, 915 (1930).
[12] W. Harold Smith, Charles Proffer Saylor, and Henry J. Wing, BS J. Research 10, 479 (1933) RP 544. W. Harold Smith and Charles Proffer Saylor, J. Research NBS 13, 453 (1934) RP719.

material was used in this investigation. The rubber was purified and separated into sol and gel fractions under conditions which aimed to preserve its structure and to avoid the effects of light and of oxygen. Oxidation of the rubber was minimized by allowing it to remain in contact with the natural antioxidants which are in crude Hevea rubber, until the final stage of purification. At low temperatures the hydrocarbons in massive rubber crystallize without a solvent. Specimens of "frozen" sol and gel were prepared by maintaining the samples at −25° C for 30 days. Other specimens of crystalline sol and gel rubber were prepared at low temperatures from ethereal solutions of the fractions.

The production of a diffraction pattern by stretched rubber, and the changes which occur when unstretched rubber is frozen and when it separates from an ethereal solution at low temperatures as discrete particles have been repeatedly termed crystallization, and that word will be used in this paper.

In the application of the ordinary X-ray diffraction equipment and technique there is no resolution of interferences which correspond to the very long interplanar spacings which frequently exist in natural materials. Hence, special apparatus and methods have been developed in the X-ray laboratory of the University of Illinois, in which a magnetic field is used to deflect the scattered electrons which ordinarily fog the film. Definite and reproducible evidence has been obtained of very large spacings in collagen, gelatin, keratin, and other materials, including gel rubber.

For the work with stretched gel rubber an ordinary flat-film camera was used. The distance from specimen to film was 5 cm. For the work with frozen sol, gel, and total rubbers, and rubber crystals deposited from solution, special apparatus and technique were again required to obtain the diffraction patterns at temperatures below the melting point of the crystals.

The crystallized rubber specimens were examined by two specially constructed types of cameras. One was a cylindrical camera, shown in figure 1, in which a low-temperature specimen holder, pictured in figure 2, was inserted in place of the wedge sample holder used for powder specimens. The entire holder was cooled by the exhaust from a liquid-air reservoir, and the cold air passed out alongside the specimen. The sides of the cylindrical camera were closed to prevent condensation of moisture on the specimen. The air in the camera was readily precooled by placing solid carbon dioxide within it. The other low-temperature camera is shown in figure 3, and had the advantage of a longer distance from specimen to film for the accurate determination of the longer spacings. It consisted simply of a funnel, in the apex of which was situated the pinhole and specimen, the latter held in place with aluminum washers. Cooling was accomplished by means of solid carbon dioxide and acetone. The open end of the funnel was fastened to a wooden frame which held a flat film. The collimator (not shown in the drawing) which defined the beam of X-rays, and which touched the camera, was constructed of wood to prevent the condensation of moisture upon it and to avoid the conduction of heat to the specimen.

In all X-ray investigations of rubber we have employed the copper K radiation from a Philips Metalix tube operating at 26 kv and 22 ma.

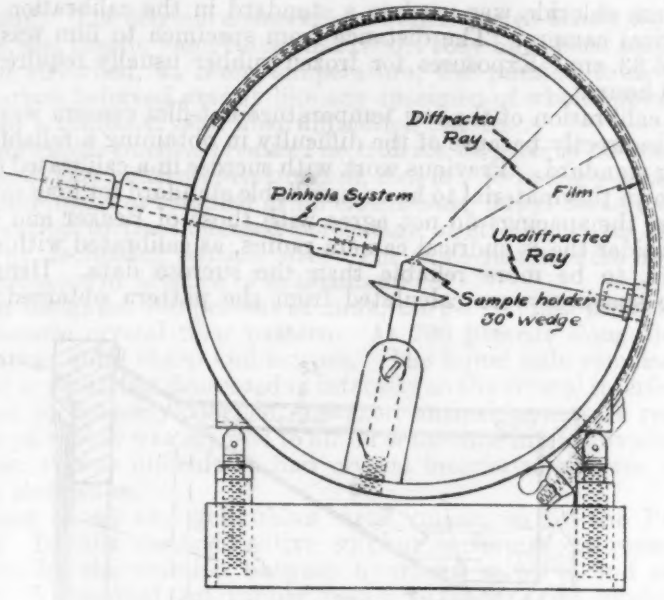

FIGURE 1.—*Cylindrical camera.*

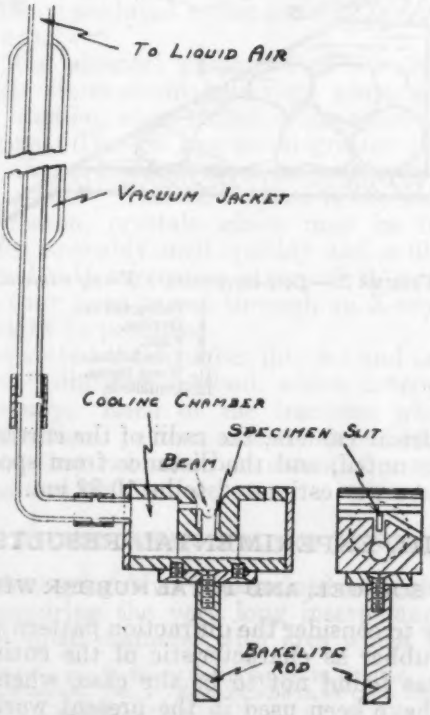

FIGURE 2.—*Low-temperature specimen holder.*

Sodium chloride was used as a standard in the calibration of the cylindrical camera. The distance from specimen to film was found to be 6.33 cm. Exposures for frozen rubber usually required from 5 to 10 hours.

The calibration of the low temperature flat-film camera was determined indirectly because of the difficulty in obtaining a reliable long-spacing standard. Previous work with sucrose in a calibrated camera had shown this material to be an unreliable standard for long spacings. At least the spacings do not agree with those of Becker and Rose.[13] We consider the cylindrical camera radius, as calibrated with sodium chloride, to be more reliable than the sucrose data. Hence, the sucrose spacings were calculated from the pattern obtained in the

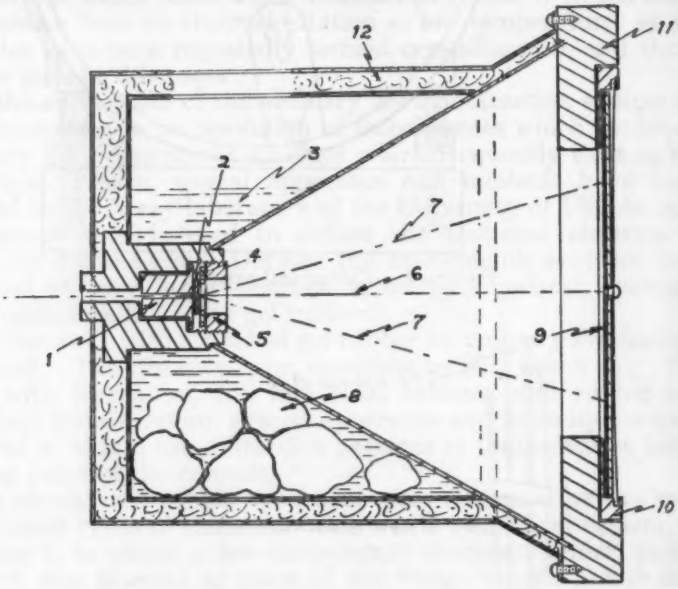

FIGURE 3.—*Low-temperature X-ray camera.*

1. Pinhole.
2. Specimen.
3. Acetone.
4. Aluminum washer.
5. Threaded washer.
6. Undiffracted ray.
7. Diffracted ray.
8. Dry ice.
9. Film.
10. Film holder.
11. Wood frame.
12. Insulation.

calibrated, cylindrical camera, the radii of the corresponding lines on the flat film were noted, and the distance from specimen to film of the flat-film camera was estimated to be 10.32 cm.

III. EXPERIMENTAL RESULTS

1. BEHAVIOR OF SOL, GEL, AND TOTAL RUBBER WHEN STRETCHED

It is customary to consider the diffraction pattern which is obtained with stretched rubber as characteristic of the entire rubber hydrocarbon. This was found not to be the case, when the sol and gel fractions which have been used in the present work were examined

[13] K. Becker, and H. Rose, Z. Physik **14**, 369 (1923).

separately. The original observations were reported briefly by Clark, Warren, and Smith,[14] and since that report they have been confirmed.

When stretched, at room temperature, the purified total rubber hydrocarbon behaved exactly like any specimen of whole rubber, and produced a similar crystal fiber diffraction pattern.

The sol rubber fraction produced no evidence whatever of the characteristic crystal fiber pattern when stretched, even at 1,000 percent elongation. The liquid halo was retained at all elongations, but it became *broader* in proportion to the increased percentage of stretch. This may be caused by decreasing particle size. The same results were observed in the presence or absence of antioxidants.

When elongated 100 percent or more, the gel fraction produced the characteristic crystal fiber pattern. At 200 percent elongation the pattern was quite sharp and intense. The liquid halo remained unchanged in width but decreased in intensity as the crystal interferences increased in intensity. When, however, antioxidants were removed and the gel rubber was exposed to air for some time in the unvulcanized condition, it was difficult to find crystal interferences, even at 400 percent elongation.

Samples of sol and gel rubber were vulcanized by the Peachey process. In this method, active sulphur is formed at room temperatures by the reaction between hydrogen sulphide and sulphur dioxide. Vulcanized sol rubber began to show faint evidence of crystal interferences when stretched more than 400 percent, which showed that sulphur had produced a profound structural effect. Vulcanized gel rubber produced a fiber pattern, but not at elongations less than 250 percent.

Differences in the physical properties of sol and gel rubber are indicated by their stress-strain behavior, when vulcanized.[15] The unvulcanized gel fraction, when milled, is the more difficult to "break down" or plasticize. The gel has much greater stiffness and more perfect elasticity; the sol is softer, more extensible, and when deformed takes a permanent set.[16] The sol fraction is the more mobile of the two. For that reason, crystals which may be formed when sol rubber is stretched probably melt quickly and a diffraction pattern cannot be obtained. If successive strips of it were stretched, immediately before they were passed through an X-ray beam, evidence of crystallinity might be produced.

Pummerer [17] separated total rubber into sol and gel by a modification of Feuchter's [18] diffusion method, which differs from that used in the present study. Each of the fractions which he obtained produced a diffraction pattern when stretched. Subsequently, Hauser [19] observed that rubber when extended very slowly, that is, isothermally, produced no interference.

2. LARGE INTERPLANAR SPACING IN GEL RUBBER

When unstretched gel rubber is examined with the equipment for detecting and measuring the very long interplanar spacings, there appears a ring of small diameter with arcs which indicate fibering.

[14] Geo. L. Clark, W. J. Warren, and W. Harold Smith, Science **79**, 433 (1934).
[15] W. Harold Smith and William L. Holt, J. Research NBS **13**, 465 (1934) RP720.
[16] See footnote 12.
[17] R. Pummerer, Kautschuk **2**, 85 (1926).
[18] H. Feuchter, Kolloidchem. Beihefte **20**, 434 (1925).
[19] M. Hunemörder and P. Rosbaud, Kautschuk **3**, 228 (1927).

(See fig. 4.) It corresponds to a spacing of 54 A, or a multiple of this value, instead of 58 A, as previously reported.[20] When gel rubber is stretched, these arcs condense into very sharp equatorial spots, corresponding to this periodicity. There is a lateral separation of molecules or crystallites of 54 A, or perhaps a multiple of it, which persists in stretched gel rubber with the fibering. An examination of sol rubber indicated that no such spacing was present. It was reinvestigated under conditions which were carefully controlled, but no evidence of large spacing interference was produced by the sol phase.

3. DIFFRACTION PATTERNS OF STRETCHED GEL RUBBER

The gel rubber, when stretched nearly to the breaking point, produced an intense diffraction pattern which was sharper than that obtained with total rubber. The diffraction data are given in tables 1 and 2. In these tables, and in those to follow, d is the distance between the set of planes, making an angle θ with the incident beam. R is radius of the diffraction spot or ring as measured on a flat film. L is the distance on the film from the diffraction line to the central spot when the cylindrical camera is used. When symbols are used to indicate relative intensities, they have the following conventional designations: s, strong; m, medium; w, weak; and v, very weak.

TABLE 1.—*X-ray-diffraction data for stretched gel rubber; see figure 5*

Flat-film camera. Distance from specimen to film 5 cm.

Pattern	Equator			First layer line			Second layer line		
	R	θ	d	R	θ	d	R	θ	d
	cm		A	cm		A	cm		A
R57	1.26	7°4.34′	6.24				1.98	10°48.1′	4.102
	1.925	10°31.41′	4.21						
R61	1.258	7°3.68′	6.253	1.60	8°52.34′	4.983	2.435	12°59′	3.421
	1.925	10°31.7′	4.207	2.20	11°52.5′	3.735			
	2.738	14°21.17′	3.100	2.44	13°0.4′	3.41			
R62	1.26	7°4.33′	6.243	1.62	8°58.56′	4.926	1.99	10°51.1′	4.082
	1.94	10°36.19′	4.177	2.215	11°56.8′	3.714	2.47?		
	2.755	14°25.64′	3.084	2.44	13°0.375′	3.412			

TABLE 2.—*X-ray diffraction data for stretched gel rubber; see figure 6*

Flat-film camera. Distance from specimen to film 5.09 cm. Pattern *R64* (with NaCl).

Equator			First layer line			Second layer line		
R (cm)	θ	d	R (cm)	θ	d	R (cm)	θ	d
		A			A			A
1.27	7°0.3′	6.30	0.87	4°51′	9.09	2.00	10°44′	4.13
1.95	10°29′	4.23	1.63	8°53′	4.98	2.46	12°54′	3.45
2.76	14°14′	3.13	2.22	11°47′	3.76			
			2.47	12°57′	3.43			

The data in table 2 are assumed to be more reliable than the data in table 1, because the distance from specimen to film was more ac-

[20] Geo. L. Clark, Rubber Age **38**, 79 (1935).

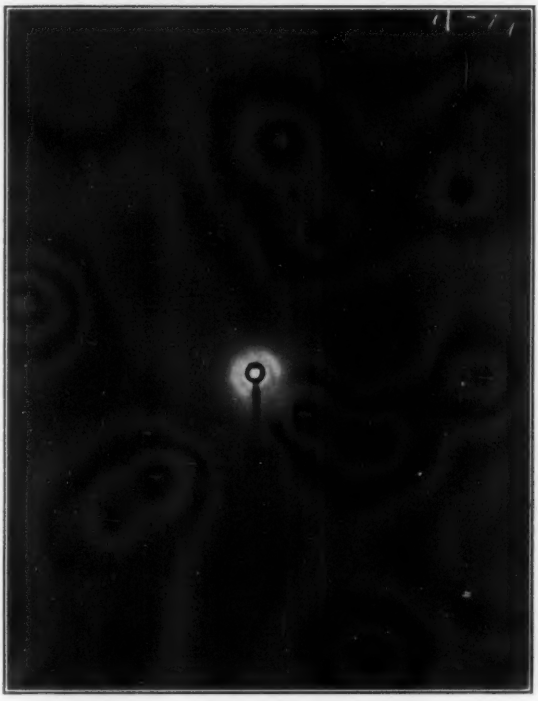

FIGURE 4.—*Long spacing in unstretched gel.*
Room temperature. Exposure 18½ hours.

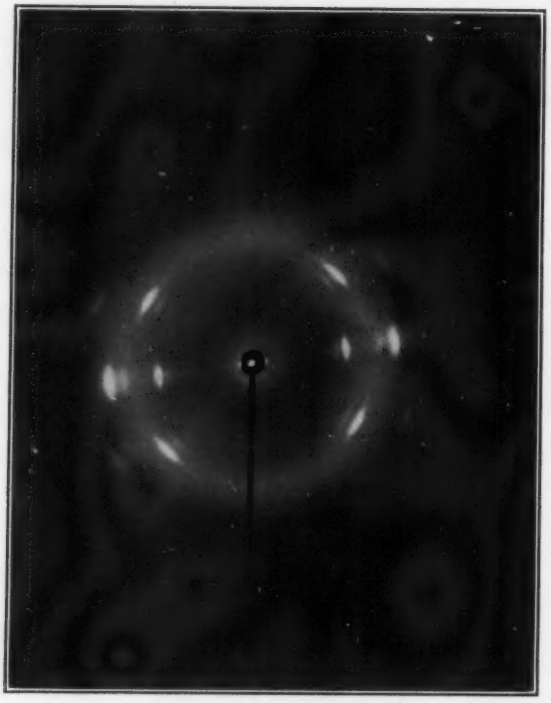

FIGURE 5.—*Pattern R57.*

Gel without sodium chloride. Stretched about 500 percent. Fiber axis normal to beam. Room temperature. Exposure 6 hours.

curately determined in this case by covering the sample with finely powdered sodium chloride. The results are in very good agreement with those of Lotmar and Meyer, as shown later in table 5. In view of the broad interferences in the pattern used by Lotmar and Meyer, it is surprising that the agreement is so good.

4. DIFFRACTION PATTERNS OF FROZEN SOL, GEL, AND TOTAL RUBBERS

In the present investigation, sol, gel, and total rubbers are examined individually, to compare the spacings and the intensities of interferences in their powder patterns, and also to compare the spacings of frozen rubber with those of stretched rubber at room temperature. Two types of patterns were taken of each kind of frozen rubber, one with the cylindrical camera and the other with the flat-film box camera. The data are recorded in tables 3 and 4 and the diffraction patterns reproduced in figures 7 and 8. Uncertain interferences were not measured, as indicated by blank spaces in table 3.

TABLE 3.—*X-ray diffraction data for frozen sol, gel, and total rubbers; see figure 7*

Cylindrical camera. Distance from specimen to film 6.33 cm.

Sol—pattern *R29*			Gel—pattern *R28*			Total—pattern *R34*		
L (cm)	θ	*d*	*L* (cm)	θ	*d*	*L* (cm)	θ	*d*
	Degrees	A		*Degrees*	A		*Degrees*	A
1.44β	6.52	6.12	1.42β	6.43	6.20	1.43β	6.47	6.16
1.58	*s*7.15	6.17	1.57	*s*7.11	6.21	1.57	*s*7.11	6.21
1.77	*m*8.01	5.52	1.76	7.97	5.54	1.76	7.97	5.54
1.97	*s*8.92	4.96	1.96	*s*8.87	4.99	1.96	*s*8.87	4.99
2.12β	9.58	4.17	2.10β	9.51	4.20	2.11β	9.55	4.19
2.36	*vs*10.68	4.15	2.34	*vs*10.59	4.18	2.34	*vs*10.59	4.18
2.65	*ms*11.99	3.70	2.62	*ms*11.86	3.74	2.64	*ms*11.95	3.71
2.86	*m*12.95	3.43	2.82	*m*12.76	3.48	2.82	*m*12.76	3.48
3.21	*mw*14.53	3.07	3.26	*mw*14.76	3.02	3.28	*mw*14.85	3.00
3.56	*w*16.11	2.77	3.49	*w*15.80	2.82			
						3.67	*vw*16.61	2.69
3.86	*w*17.47	2.56	3.86	*w*17.47	2.56	3.91	*mw*17.70	2.53
4.16	*vw*18.83	2.38						
						4.36	*m*19.73	2.28
4.52	*vw*20.46	2.20	4.47	*w*20.23	2.22			
4.84	*m*21.91	2.06	4.81	*m*21.77	2.07	4.78	*mw*21.63	2.08
5.14	*w*23.27	1.95				5.09	*w*23.04	1.96
						5.48	*w*24.80	1.83

TABLE 4.—*X-ray diffraction data for frozen sol, gel, and total rubbers; see figure 8*

Flat-film camera. Distance from specimen to film 10.32 cm.

Sol—pattern *R20*			Gel—pattern *R22*			Total—pattern *R24*		
R (cm)	θ	*d*	*R* (cm)	θ	*d*	*R* (cm)	θ	*d*
		A			A			A
2.36β	6°26′	6.19	2.38	6°30′	6.13	2.36	6°26′	6.19
2.63	7°9′	6.18	2.65	7°12′	6.13	2.63	7°9′	6.18
2.98	8°3′	5.49	2.99	8°5′	5.47	2.97	8°2′	5.50
3.32	8°55′	4.96	3.34	8°58′	4.94	3.32	8°55′	4.96
3.61β	9°38′	4.15	3.64	9°43′	4.12	3.62	9°40′	4.14
3.85	10°14′	4.33	3.88	10°18′	4.30	3.86	10°15′	4.32
4.05	10°43′	4.14	4.08	10°47′	4.11	4.06	10°44′	4.13
4.59	11°59′	3.70	4.62	12°4′	3.68	4.59	11°59′	3.70

Within experimental error, the sol, gel, and total rubbers produce similar patterns. The spacings in sol rubber obtained with the cylindrical camera are uniformly smaller than the others by approximately 0.04 A, but the difference probably is not significant. The flat-film camera shows the gel spacings to be uniformly smaller than the others, which may be a temperature effect, since no special precaution was taken to insure a constant temperature. Some interplanar spacings, including the important 020 interference of the frozen rubber, could not be distinguished in patterns *R28*, *R29*, and *R34*, but were satisfactorily resolved by the flat-film camera, which uses a longer distance from specimen to film.

An analysis of the (200) line with a microphotometer gives a slight indication of a doublet character.

For each type of rubber, in order to prove that the "powder" pattern of frozen rubber was characteristic of rubber, a pattern was also obtained after warming up to room temperature. In all cases the crystal interferences disappeared completely, leaving only the halos obtained from ordinary unstretched rubber. These patterns are shown in figure 9.

5. COMPARISON BETWEEN STRETCHED RUBBER AND FROZEN RUBBER, AND THE ASSIGNMENT OF CRYSTAL INDICES

The diffraction data on stretched and frozen rubber are arranged for comparison in table 5. The assignment of indices is based on the rubber structure given by Lotmar and Meyer. Values of d have been calculated from their sin θ/λ values for stretched rubber, and are also recorded in the table for comparison.

The lower value for the (002) spacing in frozen rubber, 6.18 instead of 6.30 in stretched rubber, is undoubtedly beyond experimental error and represents a significant difference which may be an effect of temperature. However, stretched rubber cooled to the same temperature as frozen rubber displays no change in its normal (002) spacing. Except for small differences in the (002) and (200) spacings, the principal interferences of frozen and stretched rubber confirm the structure of Lotmar and Meyer. Likewise the intensities compare favorably.

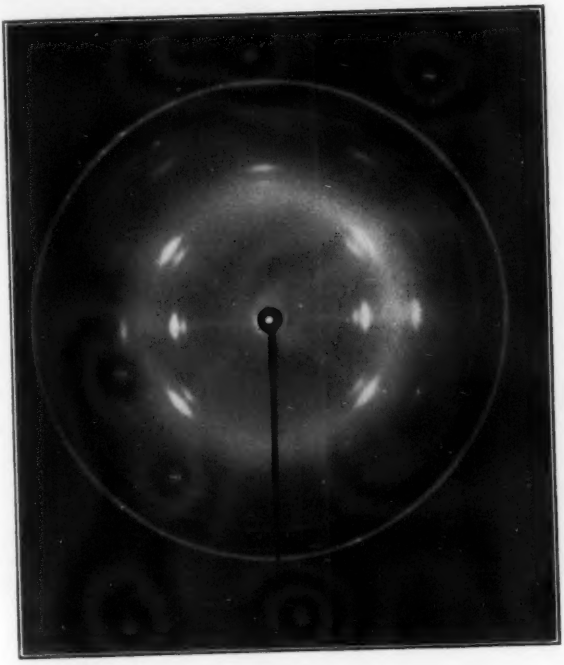

FIGURE 6.—*Pattern R64.*

Gel and sodium chloride. Stretched about 500 percent. Fiber axis 80° to beam. Room temperature. Exposure 16½ hours.

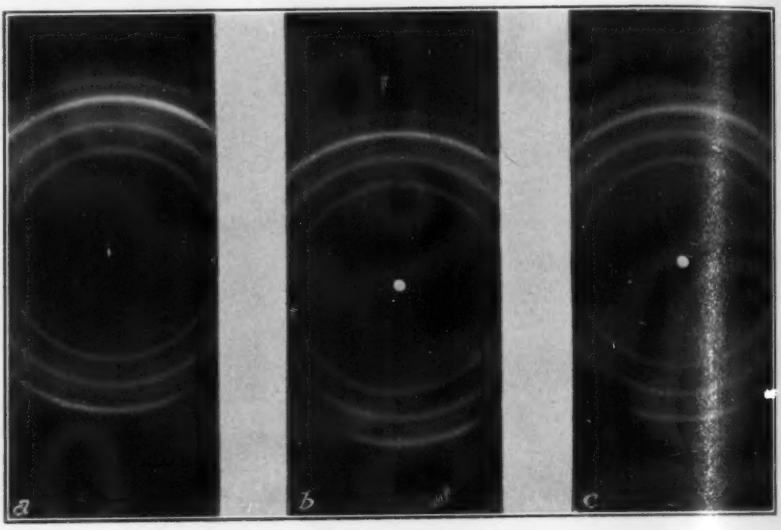

FIGURE 7.—*Frozen specimens.*

a, sol *R29*; b, *R28*; c, total *R34*. Cylindrical camera. Exposure 5 hours.

TABLE 5.—*Summary of interplanar spacings (d, in angstroms) for stretched and frozen rubber*

Lotmar and Meyer			Present investigation								
					Frozen rubber					
					Cylindrical camera			Flat-film camera		
Intensity	Indices hkl	Stretched rubber	Intensity	Pattern R64 (stretched)	Sol	Gel	Total	Sol	Gel	Total
		A		A	A	A	A	A	A	A
s	002	6.29	s	6.30	6.17	6.21	6.21	6.18	6.14	6.18
mw	111	5.50	mw		5.52	5.54	5.54	5.49	5.47	5.50
s	012	5.00	s	4.98	4.96	4.99	4.99	4.96	4.94	4.96
vs	200	4.24	vs	4.23	4.15	4.18	4.18	4.33	4.30	4.32
m	020	4.10		4.13				4.14	4.11	4.13
ms	210, 013, 211	3.76	ms	3.77	3.70	3.74	3.71	3.70	3.68	3.70
w	120, 121	3.70								
w–m	21$\bar{1}$, 12$\bar{1}$, 022, 212	3.45	m	3.45, 3.43	3.43	3.48	3.48			
w	004	3.14	mw	3.13						
w	220, 023, 221	3.01			3.07	3.02	3.00			
vw	114	2.86				2.82				
w	22$\bar{1}$, 222	2.78	w		2.77		2.69			
w	312, 311, 214, 130, 131	2.58	w							
vw	22$\bar{2}$	2.56			2.56	2.56	2.53			
vw	124	2.39	vw		2.38					
vw	230, 231	2.29								
vw	304	2.23			2.20	2.22				
vw	224	2.20	vw							
w	22$\bar{4}$	2.08	mw							
vw	034	2.06			2.06	2.07	2.08			
vw	421, 420	1.92	w		1.95		1.96			
			w				1.83			

6. SOL AND GEL RUBBER CRYSTALLIZED FROM SOLUTIONS

In earlier papers [21] to which reference has been made, crystals of sol and gel rubber which were produced from solutions of these fractions were shown to be fine needles. They were birefringent between crossed nicols, an indication of crystallinity in some system other than cubic. Their melting behavior was reported, their analysis conformed to the composition C_5H_8, and their refractive index was the same as that of uncrystallized rubber at the same temperature. They have now been investigated by X-rays to confirm their crystalline character.

The rubber was deposited on a Cellophane disk, about 2 cm in diameter, the upper surface of which was roughened with sandpaper to hold the deposit in place. The disks had been extracted previously with hot water and with hot alcohol to remove plasticizing agents. Crystals formed slowly from dilute solutions during 2 or 3 weeks at temperatures between −38 and −48° C. In this range of temperature the velocity of crystallization is suitably repressed. The deposit was washed once with ether at −60° C, and transferred to cold 95-percent ethyl alcohol, in which it was shipped from the National Bureau of Standards to the University of Illinois, surrounded by solid carbon dioxide. At low temperatures the fluidity of ethyl alcohol is quite low, so that there was little splashing and the deposit usually adhered to the disk. At the University of Illinois, the specimen was kept cold by suspending over liquid air in a vacuum flask until the X-ray exposure could be made.

The flat-film camera maintained specimens at temperatures between −20 and −40° C during exposure. The camera, pinhole, specimen holders, and forceps were cooled by solid carbon dioxide and acetone. With the cooled forceps the specimen was transferred to a piece of porous plate placed upon solid carbon dioxide, and much of the alcohol was removed. Sometimes, especially in the early trials, the specimen was also covered by a celluloid disk. In the final experiments, no disk was used, and the specimen was simply spread over the pinhole. This had a diameter of 0.01 cm. The camera was properly aligned with the X-ray tube to give a beam of maximum intensity, before the film was inserted. The exposures required about 10 hours.

After considerable experimentation with crystalline sol a diffraction pattern was finally obtained which was reproduced several times and which definitely showed faint crystalline interferences, not suitable for accurate measurement and analysis, but confirming the crystalline nature of the specimen. The crystalline material is sometimes more compact than at other times. With the crystalline gel, powder patterns were obtained with specimens *R*38 and *R*39, which are reproduced in figure 10. Many trials were made before the proper conditions were established. It is hardly necessary to emphasize the extraordinary experimental difficulties involved in work of this kind.

[21] See footnote 12.

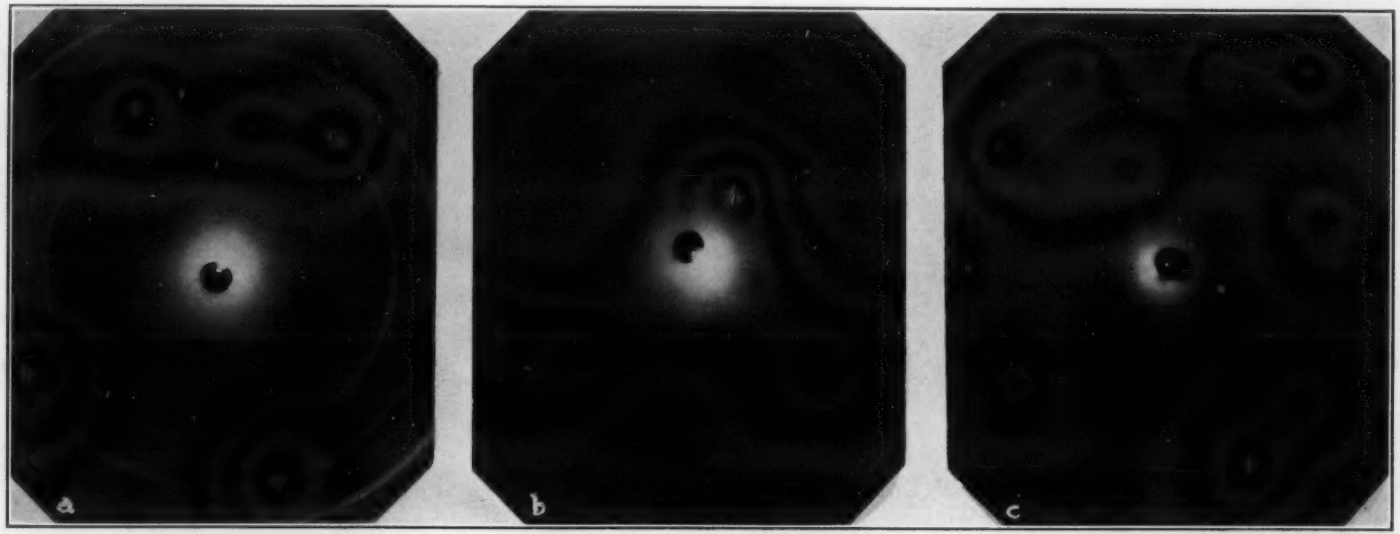

FIGURE 8.—*Frozen specimens.*

a, sol *R20*; b, gel *R22*; c, total, *R24*. Flat-film camera. Exposures 8 to 11 hours.

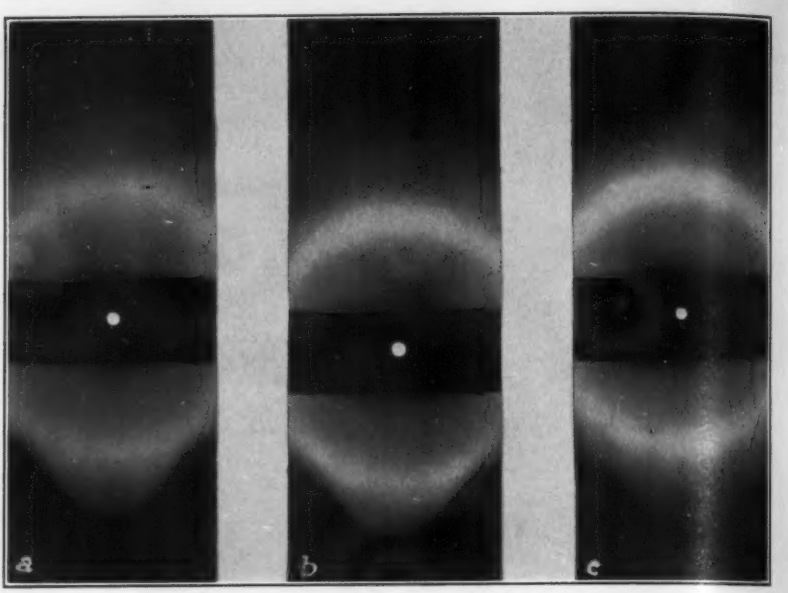

FIGURE 9.—*Specimens at room temperature.*

a, sol *R33*; b, gel *R32*; c, total *R36*. Cylindrical camera. Exposure 5 hours.

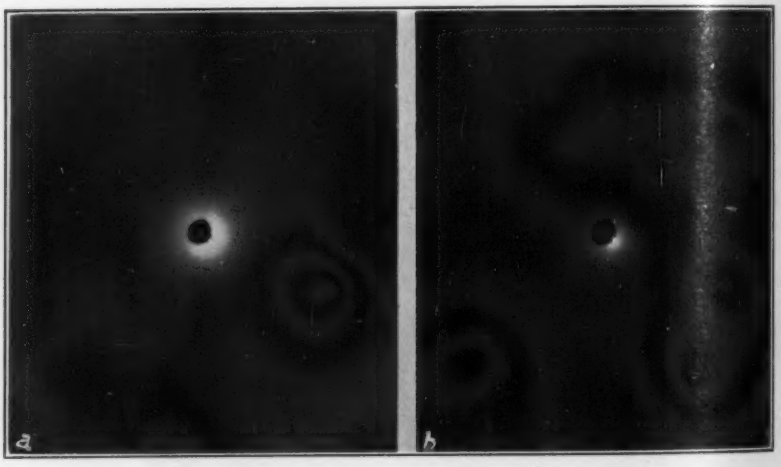

FIGURE 10.—*Gel rubber crystallized from solution.*

a, *R38*, exposure 11 hours; b, *R39*, exposure 14½ hours.

When the data in table 6 are compared with those obtained with frozen rubber, an excellent agreement is found for the three strongest interferences. There is no doubt therefore that the material is truly crystalline, and that the structures of the crystals are identical with those of crystals which form in massive, frozen rubber.

TABLE 6.—*X-ray diffraction data on crystallized gel rubber; see figure 10*

[Distance from specimen to film 10.32 cm.]

R38			*R39*		
R (cm)	θ	*d*	*R* (cm)	θ	*d*
		A			A
2.65	7° 12′	6.14	2.62	7° 7.5′	6.19
3.33	8°56.5′	4.95	3.31	8°53.5′	4.97
4.06	10° 44′	4.13	4.04	10°41.5′	4.14

IV. SUMMARY

Sol, gel, and total rubber were prepared by a method which avoided the effects of light and oxygen. The total rubber when stretched and exposed to an X-ray beam behaved like other specimens and produced the characteristic crystal fiber pattern. Stretched sol rubber produced no evidence whatever of this pattern, even at 1,000 percent elongation. With stretched gel rubber, the pattern was formed above 100 percent elongation, and at 200 percent was sharp and intense. The measurements of interplanar spacings agree excellently with the results reported recently by Lotmar and Meyer.

A large, interplanar spacing of 54 A was found in the unstretched gel. It was absent in the sol.

Specimens of frozen sol, gel, and total rubber were examined with a cylindrical, and with a flat-film camera, to compare the spacings and intensities with those of stretched gel. Within experimental error, sol, gel, and total rubber produce similar patterns. The spacings are similar to those in stretched rubber, with the exception of the (002) spacing in frozen rubber, which is 6.18 A instead of 6.30 A, the value in stretched rubber.

The pattern of gel, crystallized from solution, is similar to those of stretched and frozen rubber.

We appreciate the cooperation of L. G. Polhamus, Bureau of Plant Industry, U. S. Department of Agriculture, who supplied latex of authentic origin.

WASHINGTON, July 15, 1937.